Intranuclear Cascade Model for Deuteron- and Alpha-induced Reactions at Intermediate Energies

モニラ, ジャナツル, コブラ

https://doi.org/10.15017/1931898

出版情報：九州大学, 2017, 博士（工学）, 課程博士
バージョン：
権利関係：

Doctoral Dissertation

Intranuclear Cascade Model for Deuteron- and Alpha-induced Reactions at Intermediate Energies

By

Monira Jannatul Kobra

Department of Applied Quantum Physics and Nuclear Engineering

Graduate School of Engineering, Kyushu University, Japan

Table of Contents

1 Introduction

With the advent of science and technology, particle transport codes attract growing interest in basic science, technology and applications in recent years. The physical processes considered for hadrons transport include electromagnetic and hadronic processes, the latter of which is simulated by using nuclear reaction models. Nowadays, nuclear reactions are modelled in two stages: the first stage is cascade process and the second one is the static process followed by the cascade process. To describe the fast process, we have developed a code[1] that has been incorporated into the widely used Monte Carlo Particle and Heavy Ion Transport code System (PHITS)[2]. Background and the purpose of this work are described.

1.1 Accelerator Driven System (ADS)

The energy needs of our society have been increasing continuously over the last century. We search for new sources as well as would like to utilize the sources efficiently we already have. About 80% of our energy source oil, gas, coal etc. The energy production by these sources increases the CO_2 emission, one of the main causes of global warming. The alternative energy source can be the nuclear power plant, a CO_2 free energy source. This led to increase the number of nuclear power plants and to make the nuclear plants as sustainable as possible. However, the nuclear power generation in future will depend on solving three issues[3] i) no quick exhaustion of nuclear fuel ii) safety and security of power plant iii) nuclear waste management.

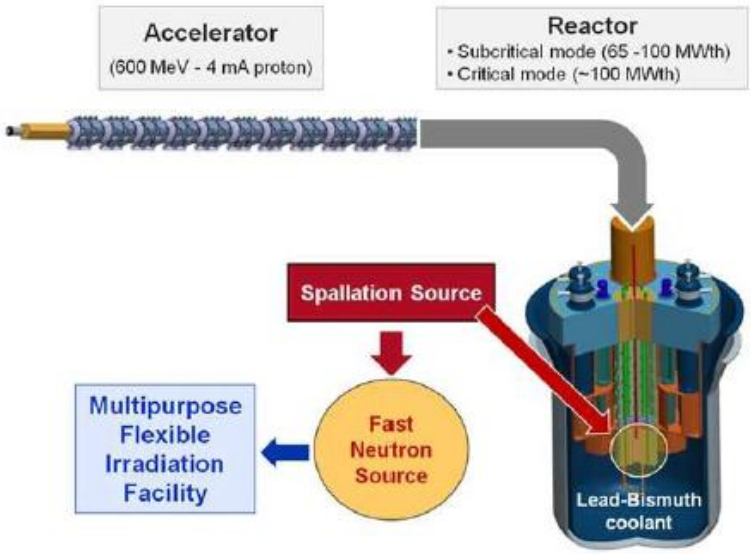

Fig. 1.1 Schematic representation of an ADS.[3]

First, I will talk about the third issue, nuclear waste management problem. The waste of nuclear power contains highly radiotoxic, long-lived isotopes. The usual solution is to keep the nuclear wastes underground for about ten thousand years. The process includes long-term monitoring, high cost, and it is also difficult to handle. To manage the highly radiotoxic waste, the alternative idea is to separate (or partitioning) the long-lived waste isotopes from the utilized fuel using the transmutation technique by the acceleration driven system (ADS). The technique involves a proton beam of few hundred MeV from an accelerator hit a spallation target surrounded by a blanket assembly of nuclear fuel located in the centre of the reactor. Usually, 10-15 spallation neutrons emit per incident high-energy proton. The spallation neutrons eventually transmute the waste isotopes lowering the half-life from hundreds of thousands of years to several hundred years. Fig. 1.1 shows a schematic diagram of an ADS project.

The incorporation of ADS technology in nuclear power generation may enhance the safety of the power plant by altering the geometry of the reactor chamber. The plan is:

available neutrons for fission chain reactions in the chamber will not allow to multiply in successive reactions and having them take off the reactor. Meanwhile, the fast spallation neutrons colliding with moderator turn them thermal neutrons and sustain the nuclear fission process. Therefore, the shutdown of the accelerator will stop the reactor. The reactor will have enhanced safety. In addition, to solve the nuclear fuel exhaustion problem, ADS technology can be useful. Study says if the current rate of uranium consumption continues the available fuel will last only for about 100 years. Uranium is the most common nuclear fuel until now. The use of naturally abundant thorium as a new primary fuel has been tantalizing for many years. The fertile thorium upon absorbing fast neutron will transmute to fissile U^{233}, which is an excellent fuel.

Considering the huge applicability, extensive research on ADS technology has been going on. To run the project, the problems with its size, high technologic requirements, etc. need to solve. Many such projects have been running all around the world to carry out the experiments, test the accuracy of models describing spallation, transmutation reactions etc. The aim of such investigations is to design the optimal parameters required for ADS system. optimization of the device requires simulation tool, particle transport codes. The macroscopic simulation tool provides information on the reactor in operation e.g. what waste to expect or what kind of shielding should prepare etc. It is very important for the tool that uses nuclear reaction models to provide precise information. Therefore, the nuclear reaction model used in transport codes should also be precise enough. It uses Intranuclear cascade (INC) model to simulate nuclear reactions. Besides emission of spallation neutrons from the high-energy proton-induced nuclear reactions, deuterons, alpha particles etc are also ejected in ADS. The nuclear model should capable of simulating secondary particles initiated nuclear reactions besides handling proton-induced nuclear reactions.

1.2 Heavy Ion Cancer Therapy

Particle physics technology has improved dramatically the cancer treatment and many other applications in medical science. Besides surgery, radiotherapy manifests a great advantage to treat the localized malignant tumour. High energy X-rays have been used for cancer treatment. In last two decades, charged particles e.g. proton, helium, carbon therapy have gained high interest.[4] The success of the radiation therapy in cancer treatment depends on providing the right amount of dose to the cancerous cell without affecting surrounding normal tissues. The primary reason to choose the particle radiotherapy over the most advanced X-ray therapy is the sharp increase of dose at the well-defined depth (Bragg-peak, Fig. 1.2) and rapid fall-off beyond that maximum. By contrast, dose with X-ray decreases exponentially with tissue depth.

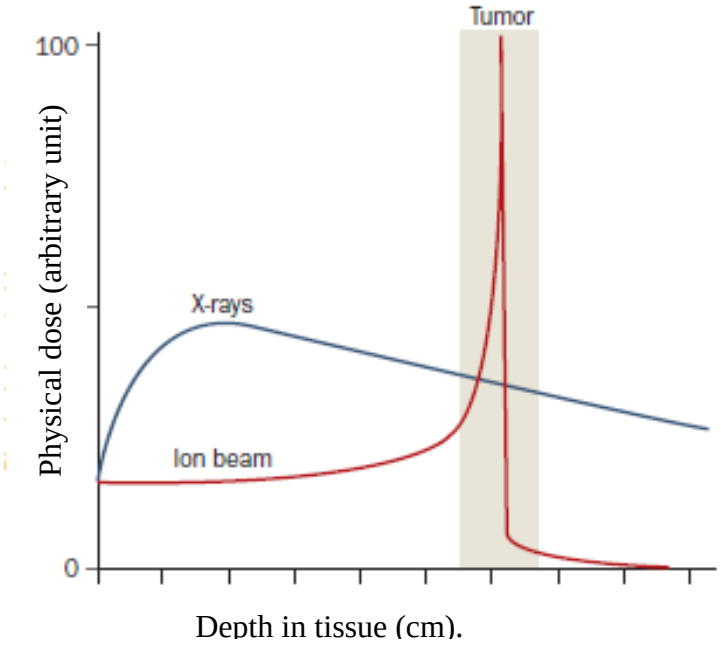

Fig. 1.2 Comparison of the depth-dose relationships for x-rays and charged particles.[5]

For the heavy-ions, the ratio of Bragg peak dose to the entrance dose is larger. Particles heavier than proton are referred as heavy-ions in oncology. High linear energy transfer (LET) for heavy-ion radiotherapy provides biological effects of high relative biological effect (RBE) and low oxygen enhancement ratio (OER) in the Bragg peak region. Although the larger charge exhibits greater effectiveness, proton and helium reveal almost the same biological effects. Neon and Carbon deliver higher biological effects of high RBE and low OER in the Bragg peak region. The RBE ratio (Bragg peak vs entrance region) is highest for Carbon. The RBE is even higher for Argon but nuclear fragmentation extends the dose even beyond the Bragg peak. The pioneering work of heavy-ion radiotherapy started with helium and neon ions at the Lawrence Berkeley Laboratory, University of California in Berkeley in 1977. World's first heavy-ion radiotherapy has been started at Heavy Ion Medical Accelerator in Chiba (HIMAC) in National Institute of Radiological Sciences (NIRS), Japan. NIRS has been treating cancer with high-energy carbon ions since 1994.

To have specific information about biological and physical dose delivered on the human body during heavy-ion radiotherapy, particle transport codes are indispensable. Late effect of low dose exposure is a serious issue for childhood cancer treatment with carbon radiotherapy. Fragments produced in the carbon incident reactions emitted at large angle with high energy beyond the irradiation field that causes an amount of dose in normal tissues. INC utilized in transport codes requires to capable of simulating fragments induced nuclear reaction for accurate dose calculation. The fragments consist of the cluster deuteron, alpha etc. particles. In addition, the theoretical success of alpha-induced reactions will open the pathway for INC model to expand for carbon-incidence radiotherapy dose calculations.

1.3 Space Radiation

Cosmic rays involve two types, galactic cosmic rays (GCR), which originates outside the solar system but within the galaxy, and high-energy particles emitted by the sun, which is called solar particle events (SPE). The compositions of these two types of rays are different and have a distinct contribution of equivalent dose to the exposure. When primary cosmic rays interact with the earth atmosphere, they are converted to secondary particles. The dominant energy range of the cosmic rays is 10 MeV/nucleon to several GeV/nucleon. Fig. 1.3 shows relative abundance of the galactic cosmic rays up to z =26. The primary GCRs contains 10-12% alpha and the alpha-induced reactions are the primary source of ^{2}He and ^{3}He production. Cosmic rays are the main source of radiation in a manned space mission.

To understand the biological effect of exposure to ionizing radiation in the space exploration missions or for the workers at International Space Station (ISS), research is going on. Currently, NASA radiation guideline is only to missions in lower Earth orbit (LEO) and there is no guideline for the missions beyond LEO. The biological effect of radiation exposure is an indispensable concern for the manned mission. The experience of the manned mission is only about four decade and limited to near Earth's orbit. The possibility of the late and long-term effect of cosmic rays demands to understand well.

To build a theory of cosmic rays, it is very much important to understand the composition of the primary cosmic rays, its source, acceleration, and the transport mechanism. Accurate simulation of the nuclear reactions by cosmic rays and interstellar matter is highly expected. The cross section and energy spectra of the secondary particles resulting from the nuclear reactions are important parameter to solve the issues. To build a cosmic ray database and to demonstrate the transport of cosmic rays, theoretical models are indispensable.[6]

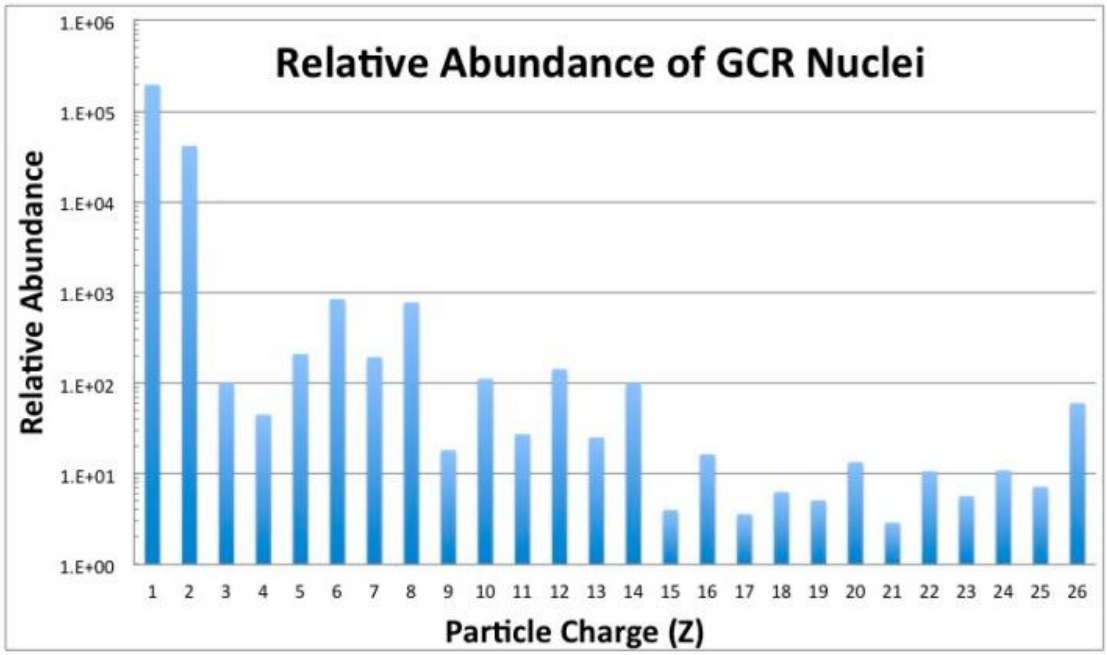

Fig. 1.3 Relative abundance of GCR nuclei from hydrogen (Z = 1) to iron (Z = 26).[7]

The INC model in transport tool like PHITS is important to estimate dose received by astronauts in a spaceship. High-energy cosmic rays or secondary particles not only harmful for an astronaut but also they destroy the devices like computers, which are the very fundamental requirement in spacecraft for getting commands from earth or sending scientific data from the space. Single event upset is one of the issues caused by heavy particles. The single event upset occurs when the high energetic heavy particle strikes sensitive portions of an electronic device interrupting its correct operation.

1.4 Nuclear Fission Reactor

Nuclear fission is the fragmentation of atomic nuclei into two lighter nuclei of comparable masses. Two German chemists, Otto Hahn and F. Strassmann in 1939, discovered nuclear fission reactions, one of the most important discoveries in nuclear

physics that allows the utilization of internal nuclear energy for the practical purpose. Nuclear reactors are devices where the controlled chain reactions are maintained to have the steady flow of neutrons generated by fission of heavy nuclei accompanied by the release of energy that is used for the practical purposes. Enrico Fermi led to build the first nuclear reactor and launched in December 1942. Nuclear models and simulation tools are the very important tools for nuclear energy research. To estimate the heat generation, material damage by neutrons and nuclear waste management, nuclear models and data libraries are essential tools. Scientists and engineers have been working to make the reactors more efficient through nuclear models and simulations. It is almost impossible to observe what is happening inside the reactor. Nuclear models and simulation tools not only allowing the scientists to understand what is occurring inside as well as observing the impact on the environment. A diagram of nuclear fission chain reaction is presented in Fig 1.4.

Energy released by fission, Q_f of the nucleus (A, Z) that fragments into masses M_1 (A_1, Z_1), M_2 (A_2, Z_2) with binding energy W_1 (A_1, Z_1), W_2 (A_2, Z_2), respectively, is

$$Q_f = M(A,Z)\,c^2 - [M_1(A_1,Z_1)\,c^2\, M2(A_2,Z_2)\,c^2] = W_1(A_1,Z_1)\,W_2(A_2,Z_2) - W(A,Z) \quad (1.1)$$

When a fissile element like ^{235}U absorbs a neutron, it may undergo fission reaction. The heavy nucleus will split into two or more fission products releasing energy, gamma radiation and neutrons. Under certain condition, produced neutrons may contribute the chain reaction.

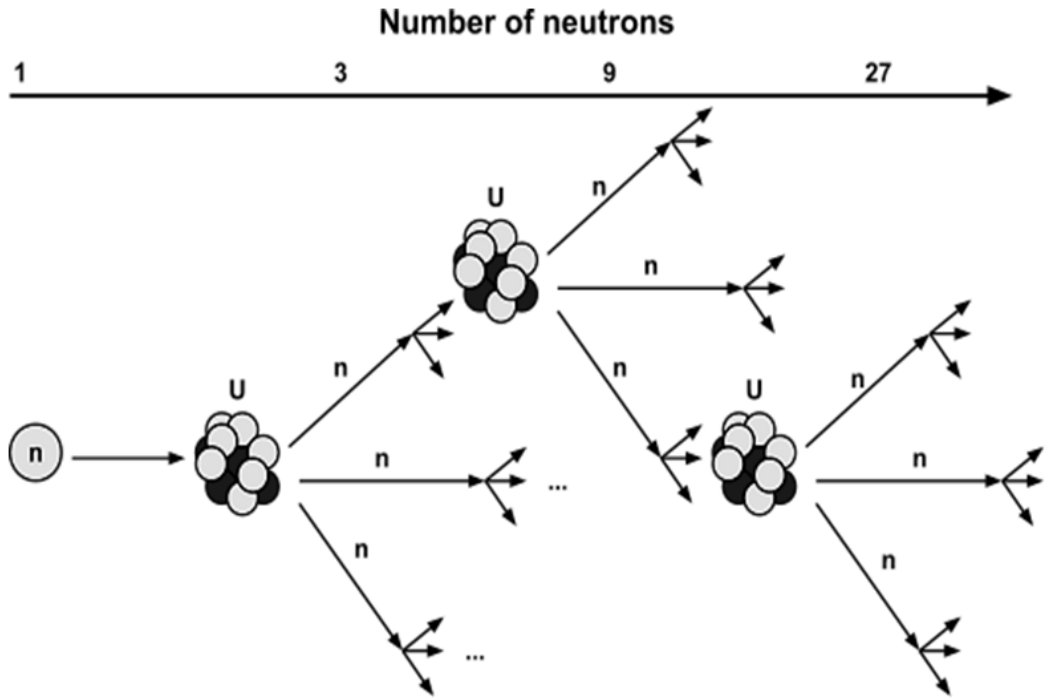

Fig. 1.4 The Fission nuclear reaction.[8]

1.5 Nuclear Fusion Reactor

A fusion reactor is a device that permits the controlled release of fusion energy. Nuclear fusion is the process by which two or more light nuclei fuse together. The process is accompanied by the release of huge energy due to the difference in mass between reactants and products. Any practical fusion reactor has not developed yet. Deuterium and tritium are considered as best fuel in a fusion reactor. Before commercial use, huge theoretical research and simulations should run and that is what is going on in many parts of the world. Macroscopic simulation tool like PHITS is an important ingredient for this kind of research.

1.6 Particle Transport Codes

Particles and heavy ions have been used in various fields of science and technologies e.g. nuclear physics, material sciences, space and geosciences, accelerator technologies, medical sciences, etc. In addition, various applications related to high-energy radioactive ions are being planned. Spallation products from high-energy ions are also planned to be used in nuclear physics. In the design of this kind of numerous facilities, it is extremely important to deal with transport and collision of various particles and heavy ions over a wide energy range. To handle the issues like estimation of shielding or estimation by tracing high-energy particles, the particle transport code is an essential. The transport codes provide macroscopic simulations by using microscopic various models. There are many particle transport codes like FLUKA, Geant4, PHITS etc. and we have then been using the codes in various research and application fields. In this section, a widely used transport code, PHITS, as well as other transport codes are discussed.

1.6.1 PHITS

PHITS stands for particle and heavy ion transport code system. It is a three-dimensional Monte Carlo particle transport simulation code. Several institutes in Japan and Europe through the collaboration have developed PHITS; Japan Atomic Energy Agency has been managing the whole project. Fig. 1.5 shows a list of institutes currently involved in the development of PHITS. This widely used transport code is written in FORTRAN, and developed based on the transport code NMTC/JAM[9].

PHITS uses various nuclear reaction models and data libraries to deal with the transport of almost all particles, e.g., neutron, protons, photons, electrons, heavy ions over a wide energy 10^{-5} eV to 1 TeV/u. The application of PHITS can be divided into two categories; namely transport process and a collision process. In the transport process, the motion of

particles is simulated even in external magnetic and gravitational field. During the motion of charged particles and heavy ions in matter, ionization processes take place that is named as transport process. Another physical process is the collision of the particles and heavy ions with nucleus in the matter. The decay of the particles is also included in collision processes. PHITS determines the mean free path using the total reaction cross section of particle, which is important to determine next collision points.

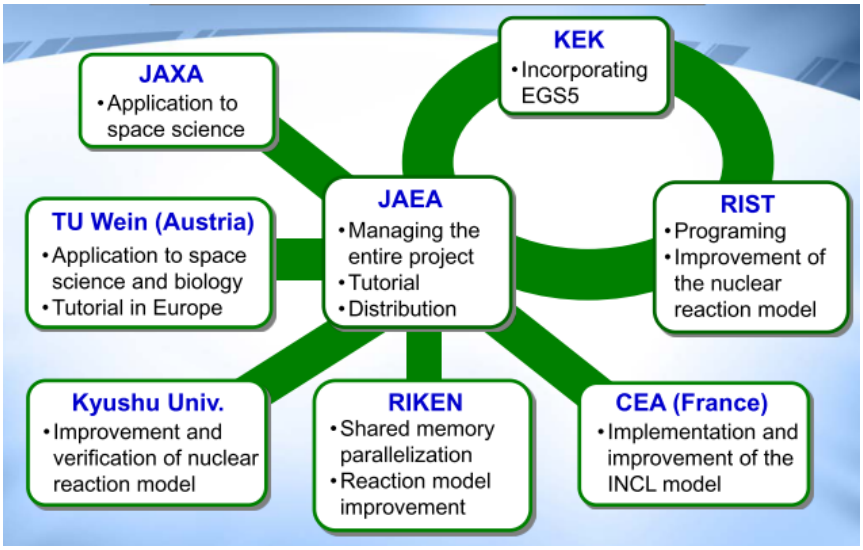

Fig. 1.5 Institutes involved to the development of PHITS[10].

The physics models used in PHITS for simulating atomic and nuclear collisions are summarized in Fig 1.6. For the transport of neutrons energy 20 MeV down to 1 meV, PHITS uses data library. For the high energy hadrons-induced nuclear reaction, the model JAM[11] is used, while for intermediate energy nuclear reactions INCL4.6 are employed to simulate dynamic stage of nuclear reactions. As alternative options, modified BERTINI and INC-ELF[1] are used in this region. The quantum molecular dynamic model, JQMD, is utilized to simulate nucleus-nucleus reactions. INCL4.6[12] is a default nuclear model for the simulation of deuteron-, triton-, ^{3}He, and α-induced nuclear

reactions. If the excitation energy of the residual nucleus is very high, statistical multi fragmentation model, SMM, is implemented before the evaporation model. Data library is used for the atomic collisions. Besides, some other models are also used; details are given[2,13].

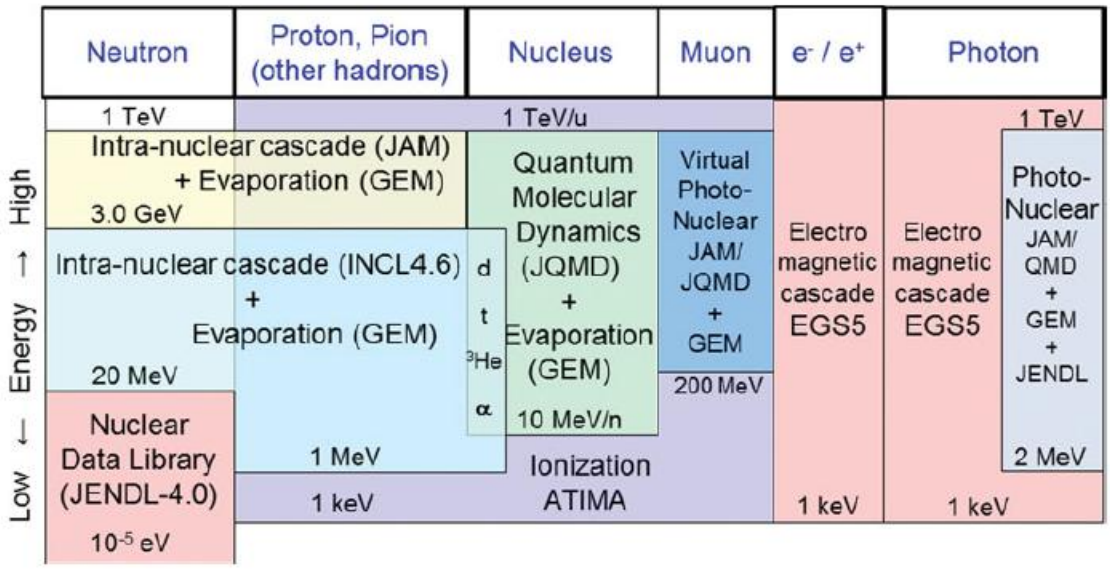

Fig. 1.6 The recommended Physics models for PHITS2.88 to simulate nuclear and atomic collisions.[14]

The important functions of PHITS are i) the event generator mode for low energy neutron interaction ii) the beam transport function, iii) the function for calculating the displacement per atom (DPA) iv) the microdosimetric tally function.[10] All the functions make it useful for specific fields.

The event generator mode and microscopic tally functions are used mainly for medical purposes such as patient estimation for radiotherapy and computed tomography examination. The mode is also indispensable for estimation of soft error in the semiconductor. For both the neutron and charged particle beam line design, the beam transport functions are useful. The DPA function is used to evaluate radiation damage in

material structure. To evaluate the deposited energy in microscopic sites, the microdosimetric function is used. PHITS has been extensively in J-PARC project to build the shielding, target, neutron beam lines due to its features. Several projects that use PHITS are also currently in progress. The PHITS-based treatment planning system has been initiated as well. It is to be noted that the INC-ELF utilized in PHITS is the previous version of the model used in the present research.

1.6.2 LAHET

LAHET[15,16] is a Monte Carlo code to simulate particle transport and nucleons, pions, light ions interactions with matter. LAHET code system has been developed at Los Alamos National Laboratory, USA based on the LANL version of HETC Monte Carlo code that was developed at Oak Ridge laboratory.

To describe nucleon-nucleon interaction, it uses Bertini model[17]. Bertini INC model is a default option in LAHET. As an alternative to Bertini INC, it employs ISABEL INC[18] model, which is an extension of Yariv and Freankel's VEGAS code having a capability to treat hydrogen and helium ions as projectiles. As an option, LAHET utilizes pre-equilibrium EXCITON model for the subsequent de-excitation of the residual nucleus.

LAHET has two options for the fission induced by the high-energy interactions. The ORNL model and the Rutherford Appelton Laboratory (RAL) model by Atchison. RAL is the default model in LAHET and it allows fission for $Z \geq 71$. LAHET utilizes Fermi Breakup model instead of evaporation model. Fermi breakup model de-excites the excited nucleus by breakup into two or more products. The unstable product will go through the subsequent breakup.

1.6.3 Geant4

Geant4[19] is a software toolkit. It simulates the "passage of particles through matter". The earlier version of Geant4 is developed by CERN, Switzerland. The present one, Geant4, is developed through collaboration.

Quark-Gluon String (QGS) model[20] is utilized to describe the interaction of protons, neutrons, pions and kaons with the nuclei at the incident energy range 20 GeV to 50 TeV. Coupled with the gamma-nuclear model, QGS can simulate photon-induced reactions in higher energy domain. For the intranuclear cascade energy region, Geant4 uses Bertini-style cascade code and Binary cascade model[21]. In Bertini-style cascade model, main features are mainly taken from Bertini model[22,23]. As an alternative to Bertini style cascade code, Binary cascade model is utilized in Geant4. Nuclear de-excitations are simulated with Precompound model. Exciton model, Fermi breakup model and Fission model also used in Geant4 code. Chiral Invariant Phase Space model is used as an event generator in Geant4.

1.6.4 FLUKA

FLUKA is a fully integrated Monte Carlo simulation package.[24,25] The code is written in Fortran 77, and is mainly developed by CERN, Geneva, Switzerland and INFN, Milan, Italy. The applications of FLUKA extend to accelerator design and shielding, accelerator driven system studies, neutrino physics etc.

A Glauber-Gribov model is employed to describe the cascade stage of hadrons-nucleus interactions. At sufficient high energy hadron-nucleus interaction is described by (G)INC model. FLUKA utilizes the exciton model for the description of the pre-equilibrium stage. For the last stage of interactions, evaporation model of Weisskopf-Ewing approach and fission model of Atchison algorithm or Fermi breakup model is used.[26] For nucleus-

nucleus interactions, FLUKA uses DPMJET-III model[27] for energies greater than 5 GeV/n.

1.6.5 NMTC

The high-energy particle transport code NMTC/JAM is an updated version of the nucleon-meson transport code NMTC/JAERI that was developed by the joint proposal of JAERI and KEK[9,28]. NMTC code employs JAM model for the interactions at above 3.5 MeV and Bertini model below 3.5 GeV. JAM is a hadronic cascade model that simulates ultra-relativistic nuclear collisions. Later on, PHITS is derived from NMTC/JAM in addition to HETC- CYRIC.[2]

1.7 Nuclear Reaction Models

Theoretical nuclear reaction models play an important role to understand the mechanism involved in the target-projectile system and estimate the required cross sections where data are not reliable or not fully available. The characteristics of nuclear reactions varied on the projectile incident energy, nature of projectile etc. There are various models of different natures, restricted to specific energy regime or specific phenomena. Therefore, it is a long-term desire to develop the nuclear model that can have a wide range of applicability, describe the reactions involving many species of incoming and outgoing particles and have high predictive accuracy as much as possible.

The reaction mechanism proposed by Serber[29] splits the nuclear reactions in two-stages. In the first stage, the incident particle initiates a cascade inside the nucleus. At this stage, nuclear reactions between the high-energy projectile and complex target nuclei are considered as nucleon-nucleon interactions. The cross section of nucleons are taken as in free space nucleon cross section, however, Pauli Exclusion Principle governs the

consideration. The second stage is the slow stage where the residual nucleus got de-excited by the evaporation or fission process. These two stages of nuclear reactions are well separated by their timescale. In the fast cascade stage, the collision takes place in the time scale of 10^{-22} S, where the second statistical process takes place in a slower timescale of the order or 10^{-16} S. The nuclear reactions usually refer as spallation reactions (Fig. 1.7).

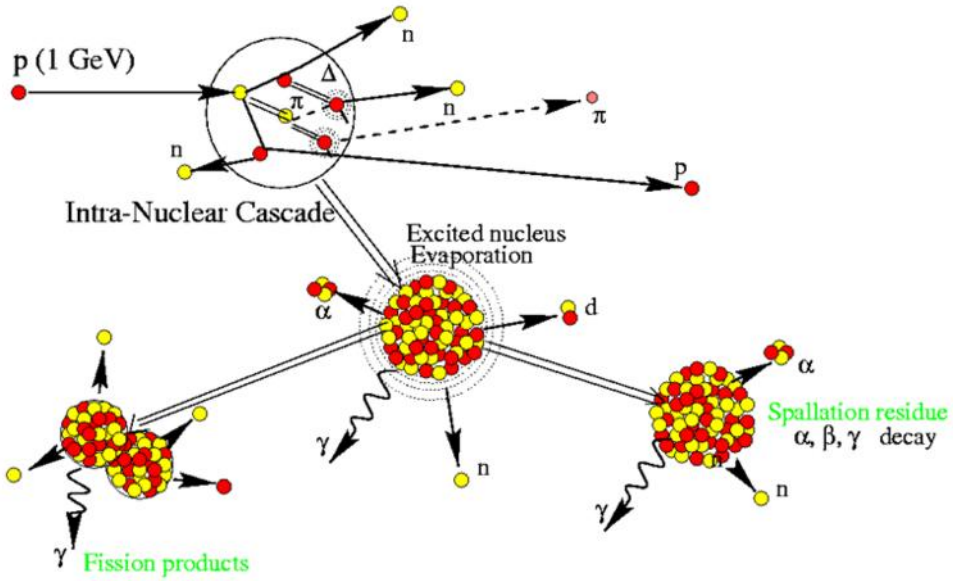

Fig. 1.7 Basic spallation reaction process.[30]

There have been developed various ideas to describe the fast cascade process including Goldberger[31], Bertini[32], Metropolis et al.[33], Chen et al.[34], Boudard et al.[35], Iwamoto et al.[36] etc. All these models use the Monte Carlo technique to calculate cascade stage of the nuclear reaction. The model name used for these kinds of calculations is known as intranuclear cascade model though there are different name proposed by the various working groups. In addition, cascade stage can also be simulated by JQMD code[37], which is based on quantum molecular dynamic (QMD). To simulate the evaporation/fission process, GEM[38], ABLA etc. is used. In some studies, between cascade and evaporation

model, a pre-equilibrium model, exciton[39], is used. However, transport codes, PHITS, utilize INC models like JAM, INCL, INC-ELF or JQMD coupled with evaporation model for the incident energy 0.1 – 3 GeV. A large number of particles, as well as clusters, emits in these reactions. The primary, as well as the secondary particles, initiated nuclear reactions require simulation having accurate predictions.

1.7.1 Intranuclear Cascade (INC) Models

Intranuclear cascade model is usually applicable for the nucleon-induced nuclear reactions where incident energy lies between intermediate to the high-energy region. There are several different INC codes as it is mentioned earlier. Some aspects are common to all of them. An overview and classification of INC model are given below.

1.7.1.1 Overview of INC Model

The INC model has been developed to explain nucleon-induced spallation reactions at high-energies. The interaction between incident particles and the target nucleons in the INC model is based on the multiple scattering theory of Serber[40] and Watson[41]. In the INC framework, nucleons in the nucleus are considered as collections of free particles and the interaction between the incident and target nucleons is considered as nucleon-nucleon (N-N) collision. Here, two-body collision is approximated as Quasi-Free scattering (QFS) with two-body collision cross section. In INC, when the kinetic energy of the projectile is high enough, it is assumed to travel in a straight-line trajectory in the nucleus, interference is not considered. A schematic diagram of INC model is shown in Fig. 1.8. In the figure, a nucleon with given kinetic energy and impact parameter enters a nucleus, initiates a two-body collision while moving in a straight-line trajectory. The nucleon scattered by the two-body collision follows a straight-line trajectory and repeat

the collision one after another. This is called multiple scattering or multi-step collision. The nucleons that acquire enough momentum will be emitted from the nucleus.

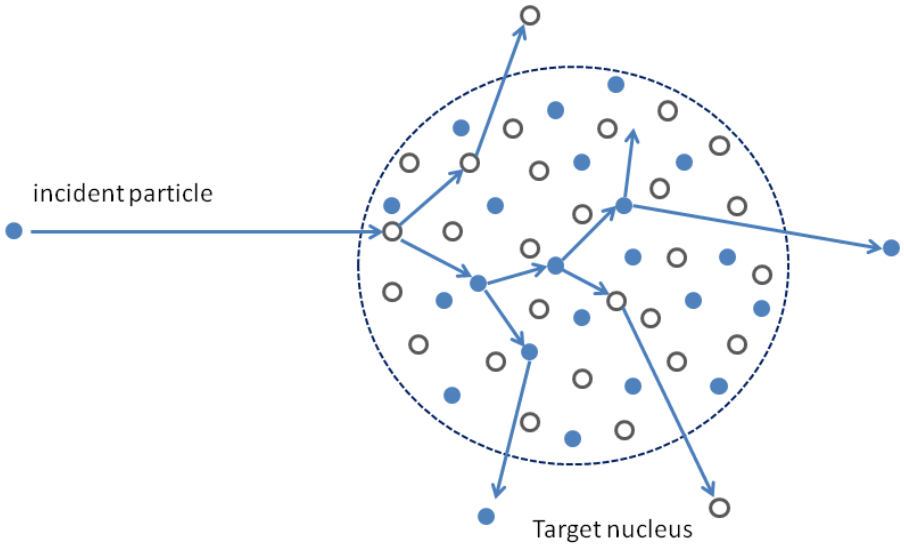

Fig. 1.8 Schematic diagram of INC model.

1.7.1.2 Classification of INC Model

All INC models can be categorized into two classes. One is space-dependent INC and the other one time-dependent INC. Time-dependent INC model studies the interaction between two collisions. Space-dependent INC model emphasizes the interaction between collections of nucleons with continuous medium characterizes by a mean free path. A bit more details of these two approaches are given below.

In the space-dependent INC model, the target nucleus is treated like a continuum with density distribution. Each participating nucleon is given mean free path according to collision cross section (nucleon-nucleon scattering cross section) of the incident particle and the nucleon in the medium. Projectiles are given mean free path at the beginning only.

The collision point x is given by the following Eq. (1.2) with the uniform random number ξ between [0, 1) and the mean free path λ,

$$x = -\lambda \ln(\xi), \tag{1.2}$$

where λ is

$$\lambda = \frac{1}{\rho \sigma_{NN}}, \tag{1.3}$$

$$= \frac{1}{\rho} \frac{A}{Z\sigma_{N_p} + (A - Z)\sigma_{Nn}}, \tag{1.4}$$

here σ_{NN} is the nucleon-nucleon collision cross section, Z is the number of protons, A is the mass number, ρ is the nucleon density, σ_{N_p} and σ_{N_n} are collision cross section between the incoming particle, and target proton and neutron, respectively. Space-dependent approach is used by e.g. ISABEL model, Bertini model, VEGAS model.

In time-dependent INC, each projectile and target nucleon is given a position and momentum. The nucleons will propagate until they come close to a certain distance, r_{ij},

$$r_{ij} < \frac{\sigma_{NN}}{\pi}, \tag{1.5}$$

here σ_{NN} is the nucleon-nucleon collision cross section. INCL is a time-dependent model. The INC model in the present research is also a time-like model. Time-dependent models are easy to handle and require less computation time.

As described above, the space-dependent and time-dependent INC largely differs depending on the method of determining the collision point, but there is no difference between the two-body scattering methods after the collision. In the next few sections, descriptions of some models that are utilized to simulate the cascade stage are represented.

1.7.2 Quantum Molecular Dynamics (QMD) Model

Quantum Molecular Dynamics can describe the cascade stage of nuclear reaction model. QMD is used in transport code to handle hadrons as well as heavy-ion induced reactions. In the following, a summary of JQMD[37] developed by Japan Atomic Energy Agency is given.

The QMD model is a semi-classical simulation method. The Gaussian wave packet is used to express each nucleon state. The Gaussian wave function is

$$\Phi_i(\boldsymbol{r}) = \frac{1}{(2\pi L)^{3/4}} \exp\left[-\frac{(\boldsymbol{r}-\boldsymbol{R}_i)^2}{4L} + \frac{i}{\hbar}\boldsymbol{r}\cdot\boldsymbol{P}_i\right], \tag{1.6}$$

where L is the width of the wave packet. $\boldsymbol{R}_i$ and $\boldsymbol{P}_i$ are the centres of a wave packet in the coordinate and momentum spaces, respectively. The total wave function is the direct product of these wave functions.

The one body distribution function is obtained by Wigner transform of wave function,

$$f_i(\boldsymbol{r},\boldsymbol{P}) = 8\exp\left[-\frac{(\boldsymbol{r}-\boldsymbol{R}_i)^2}{2L} - \frac{2L(\boldsymbol{p}-\boldsymbol{P}_i)^2}{\hbar^2}\right]. \tag{1.7}$$

The $\boldsymbol{R}_i$ and $\boldsymbol{P}_i$ time evaluation is described by Newtonian equations of motion and two body collision term. The Newtonian equations of motion are

$$\dot{\boldsymbol{R}}_i = \frac{\partial H}{\partial \boldsymbol{P}_i}, \dot{\boldsymbol{P}}_i = -\frac{\partial H}{\partial \boldsymbol{R}_i}, \tag{1.8}$$

where the Hamiltonian, *H*, is

$$H = \sum_i E_i + \frac{1}{2}\frac{C_A}{\rho_0}\sum_i \langle\rho_0\rangle + \frac{1}{1+\tau}\frac{C_B}{{\rho_0}^\tau}\sum_i \langle\rho_0\rangle^\tau + \frac{1}{2}\sum_{i,j(\neq i)} c_i c_j \frac{e^2}{|\boldsymbol{R}_i - \boldsymbol{R}_j|}\,\mathrm{erf}\left(|\boldsymbol{R}_i - \boldsymbol{R}_j|/\sqrt{4L}\right) + \frac{C_s}{2\rho_0}\sum_{i,j(\neq i)} \left(1 - 2|c_i - c_j|\right)\rho_{ij}, \tag{1.9}$$

here the first term, $E_{i,}$ is the single particle energy of *i*th nucleon. The second and third terms are the Skyrme type potential energies, the fourth term is the Coulomb energy, and the fifth term symmetry energy. In 4th term, "erf" is the error function and $\langle\rho_i\rangle$ is an overlap density of nucleon.

$$\langle\rho_i\rangle \equiv \sum_{j\neq i}\rho_{ij} \equiv \sum_{j\neq i}\int d\boldsymbol{r}\rho_i(\boldsymbol{r})\rho_j(\boldsymbol{r}) = \sum (4\pi L)^{-3/2}\exp\left[-\left(\boldsymbol{R}_i - \boldsymbol{R}_j\right)^2/4L\right], \tag{1.10}$$

with the density distribution,

$$\rho_i(\boldsymbol{r}) \equiv \int \frac{d\boldsymbol{p}}{(2\pi\hbar)^3} f_i(\boldsymbol{r},\boldsymbol{p}) = (2\pi L)^{-3/2}\exp\left[-\frac{(\boldsymbol{r}-\boldsymbol{R}_i)^2}{2L}\right]. \tag{1.11}$$

In Eq. (1.9), C_A = -219.4 MeV, C_B = 165.3 MeV, and τ = 4/3 are taken as parameters. The parameter C_i represents the number of charge in *i*th nucleon, one for proton and zero for neutron. The elementary charge is given by *e*.

In the collision term, the channels included are as follows (B is for baryon and N for nucleon):

1. $B_i + B_j \rightarrow B_i + B_j$,
2. $N + N \rightarrow N + \Delta$,
3. $N + \Delta \rightarrow N + N$,
4. $N + N \rightarrow N + N^*$,
5. $N + N^* \rightarrow N + N$,
6. $N + \pi \rightarrow \Delta$,
7. $N + \pi \rightarrow N^*$,
8. $\Delta + \pi \rightarrow N^*$.

Apart from the collision term, the decay of the baryonic resonances during propagation is as follows:

9. $\Delta \rightarrow N + \pi$,
10. $N^* \rightarrow N + \pi$,
11. $N^* \rightarrow \Delta + \pi$.

Once the equilibrium is attained, evaporation model performs the calculation of the de-excitation of the residual nucleus.

1.7.3 Liege Intranuclear Cascade (INCL) Model

Liege intranuclear cascade model[35] (INCL) has been developed by University of Liege, Belgium and CEA, France. The model has been used to simulate the dynamic stage of nuclear reactions for the cases of nucleon, pion or cluster incidence. Transport codes, PHITS, Geant4 employ INCL model to simulate cascade stage of nuclear reactions. The incident energy limit of INCL ~150 MeV to GeV range energy. INCL follows time-like approach. A stopping time is used to end the cascade process. The particle follows the straight-line trajectory.

INCL4.6[42] is a default model in PHITS for deuteron- and alpha-induced nuclear reactions. In the present study, we are focusing on cluster-induced reactions. The features related to cascade-induced and cluster production reactions of INCL4.6 are shortly represented here.

Cluster emission at INCL

A coalescence model is employed to allow the cluster emission process in this model. Different steps of cluster-emission are as follows,

i) An outgoing nucleon arriving at the surface of the target nucleus is selected to be emitted as a cluster with surrounding nucleons, if it has energy more than the threshold energy, otherwise, it will be reflected.

ii) The size of the cluster is formed by searching nucleons close in the phase space.

iii) The virtual cluster is selected phenomenologically.

iv) The selected cluster

   a. should have the sufficient energy to escape, $T_{cl} = \sum(T_i - V_i) - B_{cl} > 0$, T_i kinetic energy of nucleons, V_i depth of the potential.

   b. must successful to penetrate the Coulomb barrier.

   c. will emit if the angle of direction of the cluster satisfy, $\cos\theta > 0$, where θ is the angle between the direction of the cluster and the radial outward direction passing through centre of the cluster.

If the above conditions are fulfilled, the cluster will be emitted with kinetic energy T_{cl} in the direction of the sum of the constituent momentum of the cluster nucleons. If any of the conditions disagrees, nucleon may be emitted alone.

Handling incident cluster at INCL:

Initial nucleon distribution inside the cluster is done according to Gaussian distribution[12]. Momentum distribution follows the same Gaussian manner. The incident cluster is

considered as collections of the independent nucleons. At the beginning, the cluster centre of mass is positioned in such a way so that at least one nucleon touches the Coulomb radius i.e. the incident cluster radius is taken as same as Coulomb radius.

1.7.4 An INC Model for Deuteron- and Alpha-Induced Reactions

To understand the effects of complex projectile like deuteron and alpha on the cascade stage, a study was carried out by Mathews et al.[43] based on VEGAS model[34]. The density distribution in the target nucleus is considered as a step function distribution to approximate Fermi distribution by eight concentric regions having a constant density. The particle trajectory is classical and the collision pairs are only p-d, n-d, p-α, d-d, d- α, and α-α. Neutrons and protons are taken as similar while considering the cross section. The cascade nucleons are allowed to refracted or reflected at the potential surface. Probability of cluster breakup is,

$$P = \sigma_R(E)/\sigma_T(E), \tag{1.12}$$

where σ_R is the reaction cross section, and σ_T is the total cross section. A step function is employed to calculate the cluster breakup probability. A random number is used to select the collision partner for the incoming cluster considering the existence of cluster inside the target. While the cluster energy goes below the cut-off energy, the cascade stops. The cut-off energy for neutron is considered as Fermi energy (E_f) + 2 × average binding energy (E_B) and for proton the larger one among E_f +2 × E_B or E_f + E_B + Coulomb barrier. The cluster density distribution is same as nucleon density distribution in the target. The number of clusters present in the target is considered to fit the experimental data. The Fermi momentum of the n-nucleon cluster is taken as n-times the Fermi momentum of the individual nucleon. And the potential energy of the cluster is taken as -(E_f + E_B), with E_f is the Fermi energy, and E_B is the nucleon binding energy of the cluster. The model

was examined at the incident energy up to 380 MeV only. The predictive power of this model is low.

1.7.5 INC Model Utilized at Present Research

The research group at Kyushu University has developed an INC model originally. The model follows a time-dependent approach. The details of the model will be given in chapter 2.

The model already successfully applied for proton-induced and proton production reactions for the incident energy ~200 MeV or higher. Later on, to have a wider application of INC, the model was successfully extended at low incident energy for (p, p'x) reaction at about 50 MeV. The model is already successful in reproducing cluster production nuclear reactions. The model also incorporated in widely used particle transport codes, PHITS named as INC-ELF[1]. In this research, we will use the model name as 'INC model'.

1.8 Problems of Nuclear Models

BERTINI, JAM, JQMD, INCL are widely used models to simulate the cascade stage of nuclear reactions as described in earlier sections. It is a common expectation that a model will have wider applications considering incident energy range as well as incoming and outgoing species. Though BERTINI, JAM, JQMD are known as successful, the models cannot reproduce the double differential cross section of light fragment emission during cascade stage. Bertini and JAM cannot work with cluster-induced reactions. INCL4.6 can handle the formation of the cluster using coalescence model. On the other hand, the model shows poor predictions in case of cluster emission, especially in case of inelastic scattering. In addition, JQMD is highly recommended for nucleus-induced reactions but

the success in reproducing cluster-induced cluster production reactions is still poor. Fig. 1.9 represents the comparison of INCL and JQMD (red and green line histogram, respectively) calculation results with the experiment data (solid circles) for the ^{58}Ni (α, α'x) nuclear reactions at 140 MeV incident energy. The experimental data are taken from EXFOR[44].The calculations were executed using PHITS.

The prediction abilities of INCL and JQMD models are not always satisfactory enough. As mentioned earlier, light-cluster induced nuclear reactions need to be handled well for heavy-ion radiotherapy, space technology, ADS technology. The comparison of calculation results by the two models incorporated in PHITS coupled with evaporation model shown in Fig. 1.9 demonstrates the need to improve INC model for cluster-induced reactions.

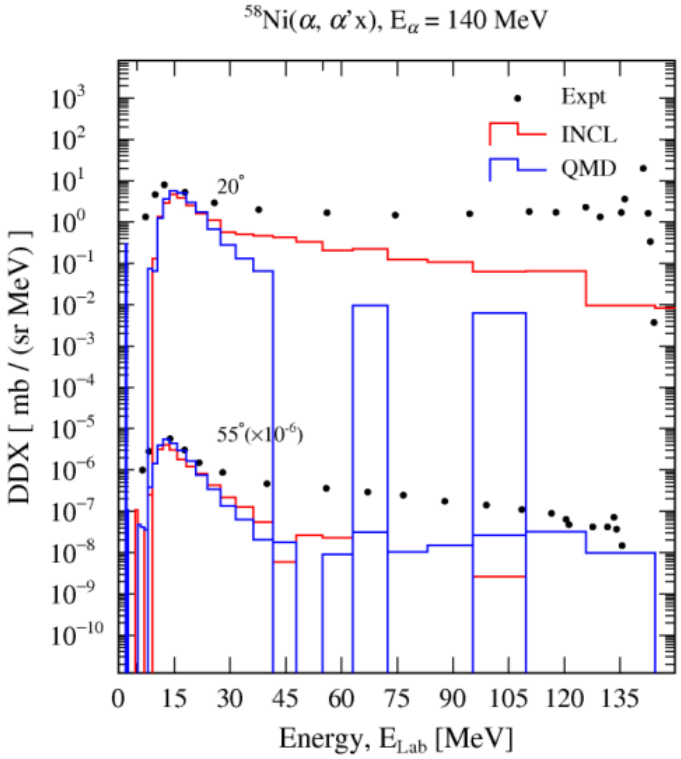

Fig. 1.9 Comparison of model result for the alpha induced reaction on ^{58}Ni at bombarding energy 140 MeV with the experimental DDX spectra.

1.9 Purpose of this Research

INC is demanded to reliable estimation for cluster-induced reactions because the late effect of low-dose exposure is a serious issue for childhood cancer treatment in heavy-ion therapy. Fragments produced in heavy-ion nuclear reactions are emitted at large angles with high-energies, and therefore healthy tissues far from the irradiation field suffer amounts of doses. It is known that the INC model and other non-perturbative reaction models including the QMD model give passably good accounts for nucleon productions, but large discrepancies for cluster production reactions in spite of great efforts. It has been therefore suggested that unpreceded physics idea is needed to improve the INC model for cluster-induced cluster production reactions. The purpose of this work is to introduce into the INC framework an idea of virtual excited state, whose wavefunction is expressed as a superposition of different cluster units. Model calculations are executed to verify the proposed model by comparison with experimental observations on deuteron- and α-induced reactions at incident energies of 22.3 - 99.6 MeV and 140 -160 MeV respectively.

1.10 Structure of the Present Thesis

This paper consists of five chapters.

Chapter 2 details of the INC code. A short description of the evaporation code is provided as well. DDX calculation procedure is very briefly described.

Chapter 3 focuses deuteron-induced nuclear reactions. The descriptions of the extension of the model for deuteron-induced reactions are discussed. The validity of the proposed model is verified comparing with experimental energy spectra for (*d,d'x*), (*d,px*) and (*d,nx*) reactions on several targets from ^{27}Al to ^{181}Ta.

In chapter 4, the alpha-induced nuclear reactions for all channels are represented. The expended model description is represented first. Later on, the proposed model is verified comparing with experimental observations for ^{27}Al and ^{58}Ni targets.

Chapter 5 draws the conclusion and discusses the future research plan.

2 Theoretical Model

2.1 INC

In this section, description of the INC model utilized in the present research is presented. The time-dependent approach is chosen since the approach allows to use the realistic nuclear density distribution.

2.1.1 Ground State of the Target Nucleus

In the INC model, it is necessary to locate the position and momentum of the nucleons in the target nucleus before entering the cascade calculation. In this study, we assume that the shape of the target nucleus is spherical. The positions of nucleons in the target nucleus are sampled according to Woods-Saxon type density distribution[45]. The Wood-Saxon density distribution is written as

$$\rho_{ws} = \begin{cases} \dfrac{\rho_0}{1+\exp\left(\dfrac{r-R_0}{a}\right)} & (r \le R_{max}) \\ 0 & (R_{max} \le r) \end{cases}, \tag{2.1}$$

where R_0 is the nucleus radius, and a is a parameter represents the diffuseness of the nuclear surface. R_{max} is the cut-off radius and is given by $R_{max} = R_0 + 5a$. Using the Negele's[45] expression,

$$R_0 = \left(0.978 + 0.0206A^{1/3}\right)A^{1/3} \quad \text{[fm]}, \tag{2.2}$$
$$a = 0.54 \quad \text{[fm]},$$

where A is the mass of the target nucleus. The momentum of each nucleon is generated according to the Fermi-Dirac distribution. The Fermi momentum, p_F, with the corresponding Fermi energy, T_F, is

$$p_F = \sqrt{T_F^2 + 2mT_F,} \tag{2.3}$$

$$T_F = V_0 - E_{bind}/Nucleaon, \tag{2.4}$$

where, m is the rest mass of the nucleon and V_0 is the depth of nuclear potential. The potential depth is assumed to be, $V_0 = 45\ MeV$. E_{bind} is the binding energy, using Bethe-Weizsacker's mass formula,

$$E_{bind} = -15.56A + 17.23A^{2/3} + 46.57\frac{(N-Z)^2}{2A} + \frac{3}{5}\frac{Z^2e^2}{1.24A^{1/3}}. \tag{2.5}$$

Fig. 2.1 shows the schematic diagram of the target nuclear potential assumed in this study.

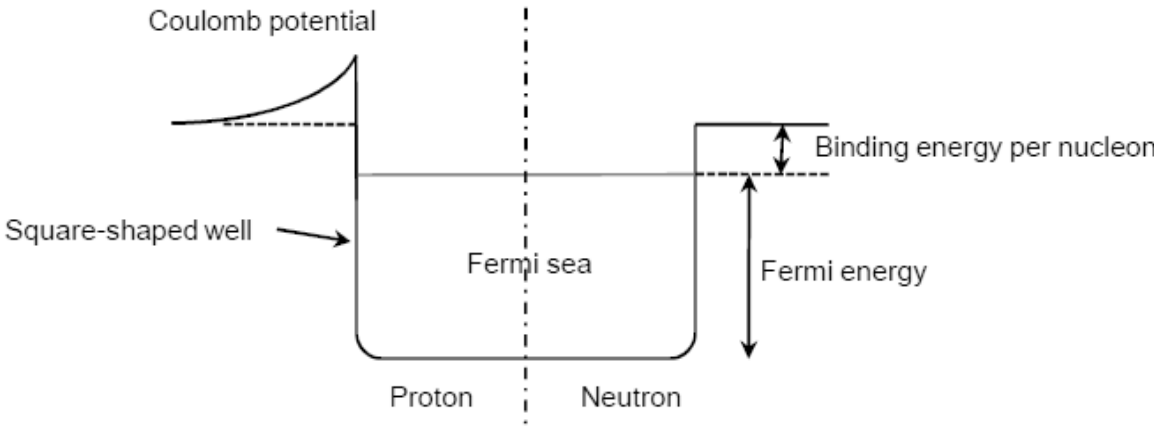

Fig. 2.1 Schematic diagram of nuclear potential.

2.1.2 Kinematics

It is assumed that incident particles move in the nucleus by obtaining potential energy when entering the nucleus. The depth of the potential is taken as, V_0 = 45 MeV. A nucleon that enters the nucleus or is allowed to move, by a two-body collision according

to free relativistic kinematics, follows Newtonian equation of motion. That is, the time evolution of nucleons obey the equation of motion as

$$\frac{\mathrm{d}\boldsymbol{r}_i}{\mathrm{dt}} = \frac{\boldsymbol{p}_i}{\sqrt{\boldsymbol{p}_i^2 + m_i^2}}, \tag{2.6}$$

where m_i is the mass of the *i*-th nucleon.

It is assumed that only nucleons having kinetic energy more than potential barrier are in motion inside the nucleus, and the rest of the nucleons are stationary. The nucleons are presumed to move in straight line. The particles can exit nucleus only if it has energy greater than given threshold energy. For the case of neutron the threshold energy is considered as same as V_0 and for the proton or charged particle, the Coulomb barrier needs to be considered as well. The Coulomb barrier,V_{coul}, is defined by

$$V_{coul} = \frac{e^2}{4\pi\epsilon_0}\frac{Z_t Z_p}{R_0}, \tag{2.7}$$

where Z_t is the proton number of the target nucleus, Z_p is the proton number of the projectile. The particle loses energy for nuclear potential of $V_0 = 45$ MeV per nucleon when it releases the nucleus.

2.1.3 Collision

When the incident particle passes through the nucleus, elastic scattering or inelastic scattering may happen with the target nucleons. The scattered nucleon may go out of the nucleus, or it can collide again with other nucleons.

During the time evolution, it is assumed that two particle can undergo collision with each other if their relative distance fulfill the condition,

$$\tilde{r_{ij}} < \sqrt{\frac{\sigma_{NN}}{\pi}}, \tag{2.8}$$

here, r_{ij} is the distance between *i*th and *j*th nucleon, σ_{NN} is the nucleon-nucleon collision (scattering) cross section, and is expressed generally by the sum of the elastic scattering cross section and the inelastic scattering cross section as $\sigma_{NN} = \sigma_{el} + \sigma_{inel}$. It is to be mentioned that in this thesis we are considering only elastic scattering. The inter-nuclear distance $\tilde{r_{ij}}$ is assumed to be Lorentz invariant,

$$\widetilde{r_{ij}^2} = r_{ij}^2 + \gamma_{ij}^2 \left(r_{ij} \cdot \beta_{ij}\right)^2, \tag{2.9}$$

$$\gamma \equiv \frac{1}{\sqrt{1 - \beta_{ij}^2}}, \tag{2.10}$$

$$\beta_{ij} \equiv \frac{p_i + p_j}{E_i + E_j}, \tag{2.11}$$

with $E_\alpha = \sqrt{p_\alpha^2 + m_\alpha^2}$ and $\alpha = i, j$.

2.1.3.1 Collision Cross Section

Nucleon-nucleon collision cross section is an important input in a nuclear model. However, the perfect description of collision cross section has not reached due to theoretical uncertainties. In the present study, we have used the nucleon-nucleon cross section by Cugnon parameterizations[46].

For proton-proton (pp) system, the elastic cross section is almost equal to the total cross section for $p_{lab} \leq 1\,\mathrm{GeV/c}$. Above this value, the data is scarce and poorer in quality than total cross section. For pp system, the parameterization is used for elastic cross sections as

$$\sigma_{\text{el.pp}}^{\text{Cugnon}} = \begin{cases} 23.5 + 1000(p_{\text{lab}} - 0.7)^4, & p_{lab} < 0.8\,\text{GeV/c}\,, \\ \dfrac{1250}{p_{\text{lab}} + 50} - 4(p_{\text{lab}} - 1.3)^2, & 0.8\,\text{GeV/c} \le p_{lab} < 2.0\,\text{GeV/c}, \\ \dfrac{77}{p_{\text{lab}} + 1.5}, & 2.0\,\text{GeV/c} \le p_{lab}. \end{cases} \quad (2.12)$$

The data for np system is more scarce. For np system, the parameterization is used as

$$\sigma_{\text{el.pn}}^{\text{Cugnon}} = \begin{cases} 33.0 + 196|p_{\text{lab}} - 0.95|^{2.5}, & p_{\text{lab}} < 0.8\ \text{GeV/c}, \\ \dfrac{31}{\sqrt{p_{\text{lab}}}}, & 0.8\text{GeV/c} \le p_{\text{lab}} < 2.0\ GeV/c, \\ \dfrac{77}{p_{\text{lab}} + 1.5}, & 2.0\ \text{GeV} \le p_{\text{lab}}. \end{cases} \quad (2.13)$$

In above two equations, p_{lab} is the momentum of the nucleon in the laboratory system. When p_{lab} is more than $1\,\text{GeV/c}$, inelastic scattering occurs, and Δ resonance and π mesons generate. Cross sections are expressed in mb. However, the inelastic scattering is not considered, as the main reaction mechanism of a nucleon-nucleon collision in the energy domain used for this research is elastic scattering.

2.1.3.2 Angular Distribution

The two colliding nucleons are scattered by the azimuth angle ϕ and the (cosine of) polar angle μ in the center of mass system. The distribution is isotropic for ϕ, but for μ, it has a characteristic distribution with forward peaked. The distribution of μ is obtained according to experimental differential scattering cross section, $\text{d}\sigma/\text{d}\Omega$. In the INC model, Cugnon et al.[46] proposed parameterizations are chosen. According to Cugnon, differential cross section, for pn system, $d\sigma_{pn}/d\Omega$ and for pp system, $d\sigma_{pp}/d\Omega$ are expressed as

$$\frac{d\sigma_{pn}}{d\Omega} = \sigma_{el,pn} N(e^{B_{pn}t} + ae^{B_{pn}u}) \sim e^{B_{pn}t} + ae^{B_{pn}u}, \quad (2.14)$$

$$\frac{d^2\sigma_{pp}}{d\Omega} = \sigma_{el,pp} e^{B_{pp}t} \sim e^{B_{pp}t}, \quad (2.15)$$

Here, σ_{el} represents the elastic scattering cross section, and N is a normalization factor. t and u are Lorentz-invariant. Mandelstam variables, t and u, are given by the following equation with respect to the (cosine of) scattering angle μ, as

$$\mathrm{t} = -2|\vec{p}|^2(\mu + 1), \quad (2.16)$$

$$\mathrm{u} = -2|\vec{p}|^2(\mu - 1). \quad (2.17)$$

The parameters a、B_{pn}、B_{pp} are given by the following equations:

$$\mathrm{a} = \begin{cases} 1 & p_{\mathrm{lab}} \le 0.8\ \mathrm{GeV/c}, \\ \left(\frac{0.8}{p_{\mathrm{lab}}}\right)^2, & 0.8\ \mathrm{GeV} < p_{\mathrm{lab}}, \end{cases} \quad (2.18)$$

$$B_{\mathrm{pn}} = \begin{cases} 0, & p_{lab} \le 0.225\ \mathrm{GeV/c}, \\ 6.2\frac{p_{\mathrm{lab}} - 0.225}{0.375}, & 0.225\ \mathrm{GeV/c} < p_{lab} \le 0.6\ \mathrm{GeV/c}, \\ -1.63p_{\mathrm{lab}} + 7.16, & 0.6\ \mathrm{GeV/c} < p_{lab} \le 1.6\ \mathrm{GeV/c}, \\ \frac{5.5 - {p_{\mathrm{lab}}}^8}{7.7 + {p_{\mathrm{lab}}}^8}, & 1.6\ \mathrm{GeV/c} < p_{lab} \le 2.0\ \mathrm{GeV/c}, \\ 5.34 + 0.67(p_{\mathrm{lab}} - 2), & 2.0\ \mathrm{GeV/c} < p_{lab}, \end{cases} \quad (2.19)$$

$$B_{\mathrm{pp}} = \begin{cases} \frac{5.5 - {p_{\mathrm{lab}}}^8}{7.7 + {p_{\mathrm{lab}}}^8}, & p_{lab} \le 2.0\ \mathrm{GeV/c}, \\ 5.34 + 0.67(p_{\mathrm{lab}} - 2), & 2.0\ \mathrm{GeV/c} < p_{lab}, \end{cases} \quad (2.20)$$

The sampling of (cosine of) scattering angle, μ is performed using direct method.

2.1.3.3 Momentum after Collision

The momentum of the particle after collision in the cm system, p'_{cm}, is given by the following equations:

$$p'_{cm,x} = p'_{cm}(s\cos\phi - \sin v \sin\varphi \sin\phi),$$
$$p'_{cm,y} = p'_{cm}(s\sin\phi - \sin v \sin\varphi \cos\phi), \quad (2.21)$$
$$p'_{cm,z} = p'_{cm}(\cos v\cos\theta - \sin v \sin\theta\cos\varphi),$$

here $s = \cos\theta \sin\upsilon \cos\varphi + \sin\theta \cos\upsilon$. However, ϕ and θ represent the azimuth and polar angle, respectively, before the collision in the cm system, and can be represented as

$$\phi = \arctan\left(\frac{p_{cm,z}}{\sqrt{p_{cm,x}^2 + p_{cm,y}^2}}\right),$$
$$\theta = \arctan\left(1 - \frac{p_{cm,z}}{\sqrt{p_{cm,x}^2 + p_{cm,y}^2 + p_{cm,z}^2}}\right), \quad (2.22)$$

φ and υ represent the azimuth angle and polar angle, respectively, after collision in the cm system.

The following expression is the relation between the momentum of the i-th particle in the cm system, $p_{cm,}$ and that of the i-th nucleon in the laboratory system, p_i.

$$\boldsymbol{p}_{cm} = \boldsymbol{p}_i + \Im_i \boldsymbol{V}, \quad (2.23)$$
$$\Im_i = \gamma\left(\frac{\gamma}{\gamma+1}(\boldsymbol{p}_i \cdot \boldsymbol{V}) - E_i\right), \quad (2.24)$$

here V and γ are defined by

$$\boldsymbol{V} \equiv \frac{\boldsymbol{p}_i + \boldsymbol{p}_j}{E_i + E_j}, \quad (2.25)$$
$$\gamma \equiv \frac{1}{\sqrt{1 - \boldsymbol{V}^2}}, \quad (2.26)$$

with $E_i = \sqrt{\boldsymbol{p}_i{}^2 + m_i{}^2}$.

The momenta p'_i and p'_j of the nucleon after collision in the laboratory system are given by the following equations:

$$\begin{aligned} \boldsymbol{p}_i' &= \boldsymbol{p}_{cm}' + \Im' \boldsymbol{V}, \\ \boldsymbol{p}_j' &= -\boldsymbol{p}_{cm}' + \Im' \boldsymbol{V}, \end{aligned} \tag{2.27}$$

$$\Im' = \gamma\left(\frac{\gamma}{\gamma+1}(\boldsymbol{p}_{cm}' \cdot \boldsymbol{V}) - E_{cm}'\right), \tag{2.28}$$

where $E_{cm}' = \sqrt{\boldsymbol{p}_{cm}'^{\,2} + m_i{}^2}$.

2.1.3.4 Pauli Blocking

In the final state of collision, Pauli blocking effect is taken into account. The simple form of Pauli blocking probability is adopted as

$$P_{Pauli} = 1 - \Theta(p_i' - p_F)\Theta\left(p_j' - p_F\right), \tag{2.29}$$

here $\mathrm{p_i'}$ and $\mathrm{p_j'}$ represent the momenta of two nucleons *i* and *j*, respectively, after collision, and Θ is a Heaviside function. Pauli blocking in INC model refers, when the momentum in either two nucleons after the collision becomes smaller than Fermi momentum, p_F, collision does not happen between those nucleons. In other words, Pauli blocking parameter becomes in Eq. (2.29), $P_{Pauli} = 1$.

2.1.4 Coupling with Evaporation Model

The INC model is given a time that stops the cascade processes and provides a way to start the evaporation process. That time is referred as stopping time and is determined by the equation,

$$t_{sw} = 80.0(A/208.0)^{0.16}. \tag{2.30}$$

Before and after the cascade calculation, the conservation laws for mass number, charge, energy, and momentum are given as

$$\mathrm{A_p + A_t = A_{ej} + A_{rem}}, \tag{2.31}$$

$$Z_p + Z_t = Z_{ej} + Z_{rem}, \tag{2.32}$$

$$T_{lab} = K_{ej} + E_{rec} + E^* + S, \tag{2.33}$$

$$p_p = p_{ej} + p_{rem}, \tag{2.34}$$

where subscripts *p* represents incident particle, *t* represents target nucleus, *ej* represents emitted particle, and *rem* represents excited nucleus after completion of cascade. T_{lab} is the incident energy in the laboratory system, K_{ej} is the kinetic energy of the emitted particles, E_{rec} is the recoil energy, and *S* is the separation energy.

During the cascade calculation, information of emitted particles is directly outputted. At the end of the cascade, information of excited nuclei is used as an input value to the next de-excitation process. In this research, we have used GEM code to calculate the further particle emission during the de-excitation of the residual nucleus at the end of cascade phase.

2.2 GEM

GEM code is a simulation program that describes the de-excitation of an excited nucleus. It is based on the Generalized Evaporation Model[38] and Atchison Fission model[47]. At the end of INC calculation, information about residual nucleus is sent to GEM code.

2.2.1 Generalized Evaporation Model

Generalized evaporation model is based on Weisskopf-Ewing's[48] formulation and is proposed by Furihata[49]. For the emission of a particle *j* from a parent nucleus *i* with total kinetic energy in the cm system between ε and $\varepsilon+d\varepsilon$, the decay probability P_j is

$$P_j(\epsilon)d\epsilon = g_j\sigma_{inv}(\epsilon)\frac{\rho_d(E-Q-\epsilon)}{\rho_i(E)}\epsilon d\epsilon, \tag{2.35}$$

where E is the excitation energy of a parent nucleus in MeV; i represents a parent nucleus with mass A_i, charge Z_i, and d is for daughter nucleus with mass A_d and charge Z_d generated after emission of ejectile j with mass A_j and charge Z_j. The reverse reaction cross section is σ_{inv}; ρ_i and ρ_j are the level densities of the parent and daughter nucleus respectively in [MeV^{-1}], and $g_j = (2S_j + 1)\, m_j/\pi^2\hbar^2$ with S_j as spin. The Q-value of the reaction is calculated according to the following equation with excess mass $\mathrm{M(A, Z)}$ as

$$Q = M(A_j,\, Z_j) + M(A_d,\, Z_d) - M(A_i,\, Z_i), \tag{2.36}$$

here the excess mass is calculated by Cameron's formula. The cross section for inverse reaction is express as

$$\sigma_{\mathrm{inv}}(\varepsilon) = \begin{cases} \sigma_g c_n(1 + b/\varepsilon) & \text{for neutrons} \\ \sigma_g c_j(1 + V/\varepsilon) & \text{for charged particles} \end{cases} \equiv \sigma_g \alpha(1 + \beta/\varepsilon), \tag{2.37}$$

where the geometric cross section, $\sigma_g = \pi R_b^2$ [fm^2], and the coulomb barrier is $\mathrm{V} = k_j Z_j Z_d\, e^2/R_c$ [MeV]. The parameter set for c_n, b, c_j, k_j, R_b, R_c are used as described by Dostrovsky et al.[50] and Matuse et al.[51]

The total decay width for the emitted particle can be obtained by integrating Eq. (2.35) with respect to the total kinetic energy ε from Coulomb barrier V up to the max value (E-Q) as

$$\Gamma_j = \frac{g_j \sigma_g \alpha}{\rho_i(E)} \int_V^{E-Q} \epsilon(1 + \beta/\epsilon)\rho_d(E - Q - \epsilon)\, d\epsilon. \tag{2.38}$$

The total level density $\rho(E)$ is expressed as,

$$\rho(E) = \begin{cases} \dfrac{\pi}{12} \dfrac{e^{2\sqrt{a(E-\delta)}}}{a^{1/4}(E-\delta)^{5/4}}, & \text{for E} \geq E_x, \\ \dfrac{\pi}{12} \dfrac{1}{T} e^{(E-E_0)/T}, & \text{for E} < E_x, \end{cases} \tag{2.39}$$

where a is the level density parameter in [MeV^{-1}], and δ is the paring energy of the daughter nucleus in MeV. E_x is determined by Gilbert and Cameron expression, and level density parameter uses the Gilbert-Cameron-Cook-Ignatyuk (GCCI) parameter sets. The pairing energy δ is expressed as sum of separate contribution from neutron and proton, $\delta = \mathrm{P}(Z_d) + P(N_d)$. The nuclear temperature T is expressed as $1/T = \sqrt{a/U_x} - 1.5/U_x$ with $E_0 = E_x - T\left(\log T - 0.25 \log a - 1.25 \log U_x + 2\sqrt{aU_x}\right)$.

Eq. (2.35) gives the probability density of the total kinetic energy ε for an ejectile and a daughter nucleus. Substituting Eq. (2.39) in Eq. (2.35), and normalizing yields

$$P_j(\varepsilon) = \begin{cases} g_j \sigma_g \alpha(\varepsilon + \beta) \dfrac{e^{(E-Q-\varepsilon-E_0)/T}}{T} \dfrac{1}{\Gamma_j} & E - Q - E_x \le \varepsilon \le E - Q \\ g_j \sigma_g \alpha(\varepsilon + \beta) \dfrac{e^{2\sqrt{a(E-Q-\delta-\varepsilon)}}}{a^{1/4}(E-Q-\delta-\varepsilon)^{5/4}} \dfrac{1}{\Gamma_j} & kV \le \varepsilon \le E - Q - E_x \end{cases} . \quad (2.40)$$

In GEM, 66 nuclides in ground state as well as in their excited states are chosen as ejectiles. The ejectiles (shown in table 2.1) are selected according to following criteria, a) isotopes with $\mathrm{Z_j} \le 12$; b) naturally existing isotopes as well as the isotopes near stability line; c) isotopes having half-life longer than 1 ms.

Table 2.1 GEM ejectile

Z	Nuclide						
0	n	-	-	-	-	-	-
1	p	d	t	-	-	-	-
2	^{3}He	^{4}He	^{6}He	^{8}He	-	-	-
3	^{6}Li	^{7}Li	^{8}Li	^{9}Li	-	-	-
4	^{7}Be	^{9}Be	^{10}Be	^{11}Be	^{12}Be	-	-
5	^{8}B	^{10}B	^{11}B	^{12}B	^{13}B	-	-
6	^{10}C	^{11}C	^{12}C	^{13}C	^{14}C	^{15}C	^{16}C
7	^{12}N	^{13}N	^{14}N	^{15}N	^{16}N	^{17}N	-
8	^{14}O	^{15}O	^{16}O	^{17}O	^{18}O	^{19}O	^{20}O
9	^{17}F	^{18}F	^{19}F	^{20}F	^{21}F	-	-
10	^{18}Ne	^{19}Ne	^{20}Ne	^{21}Ne	^{22}Ne	^{23}Ne	^{24}Ne
11	^{21}Na	^{22}Na	^{23}Na	^{24}Na	^{25}Na	-	-
12	^{22}Mg	^{23}Mg	^{24}Mg	^{25}Mg	^{26}Mg	^{27}Mg	^{28}Mg

For heavy excited nucleus, GEM code employ Atchison fission model[47] since the fission process is important for the residual nucleus. The model assumes that fission competes with neutrons emission at all stage of nuclear de-excitation with probability

$$P_f \approx \frac{\Gamma_f}{\Gamma_\mathrm{f} + \Gamma_\mathrm{n}} = \frac{1}{1 + \Gamma_f/\Gamma_n}, \tag{2.41}$$

where Γ_n is the total width of neutron emission and Γ_f is the total fission width. Fission process is assumed to occur only for the nucleus having mass number, $Z \geq 70$. Whether the fission will occur or not, will be selected randomly according to P_f.

2.3 Double Differential Cross Section (DDX) Calculation

The double differential cross section of emitted particles is calculated as follows:

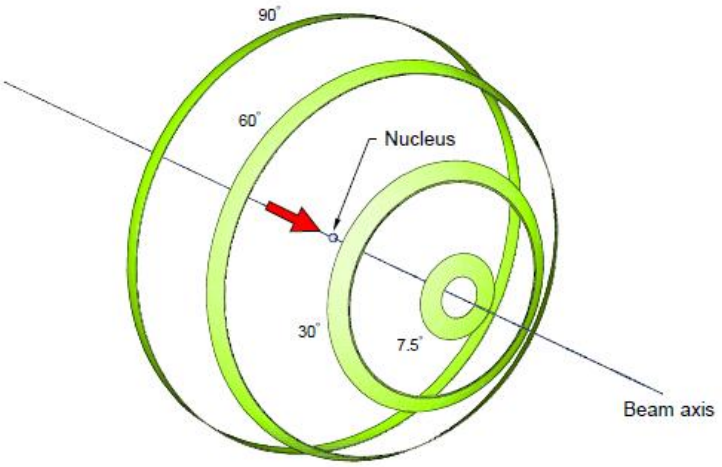

Fig. 2.2 Schematic diagram of emission angle bins.[52]

If the emission energy is E and emission angle is θ, double differential cross section of inclusive nuclear reactions are calculated as

$$\frac{d^2\sigma}{d\Omega dE} = \frac{\sigma_{inel}}{2\pi sin\theta \Delta\theta \Delta E}\frac{N(\theta;\Delta\theta,E;\Delta E)}{N_{inel}} = \frac{\sigma_{inel}}{2\pi \Delta(cos\theta)\theta \Delta E}\frac{N(\theta;\Delta\theta,E;\Delta E)}{N_{inel}}, \quad (2.42)$$

here $N(\theta;\Delta\theta,E;\Delta E)$ represents the number of particle emitted with energy E, bin width ΔE, emission angle θ and bin width $\Delta\theta$. In this present study, $\Delta\theta$ is 5° or 3°. Fig. 2.2 shows a schematic diagram of emission angle bin. And σ_{inel} is

$$\sigma_{inel} \equiv \sigma_{geo}, \quad (2.43)$$

here σ_{geo} represents the geometrical cross section as

$$\sigma_{geo} \equiv \int_0^{\infty(\approx b_{max})} 2\pi b db P_{coll}(b), \quad (2.44)$$

where b is the impact parameter, $P_{coll}(b)$ represents probability of incident particle collide with target nuclei at a given impact parameter b. $P_{coll}(b)$ can be defined as

$$P_{coll}(b) = \frac{n_{coll}(b)}{n_{tot}(b)}, \tag{2.45}$$

where $n_{coll}(b)$ represent number of collision and $n_{tot}(b)$ represents total number of incident particles within the specified impact parameter. Therefore, $\sigma_{geo}$is

$$\sigma_{geo} = \pi b_{max}^2 \frac{N_{inel}}{N_{tot}}. \tag{2.46}$$

Using Eq. (2.42), Eq. (2.43) and Eq. (2.46), the double differential cross section can be expressed as

$$\frac{d^2\sigma}{d\Omega dE} = \frac{b_{max}^2}{2\sin\theta\Delta\theta\Delta E}\frac{N(\theta;\Delta\theta,E;\Delta E)}{N_{tot}}. \tag{2.47}$$

2.4 Probability of Deflection Angle

The INC model has incorporated the concept of trajectory deflection. Due to the impacts of target nuclear potential, incoming and outgoing particle trajectory get deflects. This is known as trajectory deflection.

Elastic scattering angular distribution is used to comprehensively describe the trajectory deflection of the particles. Therefore, the interference structures are not important. The probability of angular distributions of elastic scattering[53] disregarding Coulomb scattering is taken as

$$\mathrm{P_{def}}(\epsilon,\theta,A) = \exp[-0.001(1.3\epsilon + 6\ln A - 5)\theta], \tag{2.48}$$

where ϵ is the incident energy, A is the mass number of the target nucleus.

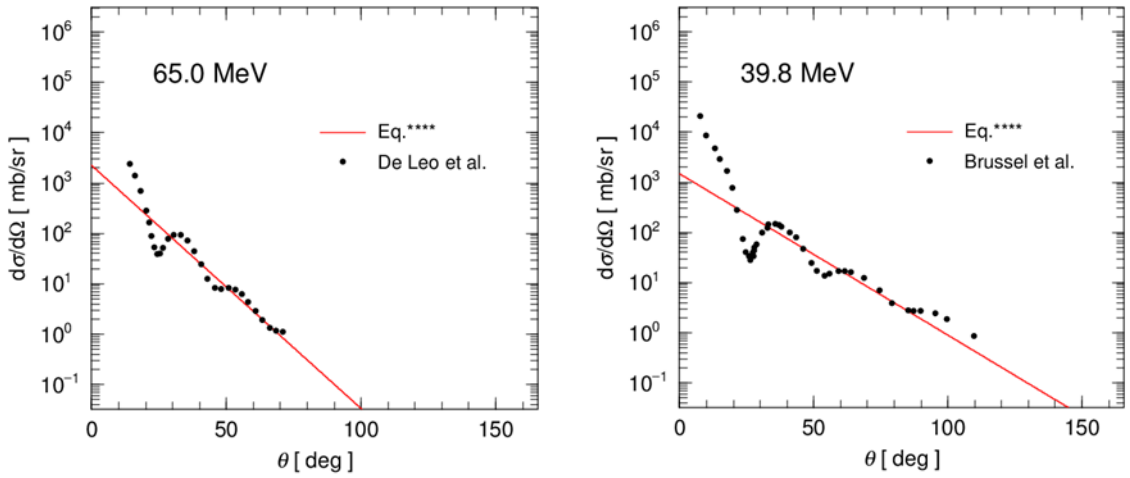

Fig. 2.3 Comparison of experimental data and calculation of Eq. (2.48) for the proton elastic scattering on ^{56}Fe at 65.0 MeV (left image) and 39.8 MeV (right image).[53]

Fig. 2.3 shows the comparison of the Eq. (2.48) and the experimental proton elastic scattering of ^{56}Fe at 39.8 MeV (right image) and 65.0 MeV (left image). Magnitudes of the calculated values are scaled to level the experimental values. The underestimation observed at forward angle is mainly due to Coulomb scattering that was ignored. However, the overall trend is reproduced well.

3 Deuteron-Induced Nuclear Reactions

3.1 Introduction

Deuteron-induced nuclear reactions are among of high interest for various applications, for instances, spallation neutron source, production of radioisotope for medical use, material science research etc. In spallation reactions, 13 neutrons are emitted per event whereas only 2.5 neutrons emit per fission event[54]. Increasing demand for powerful neutron sources has been gained interest in proton-induced spallation reactions. In such reactions, high-energy secondary particles like deuteron, alpha etc. also emit, later on, the secondary particles initiate nuclear reactions. Deuteron induced accelerator for neutron sources have also been studying simultaneously since neutron production in deuteron-induced reactions is bigger than in proton-induced one.[55,56] To handle the nuclear reactions induced by deuteron as a secondary source, INC models are very important in transport codes. In addition, to handle deuteron-induced reaction as a primary source, INC model can play a great role. Besides, understanding the breakup process in deuteron-induced reactions is also crucial. Various studies have been done to perceive the breakup process in deuteron-induced reactions.[57–59] At our present knowledge, INC model prediction capabilities for deuteron-induced nuclear reactions are not highly satisfactory yet. However, the reaction models used in PHITS, QMD and INCL, are not satisfactory enough for this kind of nuclear reactions. We would like to expand the INC model developed at Kyushu University for deuteron-induced nuclear reactions.

In this chapter, I will explain various aspects of the extended model for deuteron-induced reactions as well as validate the model. The model has been developed based on the nucleon-induced reaction model described in chapter 2. The chapter is organized as follows: at first, different features of deuteron-induced nuclear reactions are described.

The essential improvements of the model are presented later on. Then the comparison between experimental data and extended INC calculation results are shown for different targets at incident energy 22.3 – 99.6 MeV. At the end, comparisons of the experimental results with other existing models are represented.

3.2 The Bound Deuteron

The deuteron is the only two-nucleon bound system; there are no other di-nucleon systems. The ground state of the deuteron is loosely bound (E_B = 2.22461 ± 0.00007 MeV), where neutron and proton move mainly in $^3S_1$ state. The magnetic moment of deuteron, μ_d, is very close to sum of the magnetic moment of neutron and that of a proton, $\mu_{n+}\mu_p$. The difference is $\mu_n + \mu_p - \mu_d = 0.0222\mu_N$. The electric quadrupole moment of deuteron, $Q_D = 2.875 \pm 0.002\text{mb}$, which is small compared to the single-particle estimate. Considering the energy equal to ground state binding energy, $E = E_B$, one-dimension Schrodinger Equation can be written as

$$\frac{d^2u}{dr^2} + k^2u = 0, \qquad \mathbf{r} < b, \tag{3.1}$$

$$\frac{d^2u}{dr^2} - \alpha^2u = 0, \qquad \mathbf{r} > b,$$

where b is the radius of the potential. To make the mathematics simpler square–well potential is used. If we put

$$k^2 = \frac{M_n}{\hbar^2}(U_0 - E_B), \tag{3.2}$$

$$\alpha^2 = \frac{M_n}{\hbar^2}E_B,$$

and using the radial solution $u(r) = rR(r)$, the approximate solution inside and outside the potential can be written as

$$u(r) = A \sin kr, \qquad r < b, \tag{3.3}$$

$$u(r) = Be^{-\alpha(r-b)}. \qquad r > b.$$

Matching the logarithmic derivatives and wave functions at $r=b$ leads to, with $k \cot an\, kb = -\alpha$ and $A \sin kb = B$,

$$k^2A^2 = (k^2 + \alpha^2)B^2. \tag{3.4}$$

The normalization of the wave functions becomes,

$$\frac{A^2}{2k}(2kb - \sin 2kb) + \frac{B^2}{\alpha} = \frac{1}{2\pi}. \tag{3.5}$$

Using above two equations, B can be written as,

$$B \simeq \sqrt{\frac{\alpha}{2\pi}} e^{-\alpha b/2}. \tag{3.6}$$

Knowing the binding energy, α can be calculated as 0.232 fm^{-1} (ref)[60]. The range and the depth of the potential can be chosen. Usually, Schrödinger equation solution provides potential depth 21- 40 MeV.

3.3 Extended Model for Deuteron-Induced Reactions

In the deuteron-induced reaction, a nucleus-nucleus collision occurs, unlike the nucleon-incidence reactions. Therefore, to extend the INC model for deuteron-induced reactions, it is necessary to incorporate new elements. In this section, I will describe the improved model.

3.3.1 Ground State

The incident deuteron is composed of two nucleons, one proton and one neutron. Therefore, projectile ground state is needed to be treated as target nucleus described in chapter 1. The radius of the deuteron is not taken as Eq. (2.2), since it has only two

nucleons. Due to the small binding energy, the distance between nucleons in deuteron is relatively large.

If the diffuseness of the nucleus is a = 0.54 [fm], then the maximum nuclear radius is

$$\mathrm{R_{max}} = \mathrm{R_{inc}} + 5a, \tag{3.7}$$

where the projectile average radius $\mathrm{R_{inc}} = \mathrm{R_d} = 2.15\ [\mathrm{fm}]$, $\mathrm{R_d}$ represents the deuteron radius.

Assuming that the shape of the nucleus is a sphere, the position of the nucleons in the projectile is sampled according to the density Woos-Saxon distribution,

$$\rho_{ws} = \begin{cases} \dfrac{\rho_0}{1 + \exp\left(\dfrac{r - R_{inc}}{a}\right)} & (r \le R_{max}) \\ 0 & (R_{max} \le r) \end{cases}. \tag{3.8}$$

In the present study, the internal momentum of the nucleons in the incident nucleus is sampled according to the uniform Fermi gas (UFG: Uniform Fermi Gas) distribution as follows

$$\rho(p) = N_0 \Theta(p_F - p), \tag{3.9}$$

where $\mathrm{N_0}$ is a normalization parameter and Θ is a Heaviside function. The Fermi momentum $\mathrm{p_F}$ is expressed by the following equation using the corresponding kinetic energy i.e. Fermi Energy T_F as

$$p_F = \sqrt{T_F^2 + 2mT_F}, \tag{3.10}$$

$$T_F = V_0 - \mathrm{E_{bind}/nucleon},$$

Here, m is the rest mass of the nucleon, and V_0 is the depth of the nuclear potential of the incident deuteron. The specific value of the nuclear potential V_0 of the deuteron is not accurately known. Therefore, it is necessary to investigate the optimum parameters. The results of the investigation depend on experimental data (more discussion is given later).

In above equation, E_{bind}/nucleon is the binding energy per nucleon, which is taken as 1.11 MeV for deuteron.

3.3.2 Projectile Breakup

As deuteron consists of two nucleons, it may disintegrate due to nuclear potential while interacting with the target nucleus. The breakup reaction can occur on the surface of the target nucleus. The breakup of the incident deuteron is assumed to occur at the initial-state interaction. Fig. 3.1 shows the schematic diagram of projectile deuteron breakup while interacting with the target nucleus.

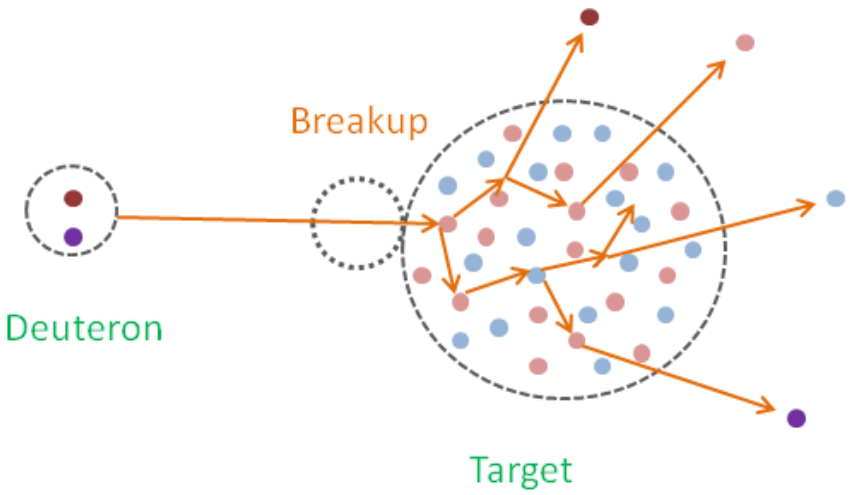

Fig. 3.1 Schematic diagram of deuteron breakup while interacting with target.

It is assumed additionally that the initial deuteron wave function is given by superposing different states. For the deuteron particle, the wave function is

$$\left|d_{init}\right\rangle = c_{d0}\left|d\right\rangle + c_{d1}\left|pn\right\rangle, \tag{3.11}$$

with the normalization of

$$\sum_{i=all} c_i^2 = 1, \tag{3.12}$$

due to orthogonality. The probabilities calculated by these wave functions are used for INC event-by-event calculations. The first term on the right-hand side of Eq. (3.11) indicates that the incident deuteron interacts with the target nucleus without disintegration. The other term represents the projectile deuteron breaks up into proton and neutron while it enters the target nucleus.

The relative yields of particles emitted from the reactions depend on the coefficients *c* in Eq. (3.11). The values of the coefficients were determined to fit the experimental data as listed in Table 3.1.

Table 3.1 Values of coefficients, *c* in Eq. (3.11).

Deuteron	
Cluster Unit	c
d	$\sqrt{70}$
p+n	$\sqrt{30}$

3.3.3 Probability of Trajectory Deflection Angle

In our INC model, the influence of the nuclear potential causes the incident particle and the outgoing particle to be deflected, which is known as trajectory deflection. In previous studies[53,61] for (*p*, *p'x*) calculations (described in chapter 2), the angular distribution of proton elastic scatterings was used to obtain a comprehensive description of the trajectory deflection. In the present study, new parameters for the probability of trajectory

deflection angular distribution of each incoming and outgoing particles are determined. In the previous chapter, the probability $W_{def,p}$ of protons to be deflected at an angle in laboratory system, θ are shown. For the deuteron, the parameters were chosen to reproduce spectral shapes of experimental DDX data as

$$W_{def,d}(\varepsilon,\theta,A)=\exp\left[-0.001(1.3\varepsilon+\ln A+6)\theta\right] \tag{3.13}$$

In addition, for the incoming and outgoing nucleons, the probability of trajectory deflections was considered as Eq. (2.48).

3.4 Search for Optimal Parameters

In this section, we investigate the depth of deuteron potential to reproduce the experimental data. Since the potential depth of deuteron, V_d, are sensitive to the spectral shapes of emitted protons, the deuteron potential was chosen to fit the experimental proton spectra as described below. In addition, the maximum impact parameter was also chosen.

3.4.1 Deuteron Nuclear Potential

The depth of the nuclear potential of the incident nucleus V_0 for deuterons was verified. For the verification, the double differential cross section of the proton spectra was used. In this case, the comparison was carried out without changing any other parameters.

The investigation was done for several cases of deuteron potential values; three cases of deuteron potential, V_d, are given bellow,

Case 1: $V_d = 10$ MeV

Let the depth of the potential is $V_d = 10$ MeV.

Case 2: $V_d = 15$ MeV

Let the depth of the potential is $V_d = 10$ MeV.

Case 3: $V_d = 20$ MeV

Let the depth of the potential is $V_d = 20$ MeV.

Fig. 3.2 shows the calculation result of the DDX proton spectra for the deuteron incidence on ^{27}Al at bombarding energy 80 MeV. The solid circles are experimental data taken from Ref[44]. As can be seen from Fig. 3.2, Case 1 (dotted line) seems to well reproduce the width of the peak of the spectrum at the emission angles but the higher energy region is largely underestimated. Case 3 (dashed line) reproduces well in the high-energy region, but the spectral width seems to widen comparing to experimental spectra. Case 2 (solid line) shows a better fit to the experimental data. Therefore, the depth of the nuclear potential of a deuteron is determined as $V_d = 15$ MeV of Case 2 (solid line). The present result of $V_d = 15$ MeV is shallower than Schrödinger equation solutions that vary between 21-40 MeV depending on assumptions as discussed in the previous section.

The impact parameter of the incident cluster is assigned randomly in the range 0–$b_{\max}$. Here, $b_{\max}$ is considered as the sum of the average radius of the projectile and cut-off radius of the target to fit with the experimental data.

These two parameters were kept fixed for all calculations of deuteron-induced nuclear reactions.

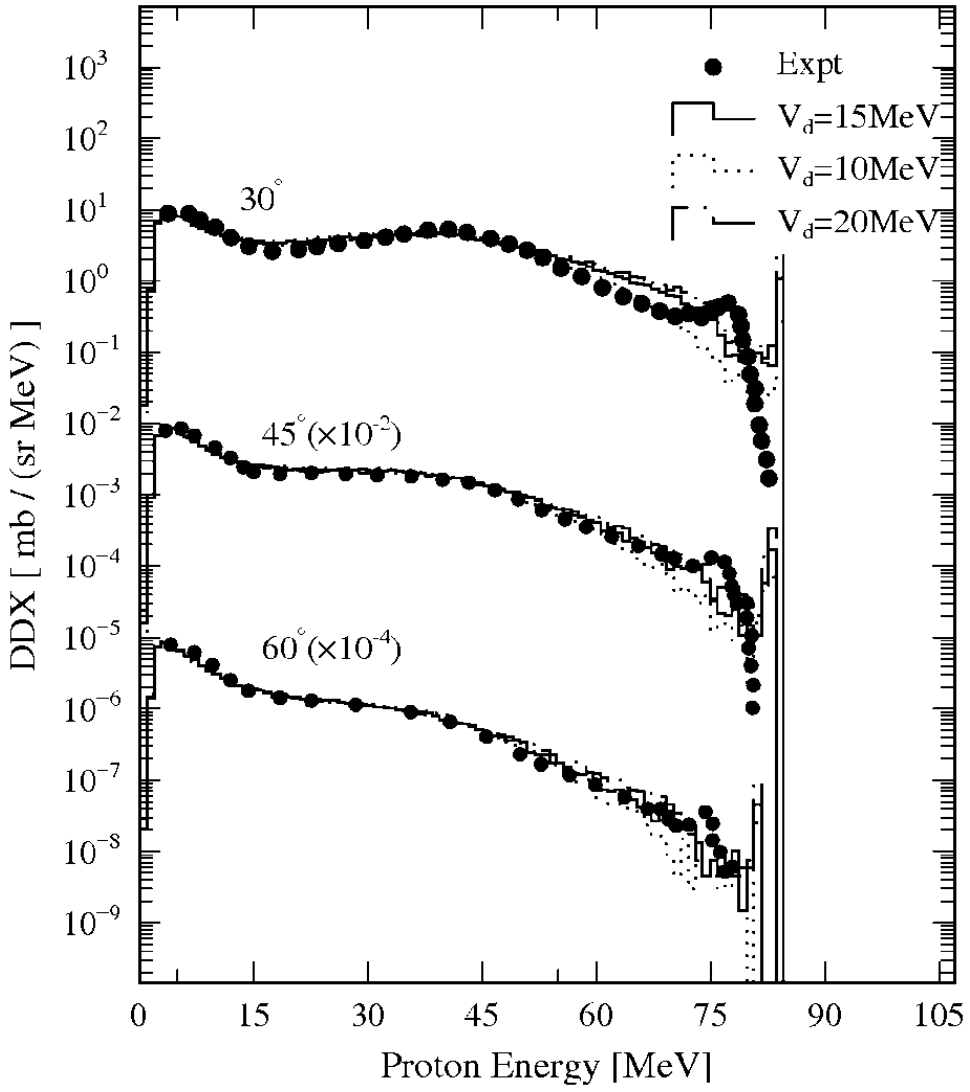

Fig. 3.2 Comparison of the calculation results for proton-production DDXs from 80 MeV deuterons bombarding ^{27}Al at angles of 30°, 45°, and 60° for different values of the deuteron potential depth. The solid circles show the experimental data taken from EXFOR[44]. The dotted, dashed, and line histograms are the INC calculation results for *d* potential depths of 10 MeV, 20 MeV, and 15 MeV, respectively. For visualization, the DDXs have been multiplied by the factors indicated.

3.5 Calculation Results and Discussions

The extended INC model was tested for deuteron-induced reactions comparing with experimental observations for the bombardment of few targets with deuteron. The comparisons of the results are presented in next few sub-sections. Closed circles represent experimental DDXs spectra and solid line histograms are the present INC calculation results respectively. In order to avoid overlap, some factors indicated in figures have been multiplied. The contribution of evaporation model, GEM, has been included in each calculation result followed by cascade stage. In the comparisons, the data of Wu et al.[58] and Ridikas et al.[56], and experimental data from EXFOR[44] are used.

3.5.1 (d, d'x) Reactions

Fig 3.3 allows comparison between experimental DDXs and INC calculation results for ^{27}Al(*d*, *d'x*) reactions at 80 MeV for 7 angular positions from 30° to 150°. Besides the experimental data from EXFOR (solid circles), numerical values from Wu et al.[58] (dots) are also included. The EXFOR database is missing some data around the elastic scattering region. Overall, the proposed model accounts successfully for the gross features of the deuteron spectra over the entire energy range.

The deuteron spectra observed from bombarding ^{58}Ni with deuterons at incident energy 80 MeV are shown in Fig 3.4. The DDX deuteron spectra have been reproduced well by the present INC model. Overestimation at higher energy regions for forward angles is observed. The peak at highest energy region is due to elastic scattering.

Fig. 3.5 shows the INC model prediction for the ^{90}Zr(d, d'x) reactions for seven angles from 20° to 135° for the incident energy 70 MeV. Besides solid circles from EXFOR[44], dots are the data from Wu et al.[58] However, with the increase of angles at higher energy regions poor prediction is observed. Overall, the predictability is quite satisfactory.

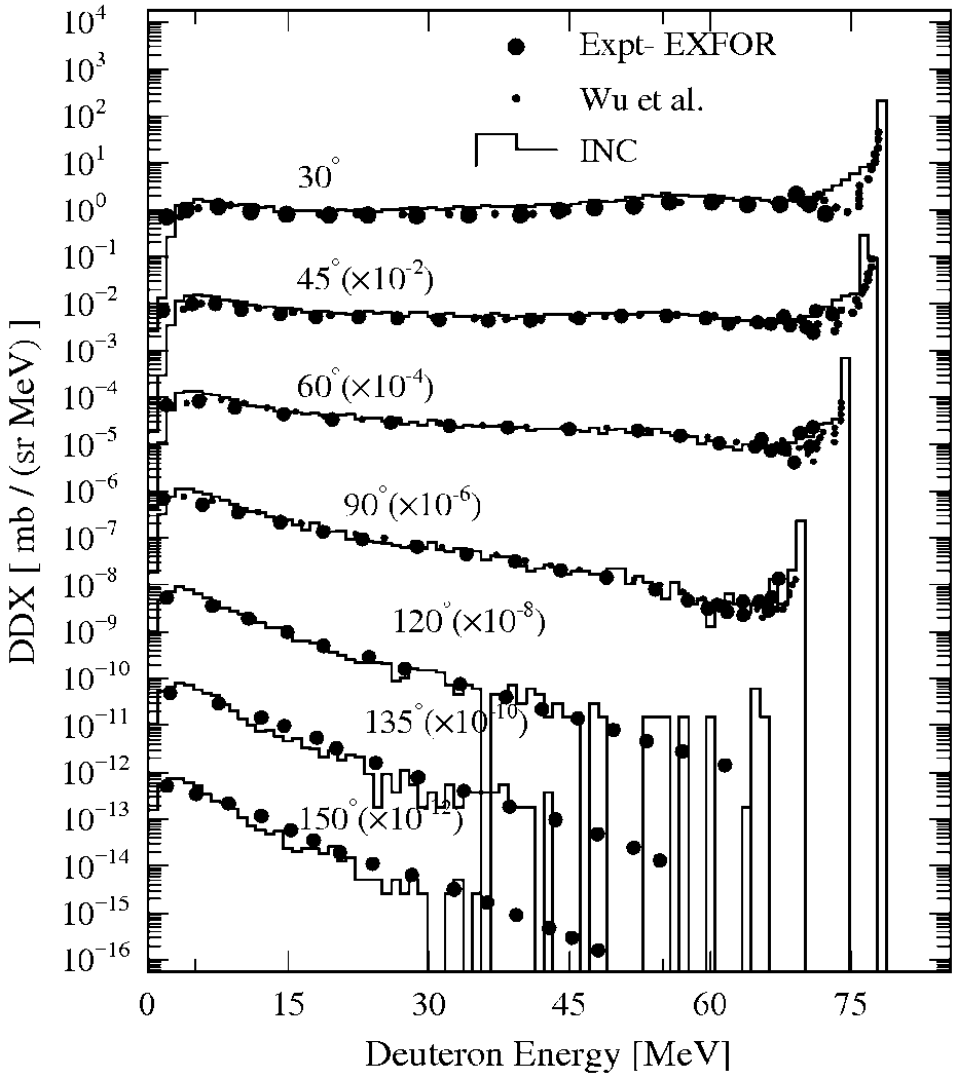

Fig. 3.3 Comparison of the experimental data and INC calculation results for deuteron energy spectra from 80 MeV deuterons bombarding on ^{27}Al at angles from 30° to 150°. The solid circles show the experimental data taken from EXFOR[44] and the dots are the experimental data taken from Wu et al.[58]. The line histograms are the present INC model calculation results. The DDXs are multiplied by factors indicated for visualization.

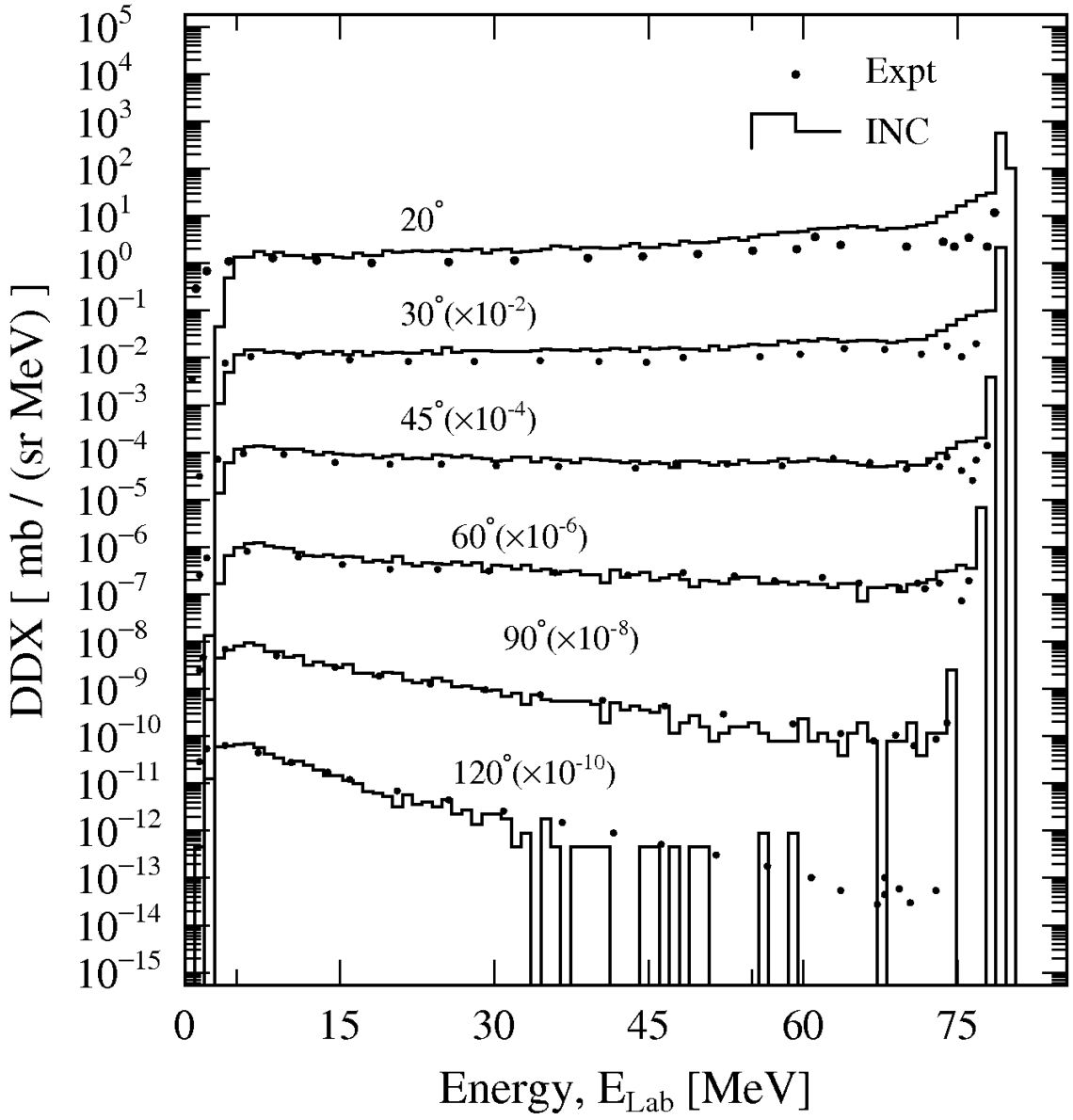

Fig. 3.4 Same as Fig. 3.3, but for ^{58}Ni(d, d'x) reactions at 80 MeV for angular positions 20° – 120°. The solid circles are the experimental data taken from EXFOR[44].

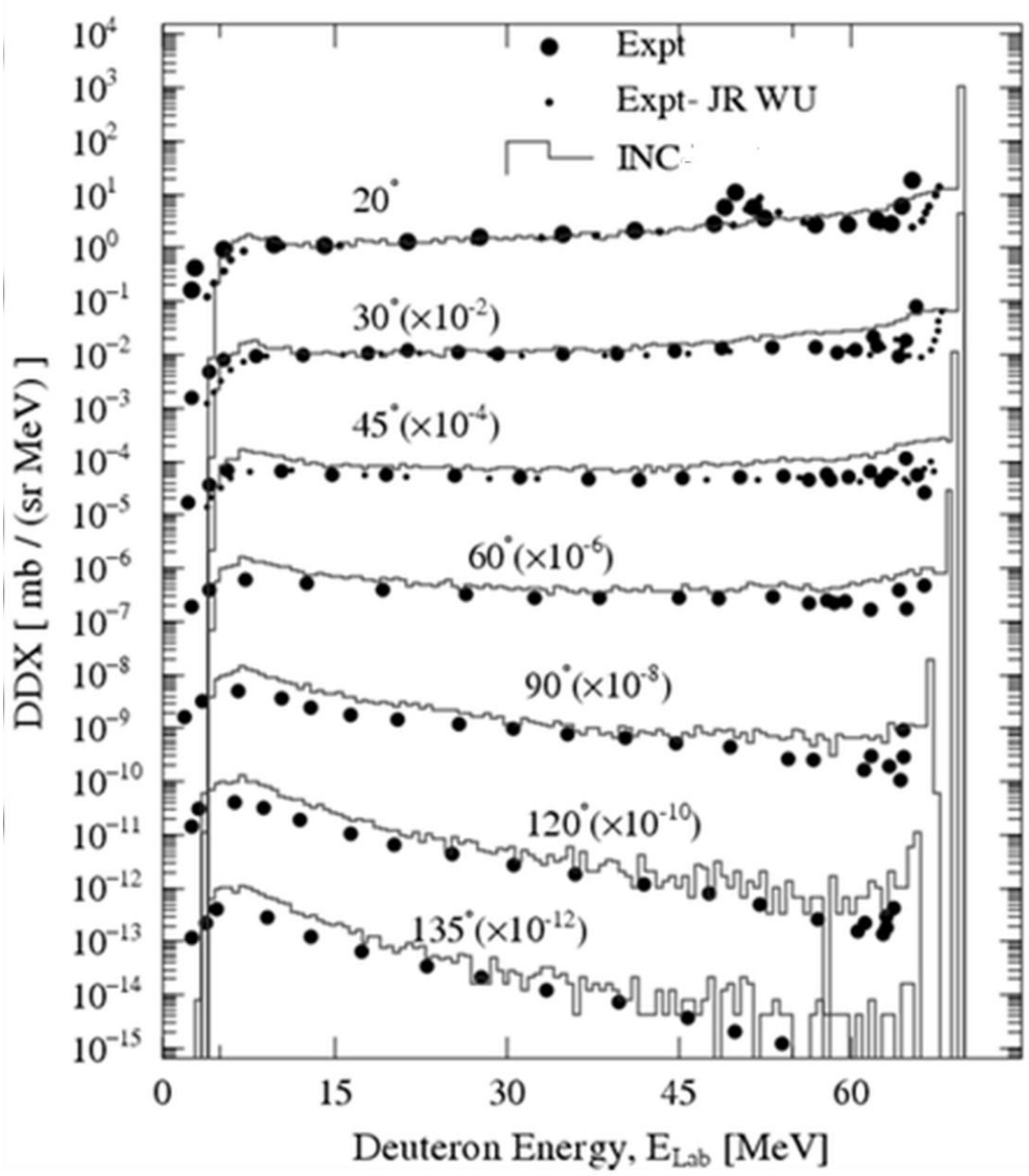

Fig. 3.5 Same as Fig. 3.3, but for ^{90}Zr(d, d'x) reactions at 70 MeV for angular positions 20° to 135°.

3.5.2 Protons Energy Spectra

The present INC model was tested to verify the validity through comparison with proton production double differential spectra for the bombardment of ^{27}Al, ^{58}Ni and ^{181}Ta with deuteron incidence at 80 or 99.6 MeV. The comparison is shown in Figs. 3.6-3.11. The breakup of the deuteron is observed at proton spectra. The broad peak at the forward most angles at almost half of incident energy are due to the breakup of the incident deuteron.[58] Reproduction of these broad peaks is also crucial.

The proton energy spectra from ^{27}Al and ^{58}Ni at bombarding energy 80 MeV are shown in Figs 3.6 and 3.7, respectively. The broad peaks at forward angles are reproduced well by the present INC model.

Figs. 3.8-3.11 show the validity of the present INC model comparing with the experimental observations for seven angular positions for the target the ^{27}Al, ^{58}Ni, ^{93}Nb from 10° to 100°, and for the target ^{181}Ta from 20° to 100° at 99.6 MeV bombarding energy, respectively. The broad peaks at 10° for ^{27}Al, ^{58}Ni and ^{93}Nb are reproduced with slight discrepancies. The overall predictability is quite satisfactory except the discrepancies at highest energy regions. Credit goes to evaporation model GEM[38] for the reproduction of low energy region. The discrepancies at low energy region in proton energy spectra for the target ^{181}Ta are also handled by evaporation model. The tendency to underestimate the observed spectra at angles 90° or more is a general trend for INC model.

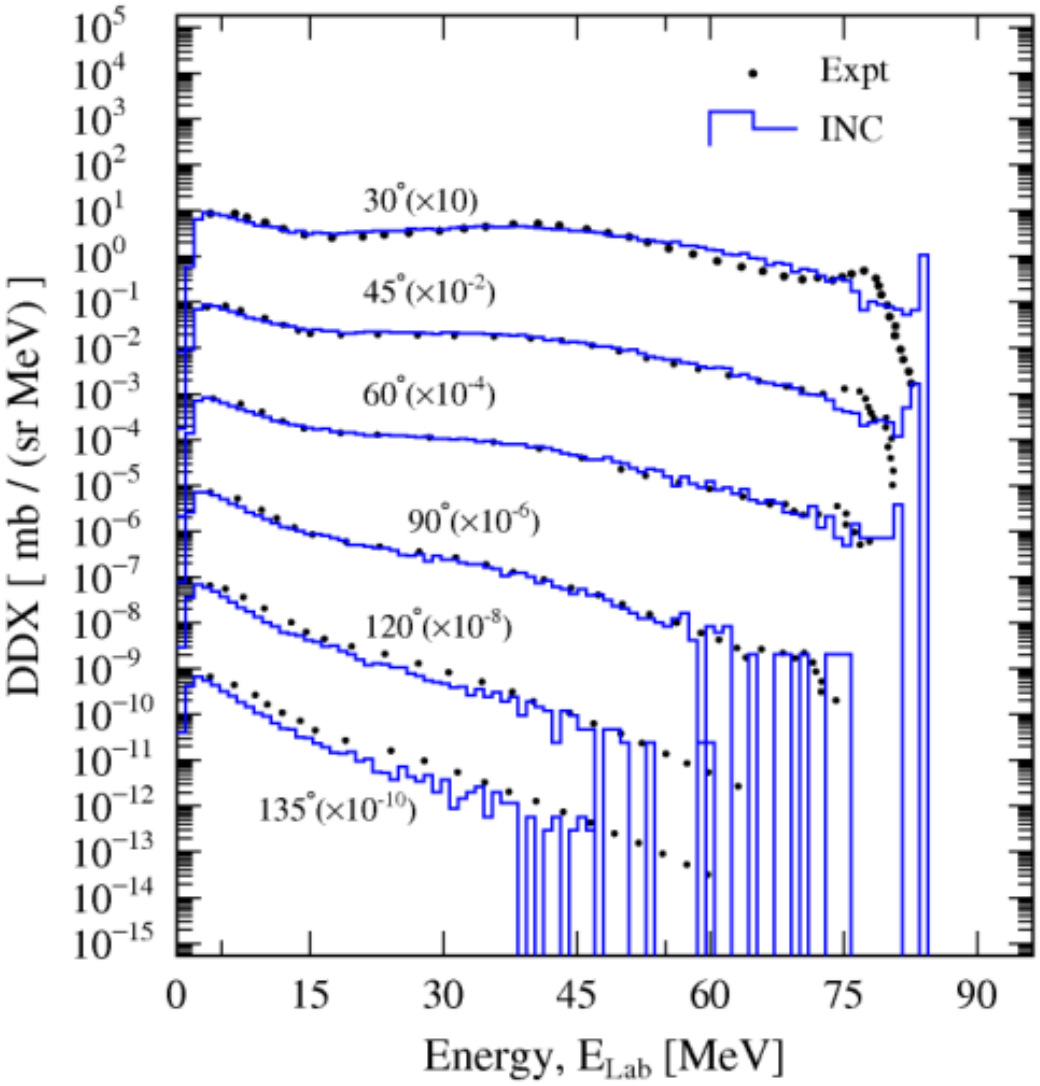

Fig. 3.6 DDX proton spectra from ^{27}Al at the angles 30° to 135° for deuteron bombarding at 80.0 MeV. The solid circles shows the experimental data taken from EXFOR[44] and the line histograms are the INC calculation results.

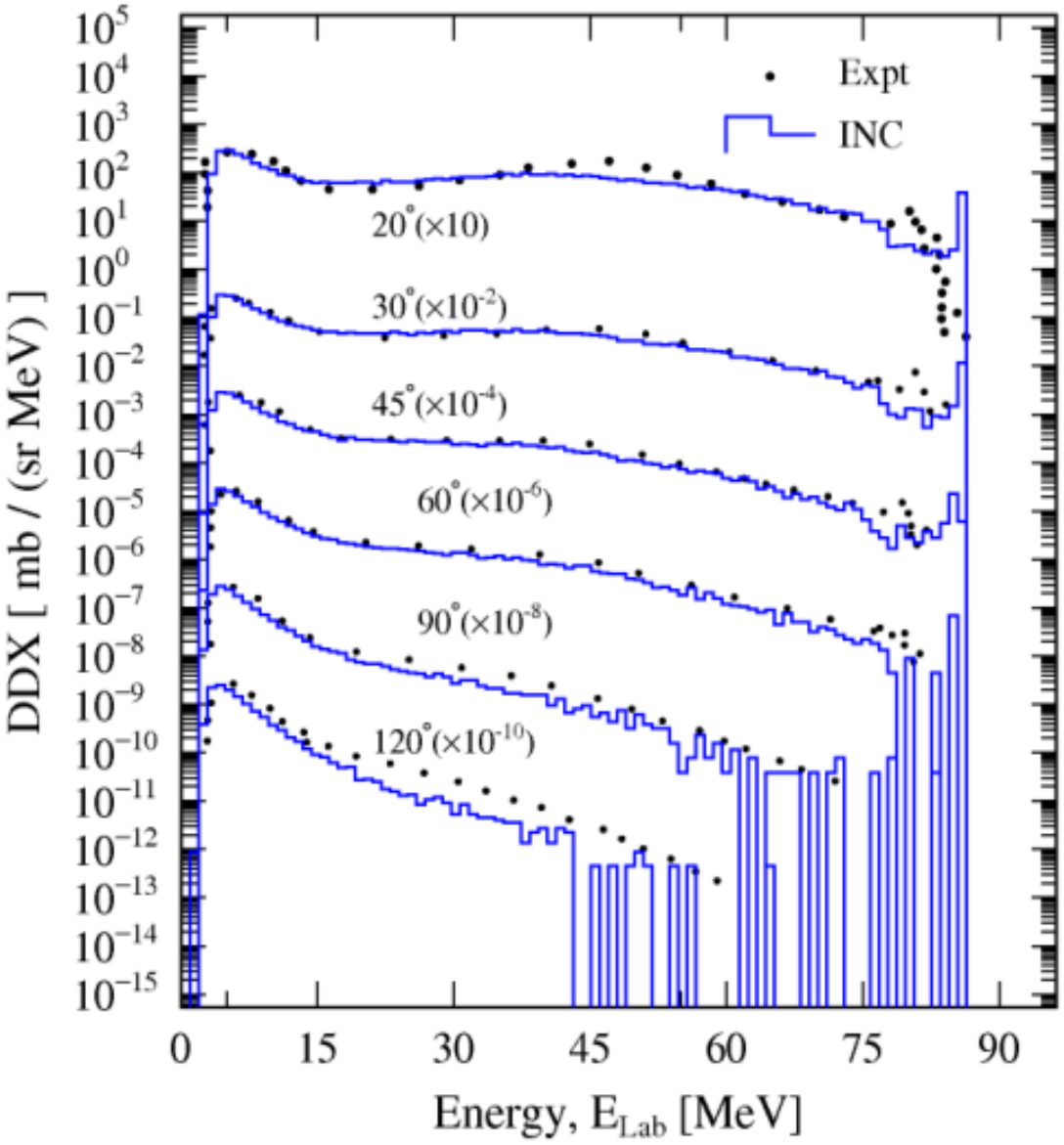

Fig. 3.7 Same as Fig 3.6, but for target ^{58}Ni at angles 20° to 120°.

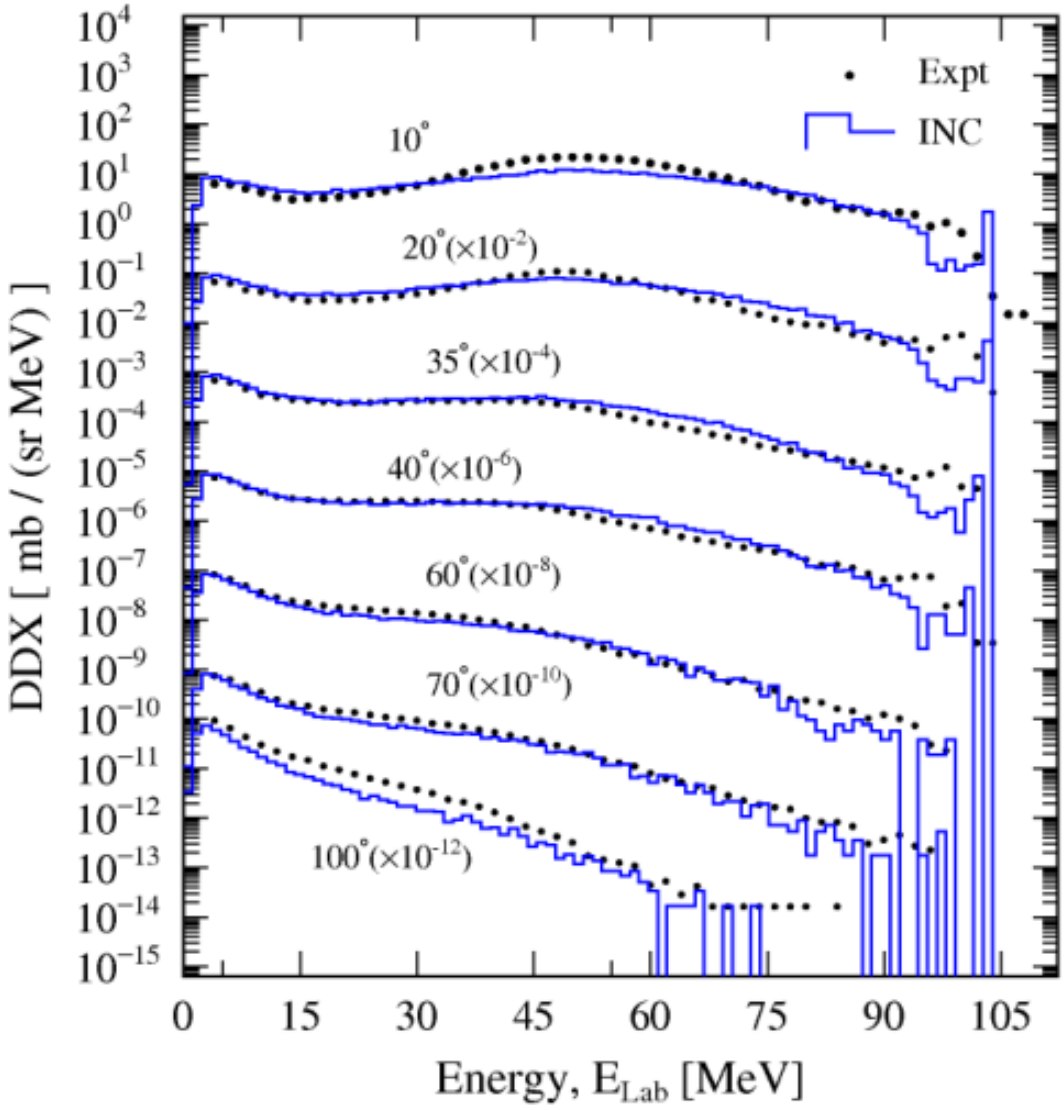

Fig. 3.8 Comparison of DDX proton spectra from ^{27}Al at the angles 10° to 100° for deuteron bombarding at 99.6 MeV with INC calculation results. The solid circles show the experimental data taken from EXFOR[44] and the line histograms are the calculation results. For visualization, the DDXs have been multiplied by the factors indicated in brackets.

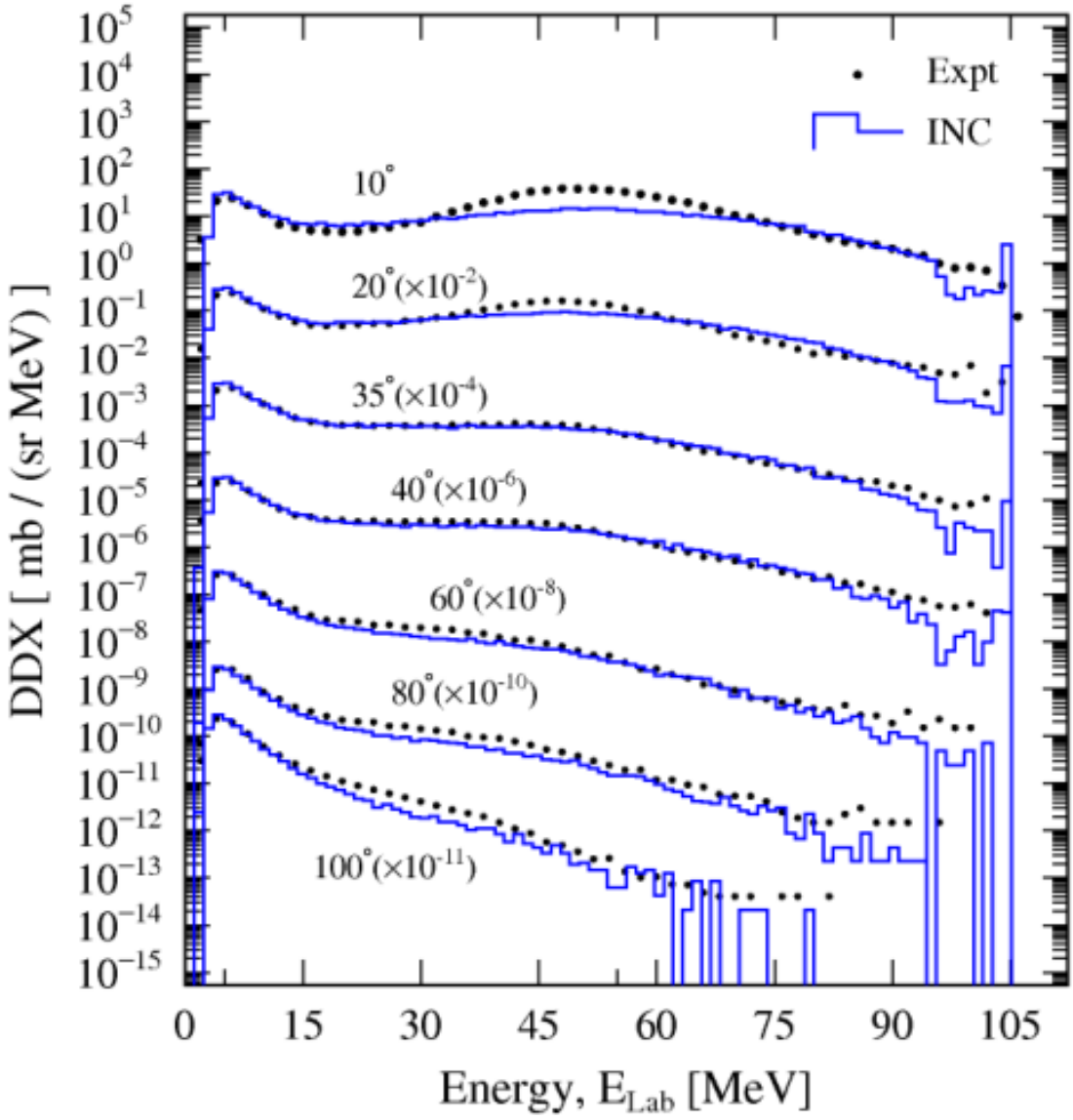

Fig. 3.9 Same as Fig 3.8, but for target ^{58}Ni.

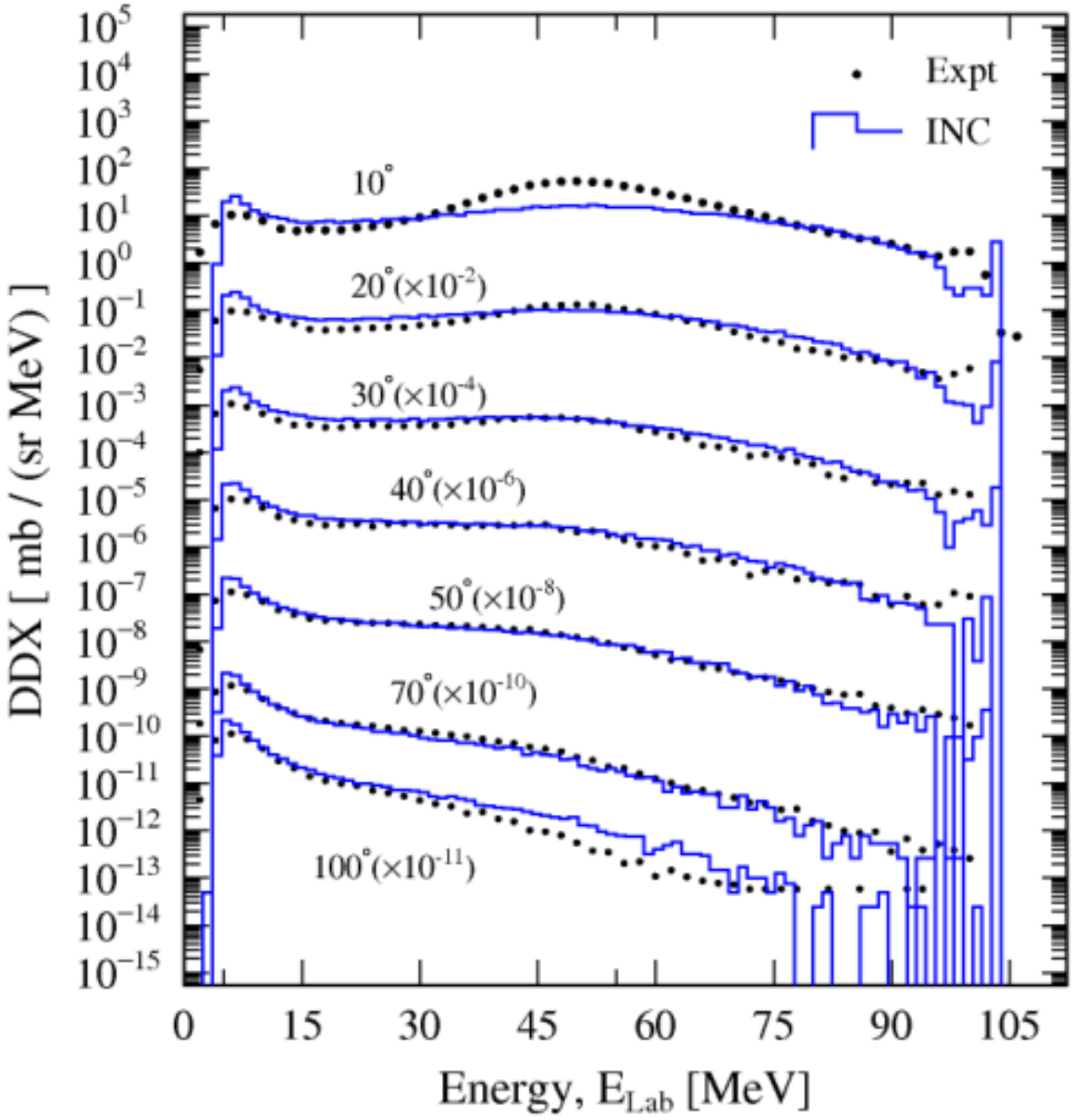

Fig. 3.10 Same as Fig. 3.8, but for target ^{93}Nb.

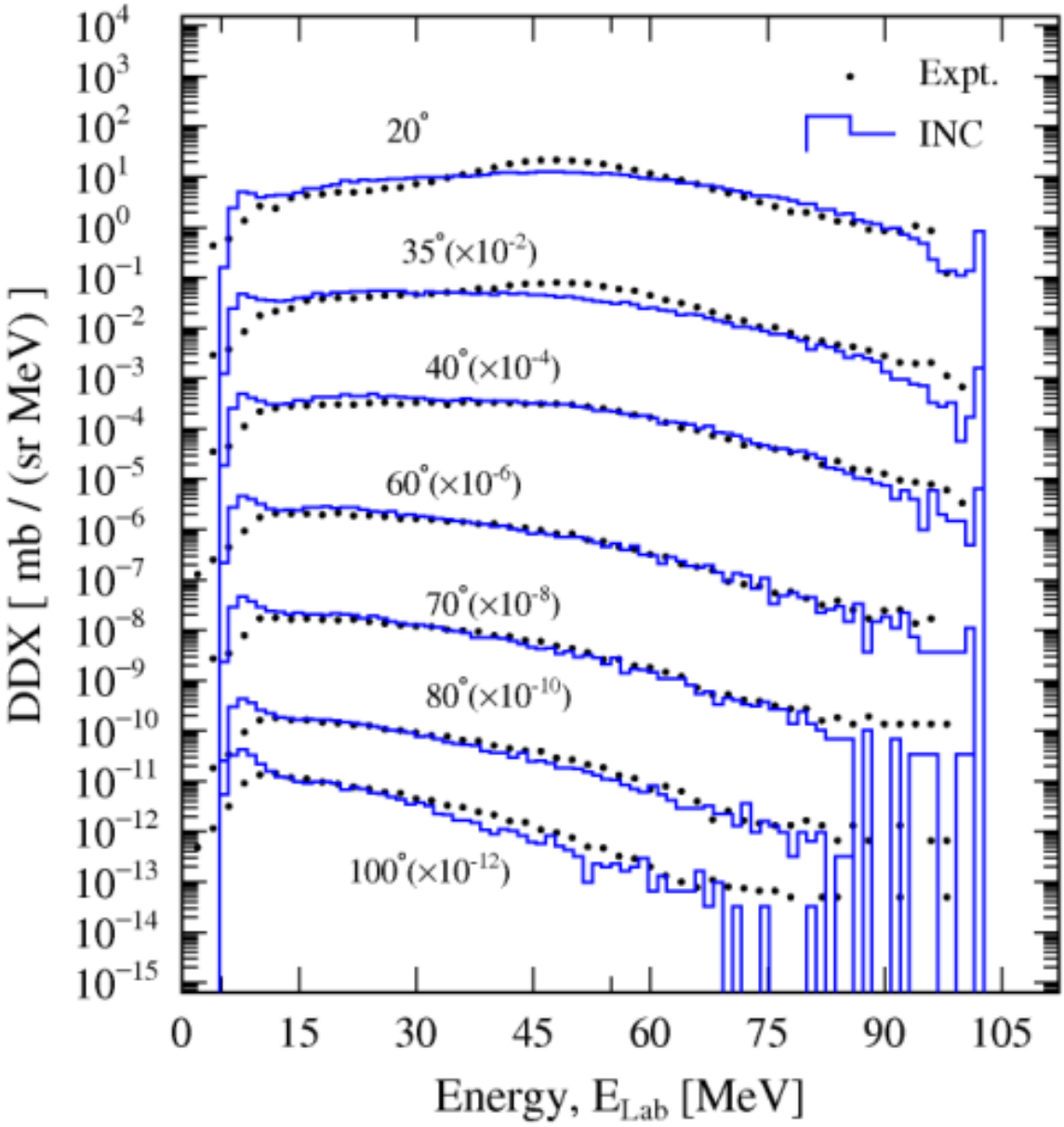

Fig. 3.11 Same as Fig 3.8, but for target ^{181}Ta at angles 20° to 100°.

3.5.3 Neutron Energy Spectra

The neutron spectra from ^{27}Al at incident energy 22.3 MeV are shown in Fig.3.12. Usually, INC models are not for such low incident energy spectra, but our model shows the relatively good prediction. Discrepancies below 10 MeV should be ascribable to the evaporation stage.

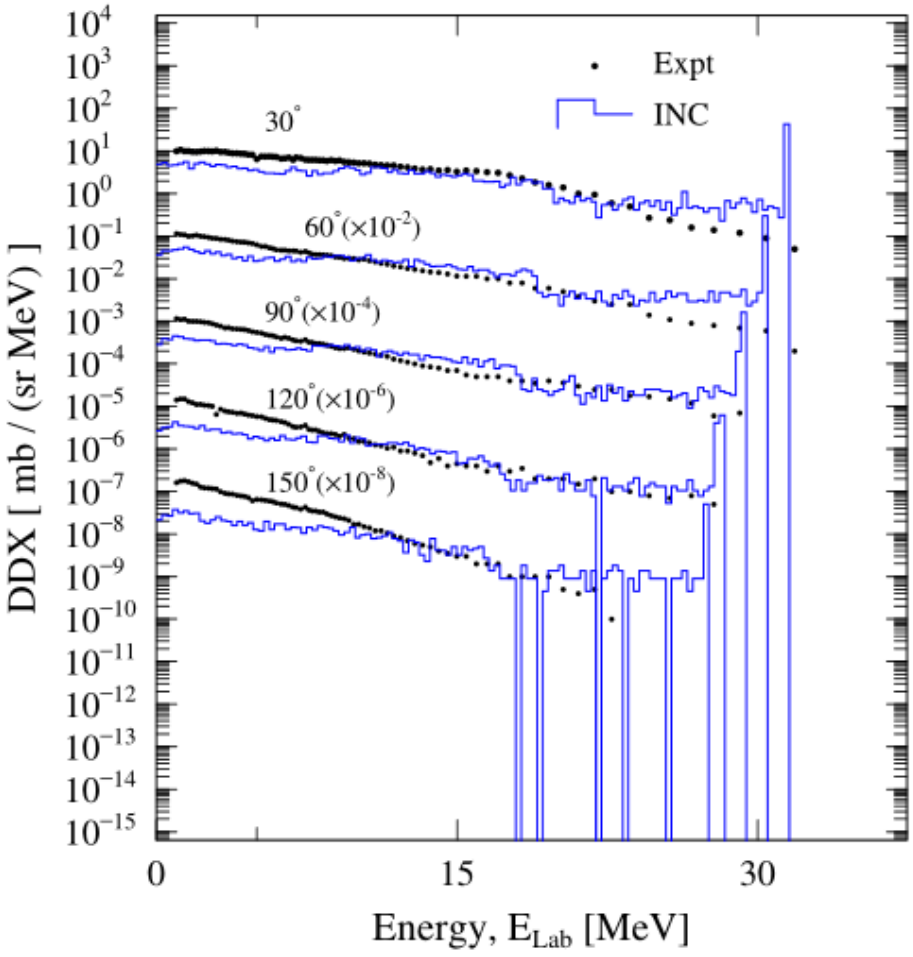

Fig. 3.12 Neutron production DDX spectra for 22.3 MeV deuterons bombard on ^{58}Ni at angles 30° to 150°.

3.6 Comparison with Other Models

INCL and QMD models are widely known for their good predictability for nucleon emission reactions. Some particle transport codes use these models for demonstrating cluster/nucleus-induced reactions. The widely used particle transport code, PHITS also rely on these models for complex nuclei induced reactions. In this section, examples of the calculation result by INCL and JQMD models using PHITS are shown in Figs. 3.13-3.17. As like the previous section, the solid circles show the experimental data taken from EXFOR[44] and dots are taken from Wu et al.[58]. The line/dashed histograms are the model calculation results. For visualization, the DDXs have been multiplied by the factors indicated in brackets in the figures.

Comparison of the PHITS-INCL and PHITS-JQMD calculation results for deuteron production DDXs from 80 MeV deuteron bombarding ^{27}Al at angles of 30°, 45°, 60° and 90° are shown in Fig. 3.13. Both the models underestimate the higher energy regions. Low energy regions are relatively well reproduced, but this calculation comes from evaporation model.

The proton spectra observed from deuteron bombardment on ^{27}Al at 80 MeV are compared with PHITS-JQMD calculation results at angles 30°, 60° and 90° in Fig. 3.14. The JQMD model prediction is not enough satisfactory. On the other hand, INCL reproduces proton spectra quite well as in Fig. 3.15 where ^{58}Ni(d, px) reactions at 99.6 MeV are displayed.

Fig. 3.16 and 3.17 show the comparison of deuteron spectra from the ^{58}Ni target with the JQMD and INCL model, respectively, for 80 MeV deuterons bombardment. The comparison shows a poor prediction of experimental data by both JQMD and INCL model at 20°, 45°, and 90°.

The prediction ability for the cluster-induced nuclear reactions by the existing PHITS models is not satisfactory, that is why the need for a higher prediction ability model is highly expected.

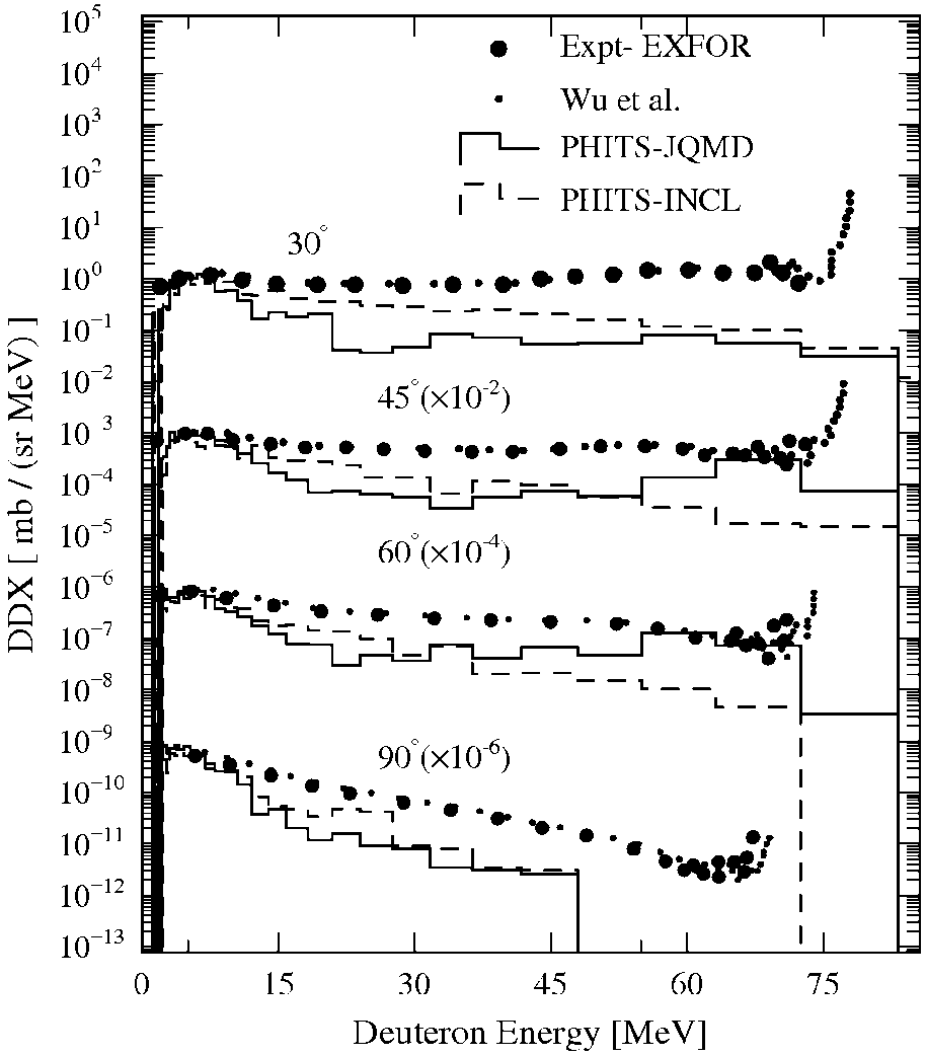

Fig. 3.13 INCL (dashed lines) and JQMD (solid lines) model calculations for ^{27}Al(d,d'x) reactions at 80 MeV in comparison with experimental values (dots taken from Wu et al.[58] and solid circles from EXFOR[44]). The DDXs have been multiplied by factors indicated in the figure (shown in bracket) for visualization purposes.

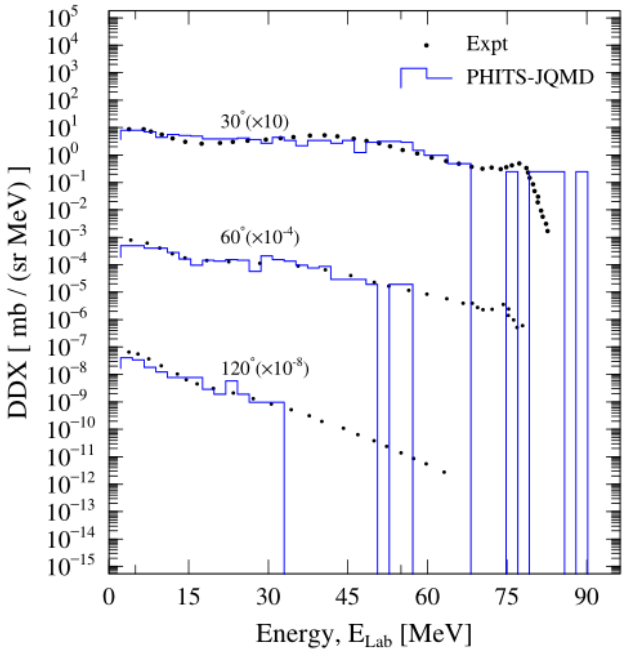

Fig. 3.14 JQMD model calculation results for the ^{27}Al(d, px) reactions at bombarding energy 80 MeV. The experimental data are taken from EXFOR[44].

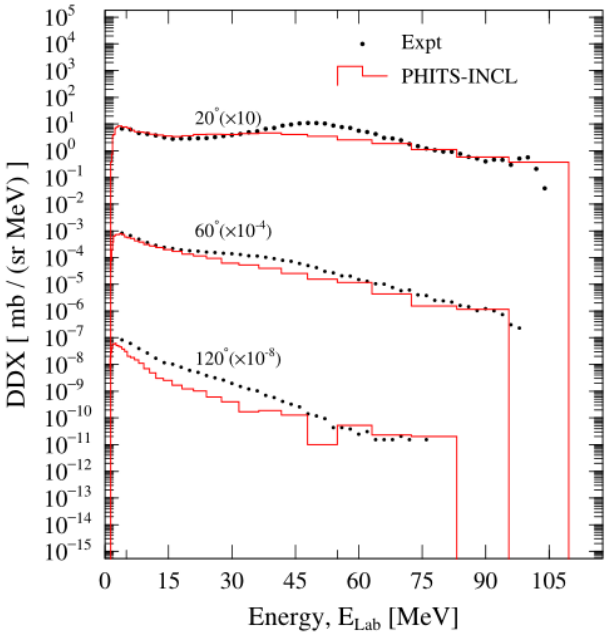

Fig. 3.15 INCL calculation results for ^{27}Al(d, p*x*) reactions at 99.6 MeV incident energy.

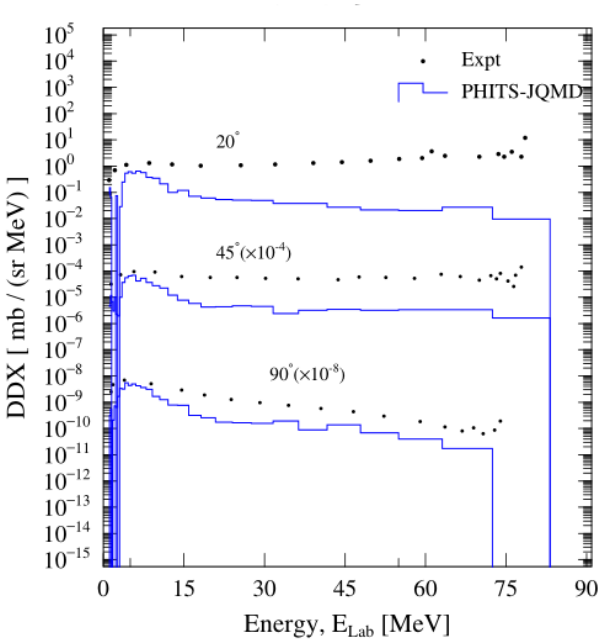

Fig. 3.16 JQMD model calculation results for the ^{58}Ni(d, d'*x*) reactions at bombarding energy 80 MeV. Solid circles are the experimental data taken from EXFOR[44].

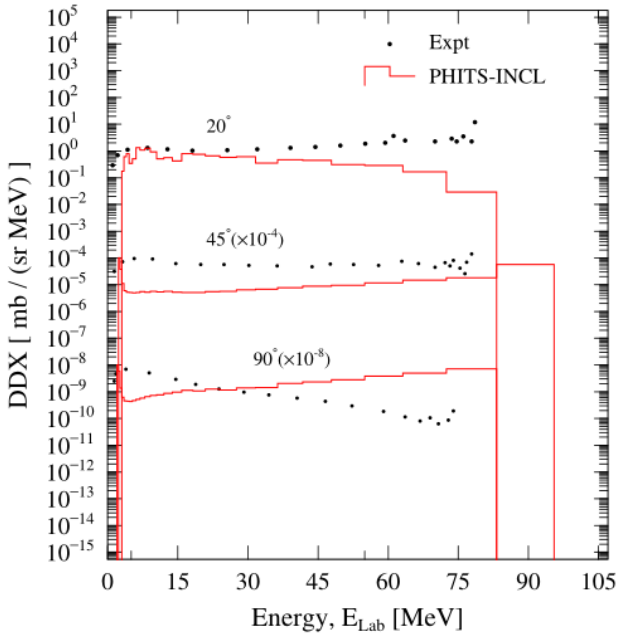

Fig. 3.17 Same as Fig. 3.16, but the comparison with INCL model calculations.

4 Alpha-Induced Nuclear Reactions

4.1 Introduction

Intermediate energy nuclear reaction models are of high interest for a variety of applications in science and technology. Nucleon induced reactions have been studying extensively. On the other hand, studies on alpha-induced reactions are relatively neglected at intermediate energies. Not only for the manifolds applications but also to have an improved understanding of reaction mechanism, it is important to study the alpha-induced nuclear reactions. In addition, the study of alpha-induced reactions has very practical significance in particle transport code as discussed in chapter 1.

INC model already shows high predictability for nucleon induced nucleon production reactions.[35,36,62,63] Though some studies have considered heavy ion reactions, were limited to proton or pion productions.[18,64,65] Some studies also have done for alpha-induced reactions but little attention was paid to cluster productions reactions.[12,43] However, none of the studies was concentrating the all-outgoing channel since all the final channels have to have similar strengths.

The INC model used in this research was expanded previously for proton production and proton-induced nuclear reactions for the incident energy of 200 MeV or higher.[66,67] Later on, the model was made applicable for low energy region ~50 MeV.[61] In this case, trajectory deflection and collective excitation, barrier transmission coefficient have been incorporated in the model. In the present study, the model has been expanded to include alpha-induced nuclear reactions, namely, (α, $\alpha'x$), (α, ^{3}Hex), (α, tx), (α, dx), (α, px), and (α, nx). The proposed model is validated by using experimental data for ^{27}Al, ^{58}Ni target at incident energies 140 and 160 MeV.

The chapter is organized as follows: improvement of the INC model is explained first. The validity of the model is checked comparing with the experimental data. At the end, the experimental data are compared with other works.

4.2 Extension of INC model

In the present study, INC model has been extended to handle the cluster-induced reactions. The major improvements of the model for the alpha-induced nuclear reactions are discussed in this section.

4.2.1 Incident Nuclear Ground State

Alpha particle is composed of four nucleons. Constituent two protons and two neutrons make α particles are in a strongly coupled state as the nucleons' wave functions are completely overlapped. The binding energy of α particle is 28.3 MeV, and the separation energies of protons and neutrons are extremely large. The nucleons in alpha are so tightly bound that radius of α particle is small and is approximately, R_α = 1.2 [fm].

Ground state of the alpha is determined in the same way as for the projectile deuteron described in chapter three (section 3.3.1). For the alpha projectile, the average radius was taken as $\mathrm{R_{inc}} = \mathrm{R}_\alpha = 1.2\ [\mathrm{fm}]$ in Eq. (3.7).

4.2.2 Projectile Breakup

One of the major extensions of the model is to improve breakup mechanism for the projectile nucleus. It is assumed that the breakup of projectile occurs at the initial state of

the interaction. Fig. 4.1 shows the schematic diagram of alpha particle disintegration while interacting with the target.

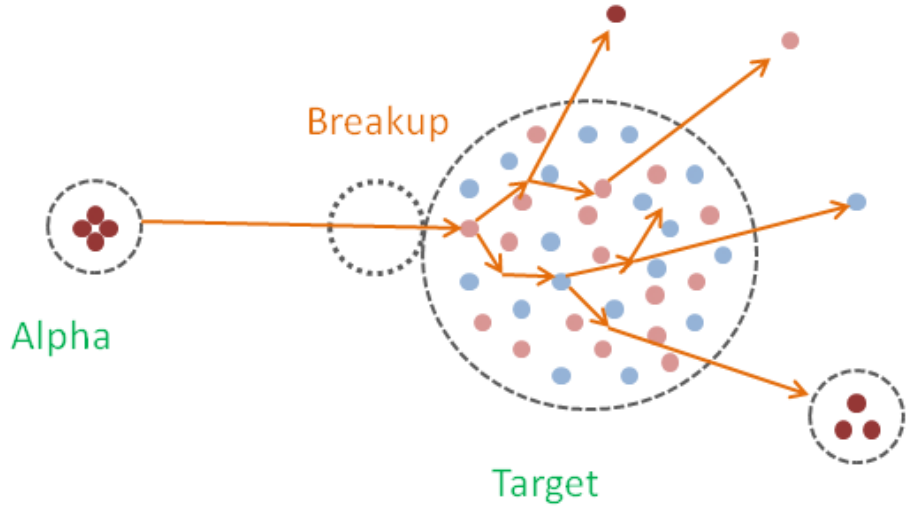

Fig. 4.1 Schematic diagram of alpha breakup while interacting with target nucleus.

.

Initial alpha particle wave function is assumed as the superposition of the different states that consists of the cluster unites. For the alpha particle, the wave function is,

$$\left|\alpha_{init}\right\rangle = c_{\alpha 0}\left|\alpha\right\rangle + c_{\alpha 1}\left|{}^{3}\mathrm{He}n\right\rangle + c_{\alpha 2}\left|tp\right\rangle + c_{\alpha 3}\left|dd\right\rangle + c_{\alpha 4}\left|nnpp\right\rangle \tag{4.1}$$

with the normalization of

$$\sum_{i=all} c_i^2 = 1$$

due to orthogonality. For every event of INC calculation the probability was calculated by these wave function. The inclusion of cluster allows to treat their composite nature. The first term of Eq.(4.1) shows that the incident alpha does not go through any breakup mechanism while interacting with target. The second term indicates that the incident

alpha disintegrates to $^{3}He + 1n$ while enters target nucleus. The resultant ^{3}He does not go any further breakup. The momentum of the fragment ^{3}He is taken as,

$$\vec{P}_{^{3}He} = \sum_{N_i=1}^{3} \vec{P}_{N_i} + \frac{3}{4}\vec{P}_{\alpha} \tag{4.2}$$

where, $\vec{P}_{N_i}$ is the momentum of the *i*th nucleon of ^{3}He and $\vec{P}_{\alpha}$ is the momentum of the projectile alpha.

The transport of the particle ^{3}He has been considered as if three constituent nucleons move in parallel with the speed of ^{3}He. During the transport, if any of the constituents get interaction with the target nucleons, momentum change of the nucleon is considered. This momentum in turn taken as momentum change of the ^{3}He itself. The 3rd, 4th and 5th terms of Eq. (4.1) represent that the incident alpha particle breakup into $t + p$, $d + d$, $n + n + p + p$ respectively. The momentum of the fragments is same as demonstrated for the 2nd term. And the transportation process of the fragments are also same as of the description of 2nd term.

The relative yield of the incident alpha fragmentation depends on the coefficients *c* of Eq (4.1). These values were determined to reproduce experimental data i.e. fitting experimental values. Table 4.1 shows the values of the coefficient to fit the experimental data for alpha incident reactions.

Table 4.1 Values of the co-efficients in Eq.(4.1) for alpha incident reactions.

Cluster Unit	Co-efficient, c
α	8
^{3}He + n	$\sqrt{8}$
t + p	$\sqrt{10}$
d+d	$\sqrt{10}$
2p + 2n	$\sqrt{8}$

4.2.3 Investigation of Potential Depth

Nuclear potential depth is not known explicitly yet. To investigate alpha nuclear potential fitting experimental data technique was followed. The investigation procedure to optimize the depth of the nuclear potential of α particles, V_{α}, was done as follows. Various estimation of nuclear potential to fit the proton production experimental energy spectra was considered. The Nuclear potential that provides the best fit was chosen. Here, three cases are shown,

Case 1: The depth of the potential is $V_{\alpha} = 30$ MeV.

Case 2: The depth of the potential is $V_{\alpha} = 40$ MeV.

Case 3: The depth of the potential is $V_{\alpha} = 60$ MeV

Fig. 4.2 shows the proton-production double differential cross section for the ^{27}Al (α, px) reaction at incident energy 140 MeV calculated at above three cases. It can be easily observed from Fig 4.2 that the calculated energy spectra compared to the experimental data provide best fit for the Case 2. Therefore, the depth of the nuclear potential of α particle was determined as $V_{\alpha} = 40\ MeV$.

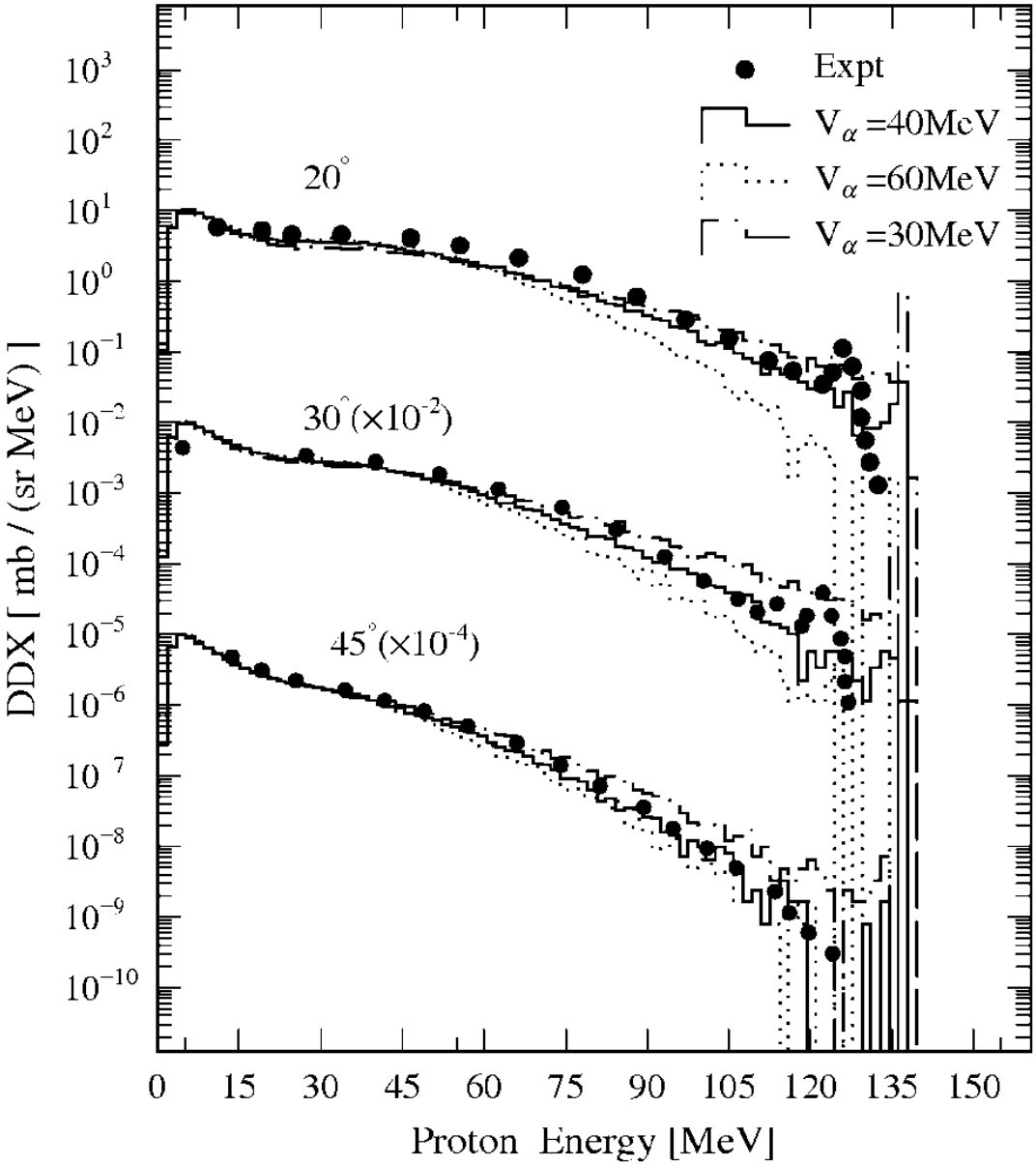

Fig. 4.2 Comparison of the calculation results for proton production DDXs from 140 MeV alpha particles bombarding ^{27}Al at angles of 20°, 30°, and 45° for different values of the potential depth of alpha particle. The solid circles show the experimental data taken from EXFOR[44]. The dash-dotted, solid, and dotted line histograms are the INC calculation results for alpha-particle potential depths of 30 MeV, 40 MeV, and 60 MeV, respectively. For visualization, the DDXs have been multiplied by the factors indicated in brackets.

4.2.4 Investigation of Maximum Impact Parameter

For nucleon incidence reaction the maximum impact parameter was taken as the target cut-off radius given by the expression shown in chapter 2 as

$$R_{max} = R_0 + 5a, \tag{4.3}$$

where R_0 is the nuclear radius and a is the diffuseness.

For alpha incident reaction, maximum impact parameter was chosen to fit the experimental data. Few cases were considered and the best one was chosen. Three cases are shown as follows,

Case 1:

Maximum impact parameter, b_{max} = Target cut-off radius (as like the nucleus incident reaction using Eq. (4.3))

Case 2:

Maximum impact parameter, b_{max} = Target cut-off radius + Projectile average radius

Case 3:

Maximum impact parameter, b_{max} = Target cut-off radius + Projectile cut-off radius

For the nucleon incident reactions, maximum impact parameter was considered equal to the target cut-off radius. For alpha-induced reaction, if the same consideration were taken, case 1 would obtain. Case 3 shows the maximum impact parameter as the sum of the cut-off radii (Eq. (4.3)) of both target and incident particle. However, as mentioned earlier, due to high binding energy alpha particle is smaller and the radius is about 1.2 fm. The maximum impact parameter for alpha particle interaction was taken as the sum of average radius of incident alpha and the cut-off radius of the target nucleus shown in case

2. For a comparison, Fig 4.3 shows calculated DDX spectra for three cases of maximum impact parameter, b_{max} for ^{27}Al(p,p'x) reactions.

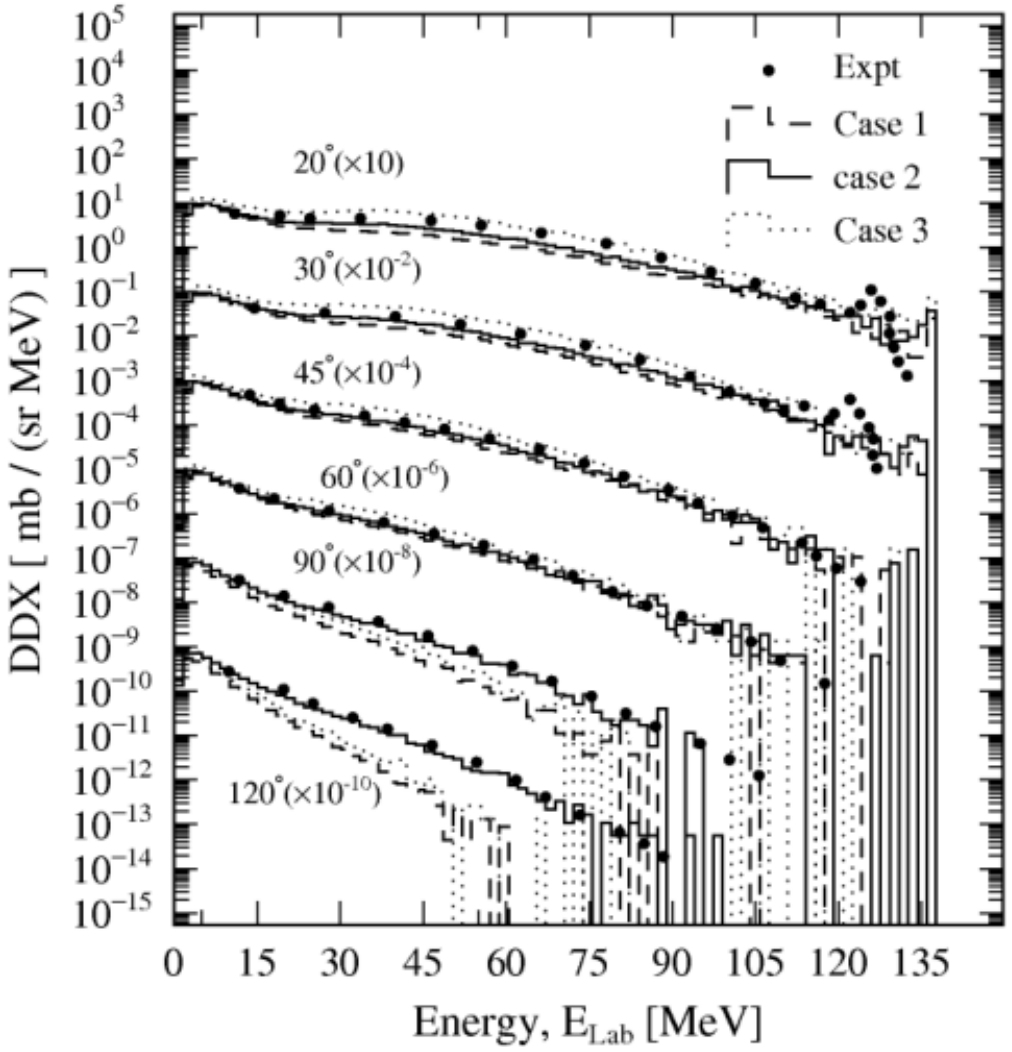

Fig. 4.3 Comparison of the calculation results for proton production DDXs from 140 MeV alpha particles bombarding ^{27}Al at six angles from 20° to 120° for different values of the maximum impact parameter. The solid circles show the experimental data taken from EXFOR[44]. The dashed, solid, and dotted line histograms are the INC calculation results for the impact parameter of case 1, case 2 and case 3, respectively. For visualization, the DDXs have been multiplied by the factors indicated in brackets.

4.2.5 Probability of Deflection Angle

The incoming and outgoing particle is deflected while enters into and goes out target nucleus due to the influence of nuclear potential. For alpha-induced nuclear reactions, trajectory deflections have a strong effect on the angular distribution of the fragments. New parameters have been chosen for the incoming and outgoing particles. In previous report[53], the probability, $W_{def,p}$ of proton deflection at laboratory angle, θ were shown (discussed in chapter 2). The parameters were chosen to reproduce the spectral shapes of experimental DDX spectra for cluster emission reactions as

$$W_{def,d}(\varepsilon,\theta,A) = \exp\left[-0.001(1.3\varepsilon + \ln A + 6)\theta\right], \tag{4.4}$$

$$W_{def,t}(\varepsilon,\theta,A) = \exp\left[-0.001(1.2\varepsilon + 6\ln A - 5)\theta\right], \tag{4.5}$$

$$W_{def,3He}(\varepsilon,\theta,A) = \exp\left[-0.001(1.2\varepsilon + 6\ln A - 5)\theta\right], \tag{4.6}$$

$$W_{def,\alpha}(\varepsilon,\theta,A) = \exp\left[-0.001(1.2\varepsilon - 10\ln A + 40)\theta\right], \tag{4.7}$$

where ε is the incident energy, A is the target mass number. $W_{def,d}$, $W_{def,t}$, $W_{def,3He}$, $W_{def,\alpha}$,respectively, represent the probability of deuteron, triton, ^{3}He and alpha particle deflection due to nuclear potential.

4.3 Calculation Results and Discussions

The proposed INC model was tested for the bombardment of alpha particle on targets ^{27}Al and ^{58}Ni at incident energy 140 MeV for all available channels, namely (α, α'x), (α, ^{3}Hex), (α, tx), (α, dx), (α, px), and (α, nx). Figs. 4.4 to 4.15 allow comparisons between the calculated DDXs spectra and the experimental data. The solid circles show the experimental data and the line histograms are the INC calculation results. The DDXs have been multiplied by the factors shown in brackets for visualization purpose. In these

comparisons, the data from Wu et al.[68] and experimental data taken from EXFOR[44]are used.

Figs. 4.4 and 4.5 represent the comparison between experimental alpha DDXs and calculated INC model results for the case of (α, $\alpha'x$) reactions with ^{27}Al and ^{58}Ni target, respectively. The highest energy peak of the alpha spectra corresponds to elastic scattering, is captured well by our calculations. The calculated alpha-production DDX spectra account well for the experimental results at all angles and over the entire energy range for both targets except little underestimation at higher angles for ^{58}Ni.

Figs. 4.6 and 4.7 show the comparison of experimental and calculated neutron energy spectra for the alpha bombardment on ^{27}Al and ^{58}Ni respectively. The present model reproduces the features of neutron spectra from ^{27}Al quite well except the discrepancy at 60º. The discrepancy observed at 60° can be attributed to experimental uncertainty. The neutron spectra from ^{58}Ni at 20º, 45º and 90º are also reproduced well. The discrepancy in low energy region at angular position 90º is mainly reproduced by evaporation model GEM, and it is beyond the capability of the INC model.

Figs. 4.8 and 4.9 allow the comparison of energy spectra for the (α, ^{3}Hex) reactions with INC calculation results for targets ^{27}Al and ^{58}Ni, respectively. The gross features of the ^{3}He energy spectra in both cases are reproduced well except the high-energy region. The calculated spectra show overestimation at 55º and 75º and underestimation at 105º for the target ^{58}Ni.

Triton spectra from the targets ^{27}Al and ^{58}Ni for the alpha bombardment are shown in Figs. 4.10 and 4.11, respectively. The overall features of the triton spectra from ^{27}Al are reproduced well by our INC model. The spectra from ^{58}Ni are also reproduced grossly. As in the case of ^{3}He production spectra, the high-energy end, where the triton production is dominant, is underestimated. In this study, one neutron stripping reaction mechanism is

not considered. We believe the incorporation of one-nucleon transfer reaction will improve the scenario.

The comparison of the calculated and experimental deuteron spectra for the targets ^{27}Al and ^{58}Ni at alpha incidence 140 MeV is presented in Figs. 4.12 and 4.13, respectively. The extended INC model reproduces well the forward angle broad peaks at the half of the incident energy that is due to the breakup of incident alpha.[69] The deuteron spectra from Al target account well by the extended INC model except at angular position 30º. The spectra from Ni also show good agreement except the underestimation at higher angle as well as energy region.

Figures 4.14 and 4.15 represent the comparison between experimental and calculated proton energy spectra from ^{27}Al and ^{58}Ni, respectively. The present model accounts well the gross features of the proton spectra from the Aluminum target. However, at small angles, a difference is observed in the high-energy region that is governed by the stripping reaction. The extended model results in overestimation at large angles (i.e., 90° and 120°). The proton spectra from ^{58}Ni show overestimation in all angle and entire energy region.

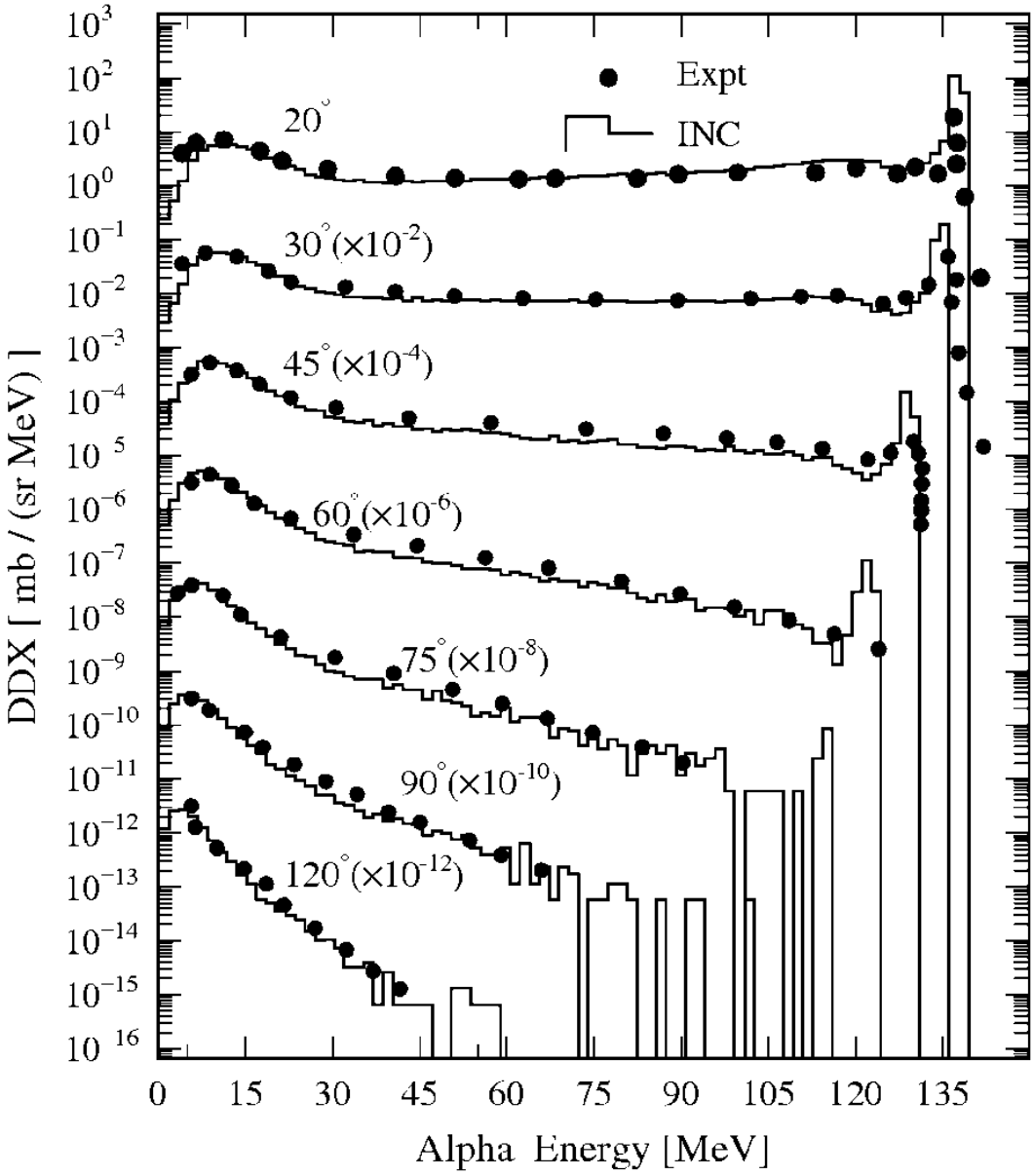

Fig. 4.4 Comparisons of experimental DDXs for ^{27}Al(α, α'x) reactions at 140 MeV with the INC model coupled with GEM model calculation results at angles 20°-120°. The solid circles represent the experimental energy spectra taken from EXFOR[44] and the line histograms are the INC calculation results. For visualization, the DDXs have been multiplied by the factors indicated in brackets.

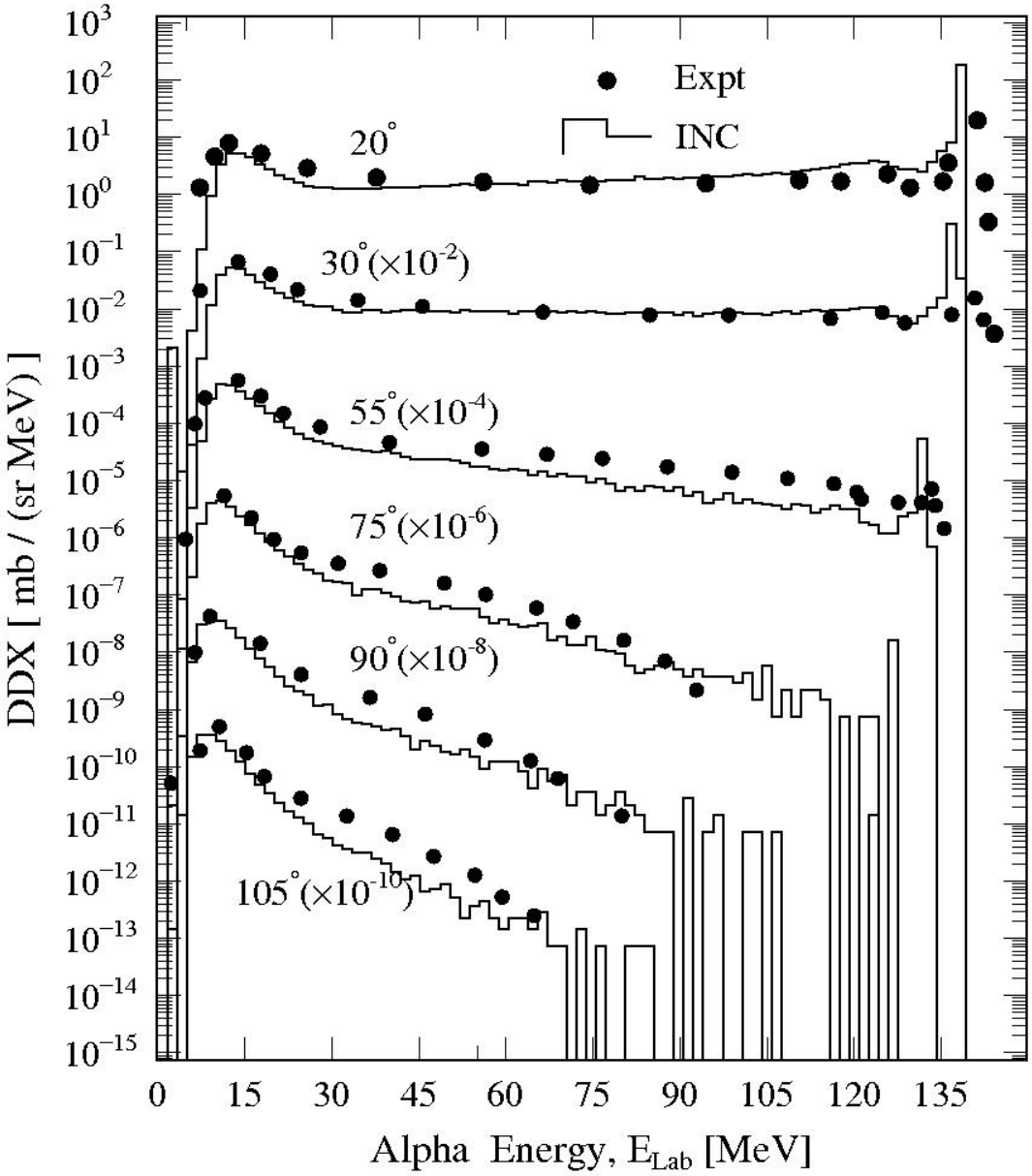

Fig. 4.5 Same as Fig 4.4, but for target ^{58}Ni at angles 20°-105°.

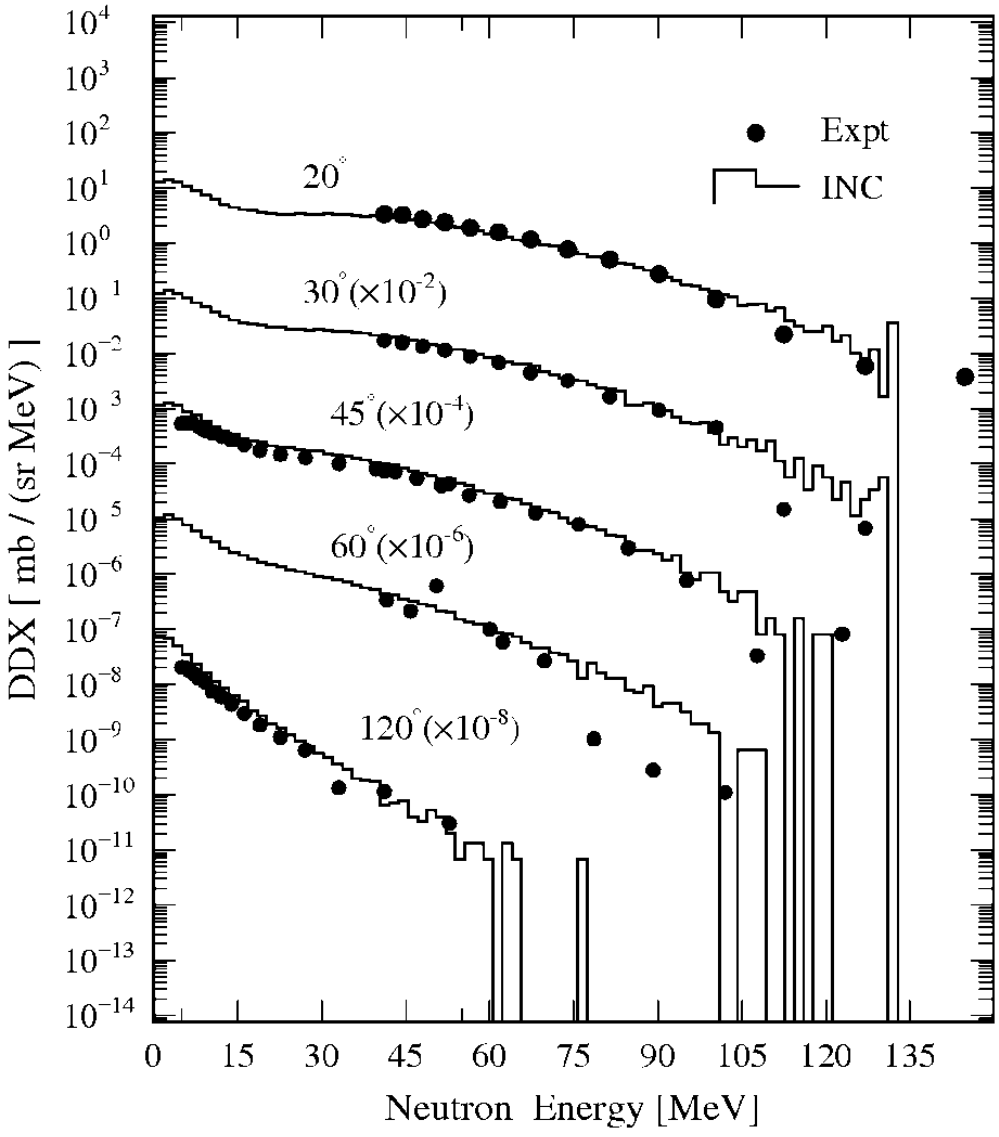

Fig. 4.6 Same as Fig. 4.4, but for ^{27}Al(α, nx) reactions at 140 MeV.

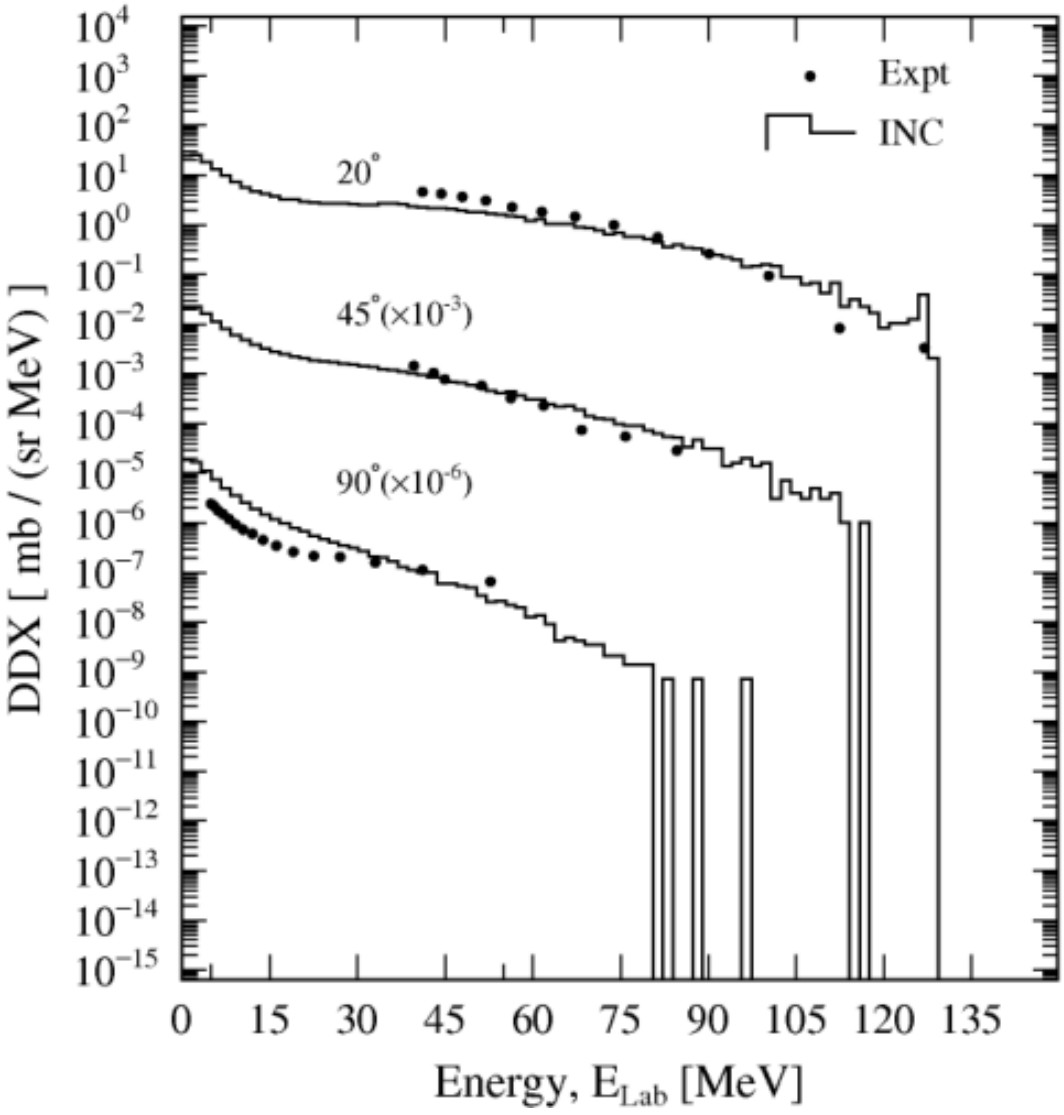

Fig. 4.7 Same as Fig. 4.4, but for ^{58}Ni(α, nx) reactions at 140 MeV for the angular positions 20°,45° and 90°.

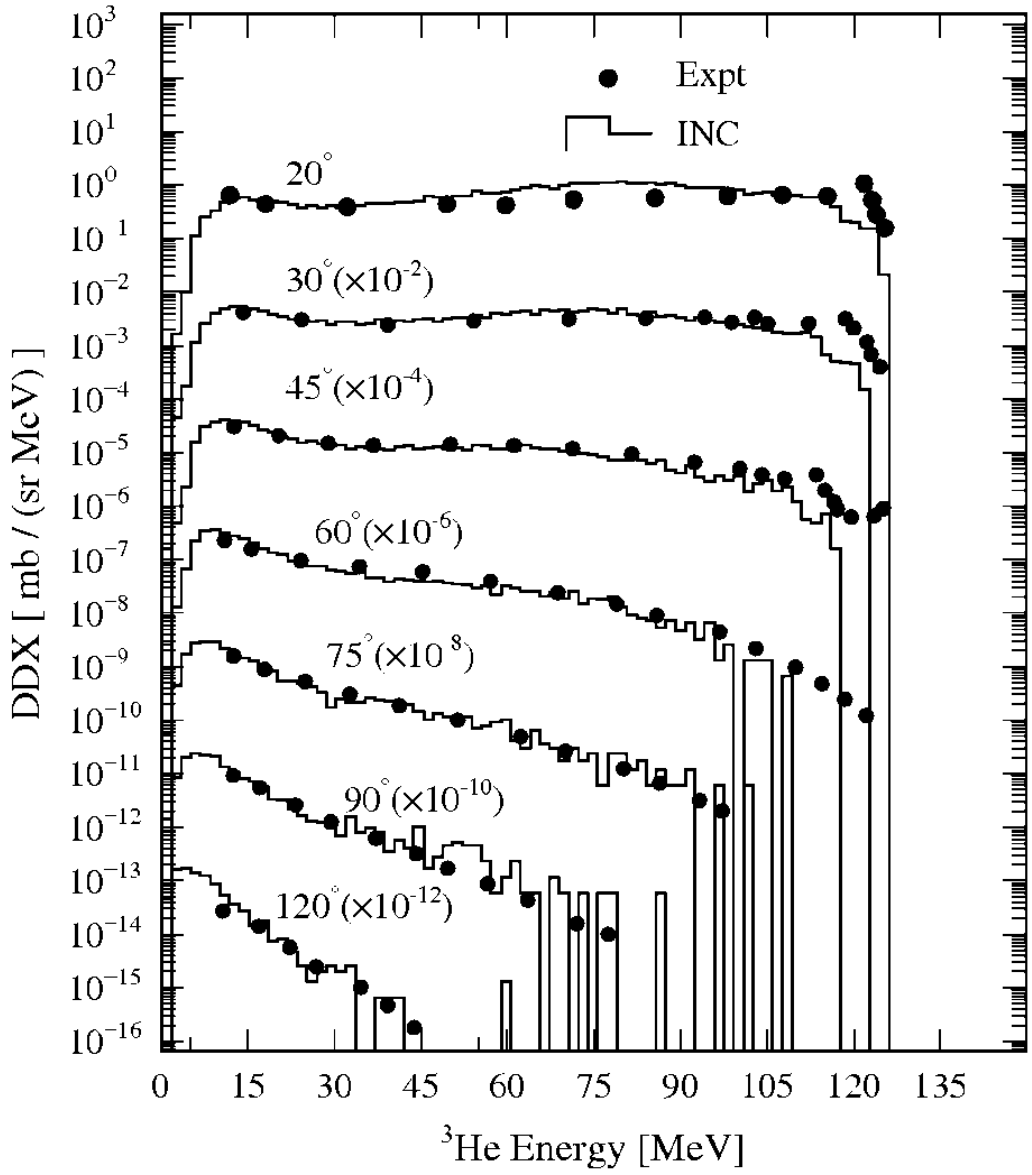

Fig. 4.8 Same as Fig. 4.4, but for ^{27}Al(α, ^{3}He) reactions. Solid circles show the experimental data from EXFOR[44].

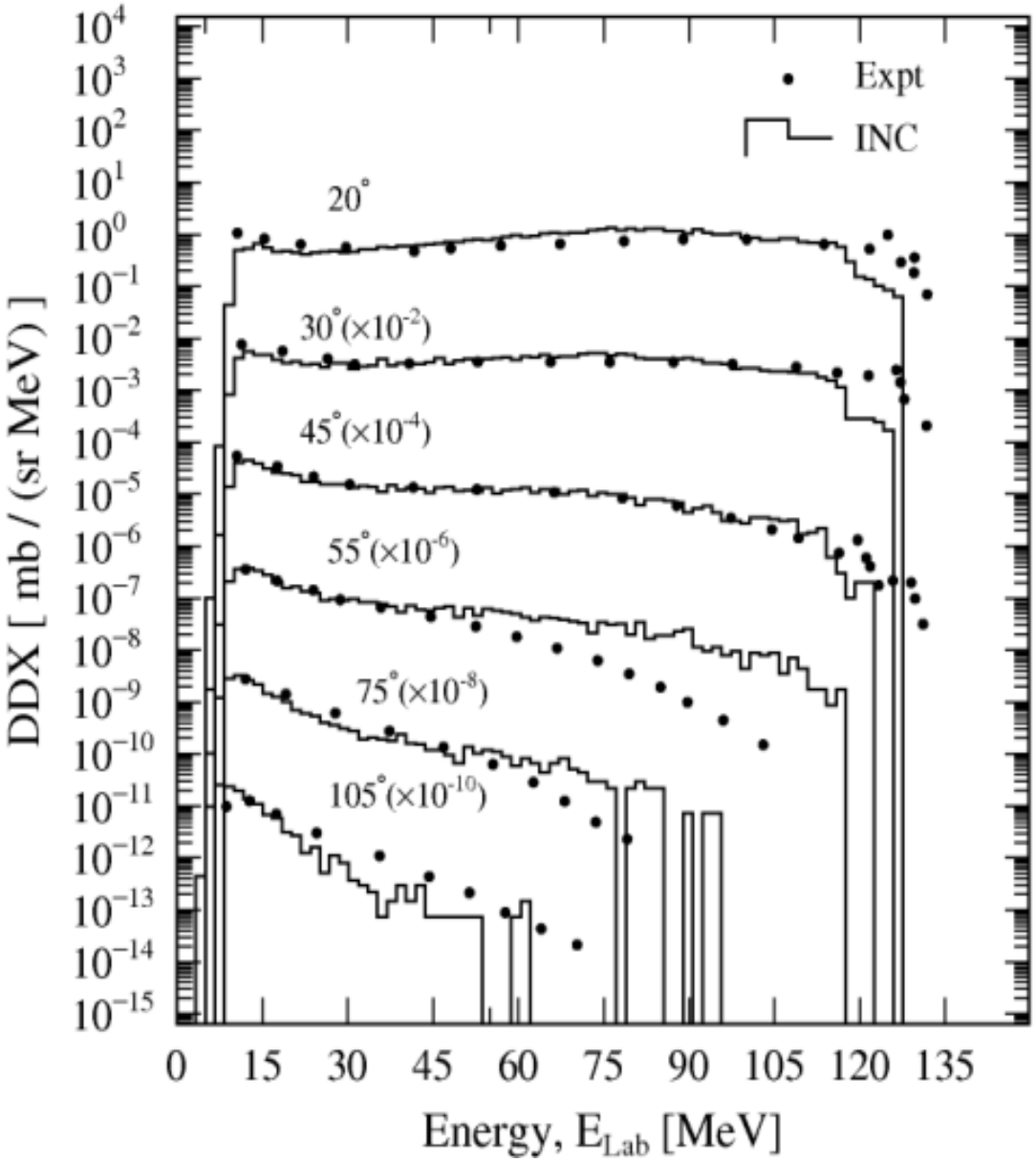

Fig. 4.9 Same as Fig. 4.4, but for ^{58}Ni(α, ^{3}Hex) reactions at angles 20°-105°.

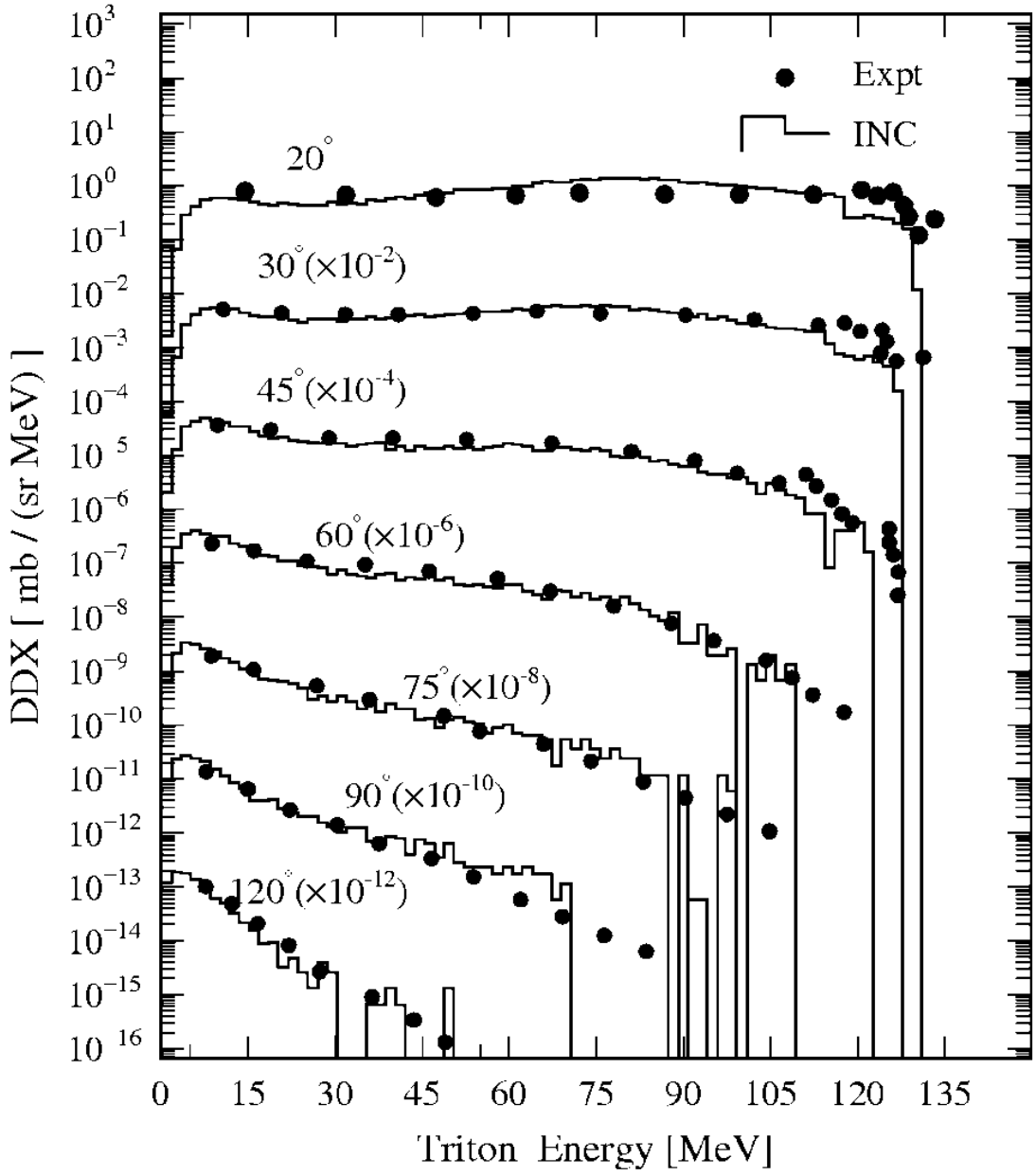

Fig. 4.10 . Same as Fig. 4.4, but for ^{27}Al(α, tx) reactions at 140 MeV.

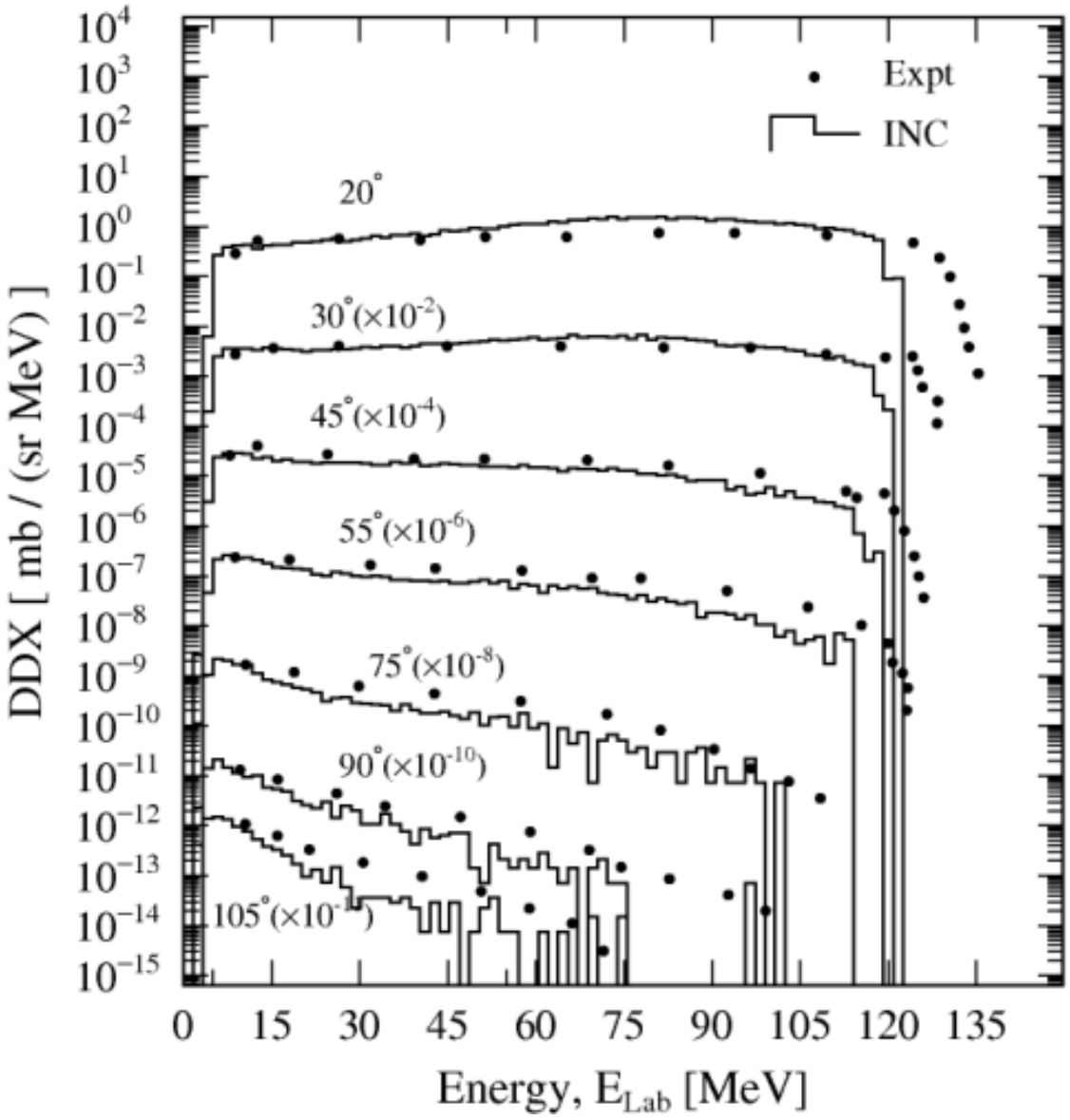

Fig. 4.11 Same as Fig. 4.4, but for ^{58}Ni(α, tx) reactions at 140 MeV for the angular positions 20°-105°.

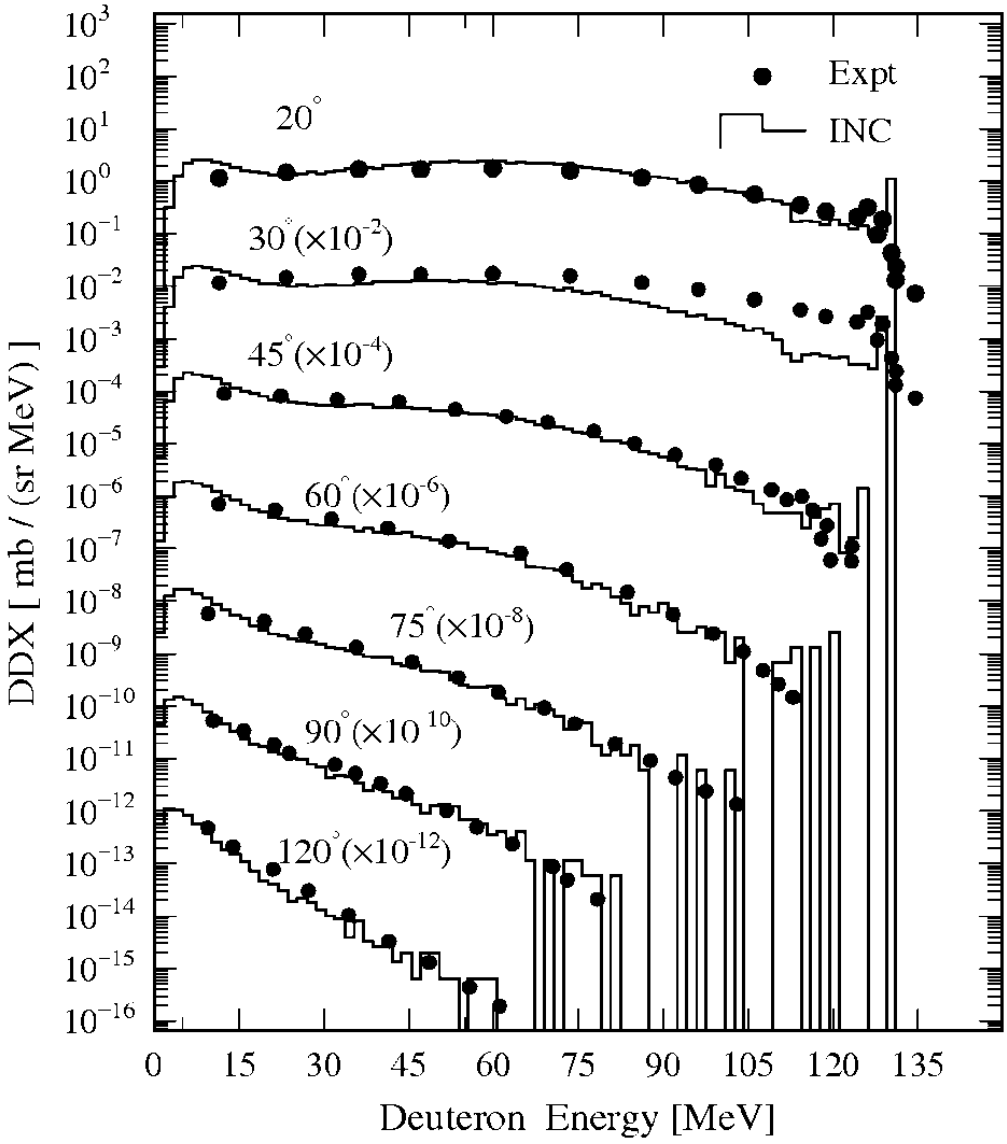

Fig. 4.12 Same as Fig. 4.4, but for ^{27}Al(α, dx) reactions at 140 MeV. Solid circles are the experimental data taken from EXFOR[44].

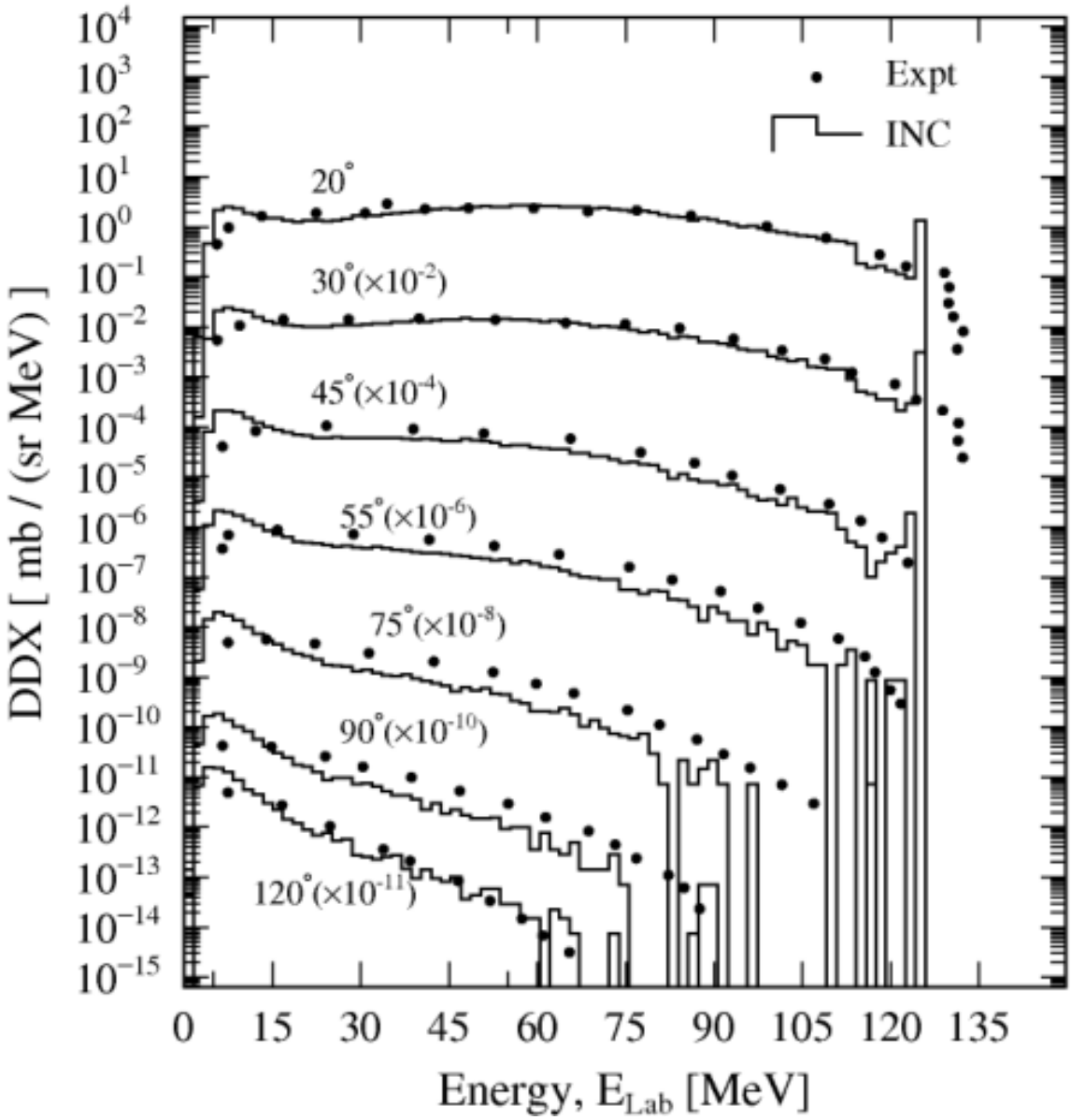

Fig. 4.13 Same as Fig 4.4, but for ^{58}Ni(α,dx) reactions.

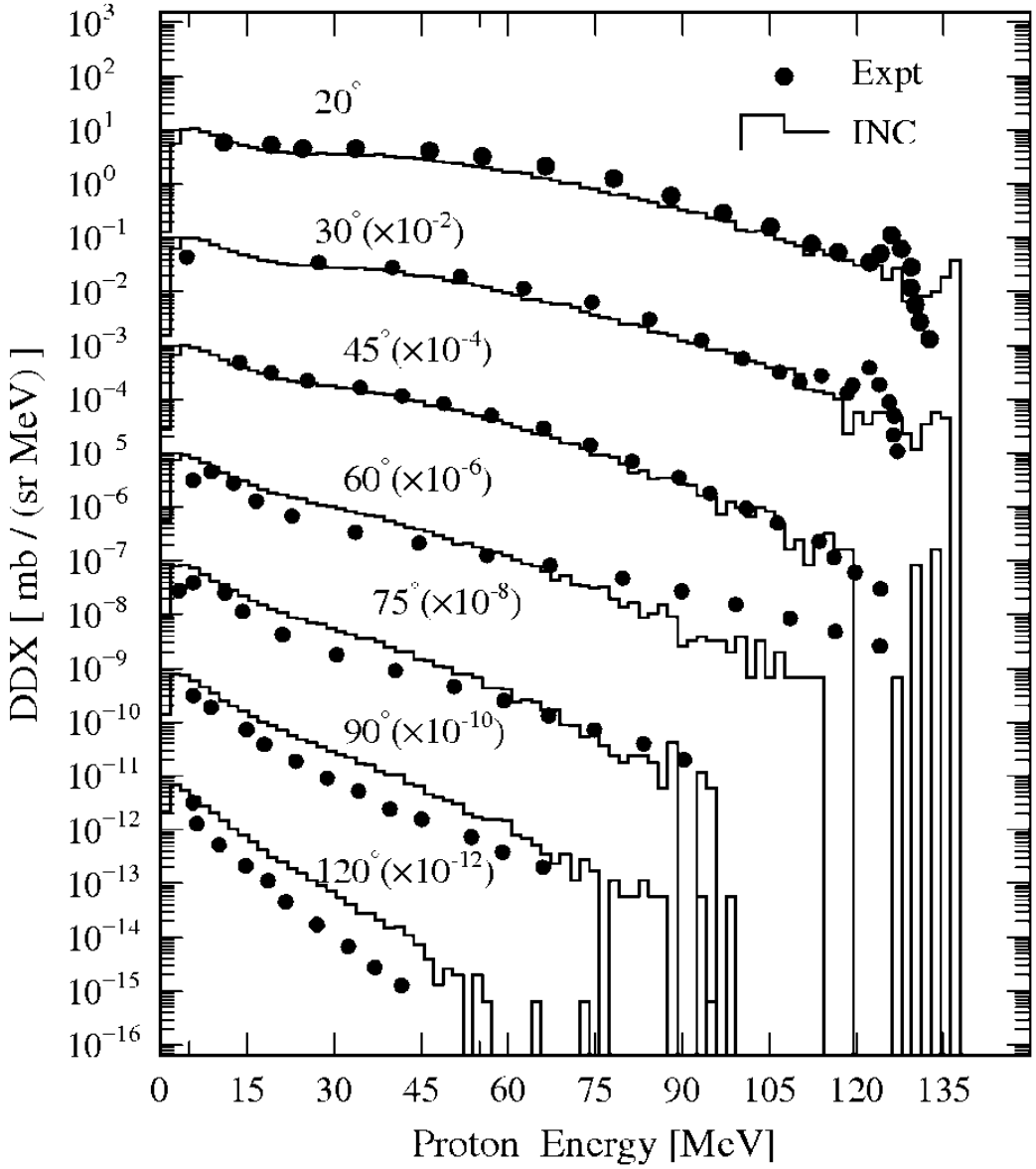

Fig. 4.14 Same as Fig. 4.4, but for ^{27}Al(α, px) reactions at 140 MeV.

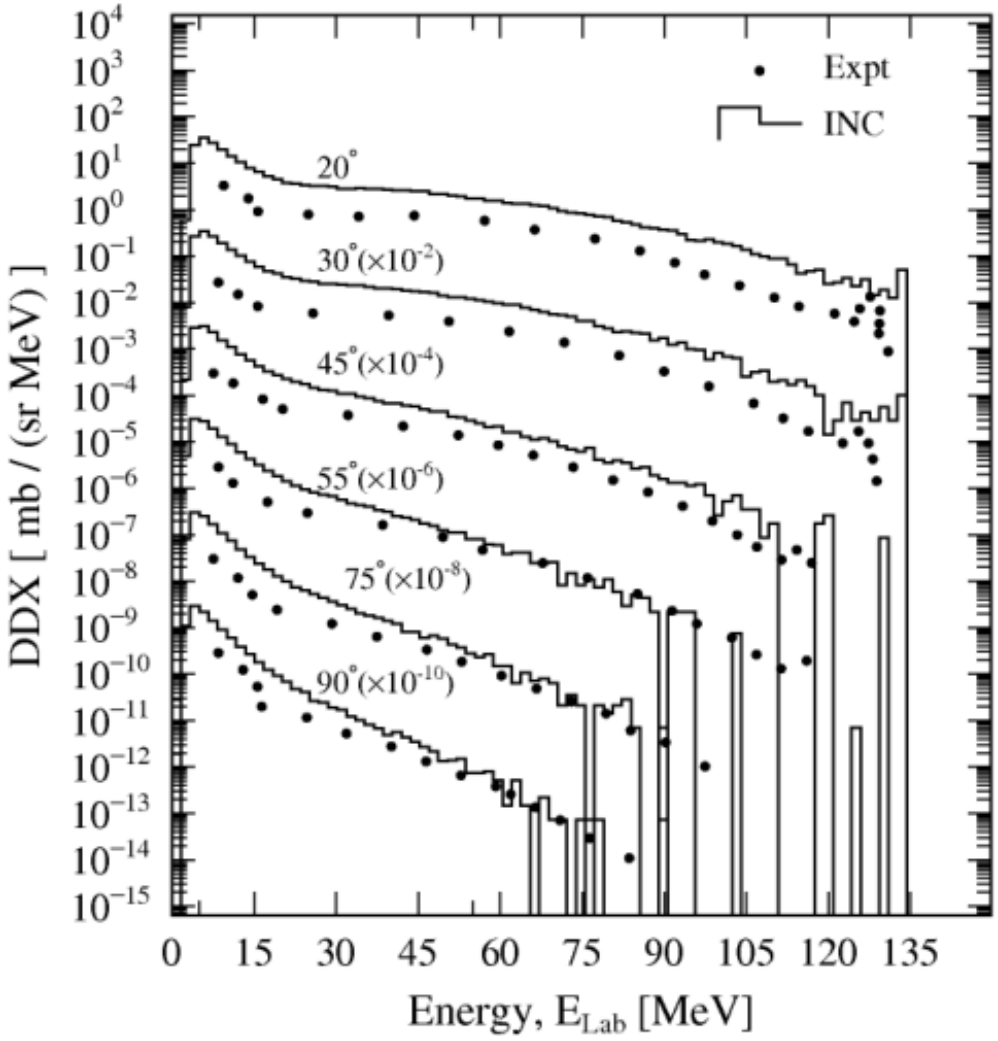

Fig. 4.15 Same as Fig. 4.4, but for ^{58}Ni(α, px) reactions.

4.3.1 INC for Forward Angular Positions

In this section, the predictability of extended INC model is represented for the forward angle energy spectra from ^{27}Al and ^{58}Ni in case of deuteron and triton production DDXs at 160 MeV alpha incident energy. The experimental data were taken from Ref[69].

Figs. 4.16 and 4.17 allow the comparison of the deuteron energy spectra from ^{27}Al and ^{58}Ni, respectively, at angles 6° to 26°. In both cases, gross features are reproduced well.

Higher energy end of the spectra in case of Al target and lower energy end of spectra from Ni shows discrepancies.

The triton spectra from ^{27}Al and ^{58}Ni are shown in Figures 4.18 and 4.19, respectively. The calculated triton spectra for the target ^{27}Al at angles 6°-26° as well as the calculated spectra for target ^{58}Ni at angles 6°-18° show good agreement with experimental data except the higher energy region. The inclusion of stripping reaction in INC model would diminish the discrepancies.

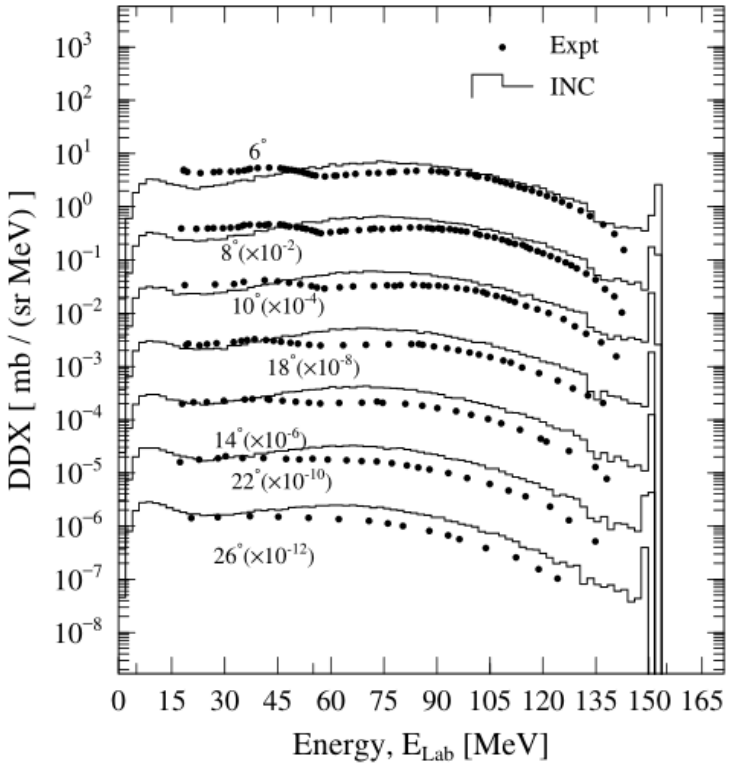

Fig. 4.16 Comparison of the experimental and calculated deuteron energy spectra for the 160 MeV alpha bombardment on ^{27}Al. Experimental data (solid circles) are taken from Wu et al.[69] Line histograms are the INC model calculation results. For visualization, the DDXs have been multiplied by the factors indicated in brackets.

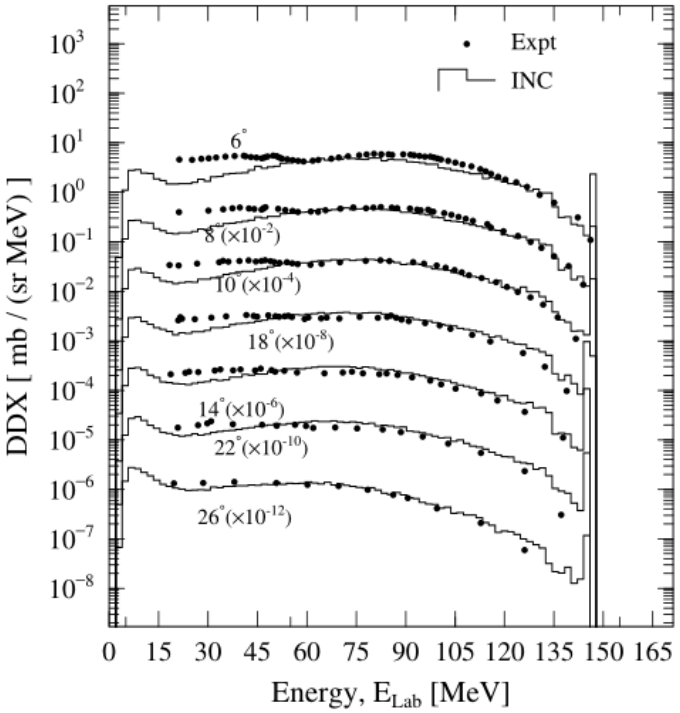

Fig. 4.17 Same as Fig. 4.16, but for target ^{58}Ni.

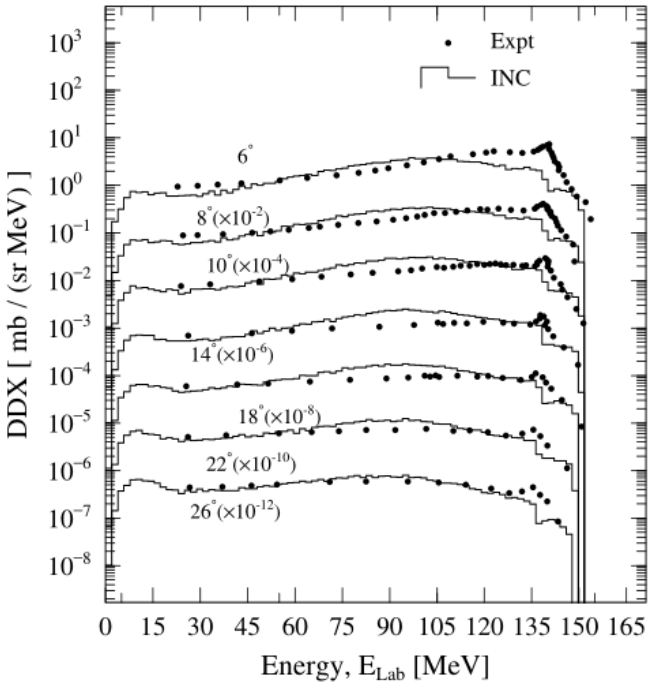

Fig. 4.18 Same as Fig 4.16, but for ^{27}Al(α, tx) reactions at 160 MeV.

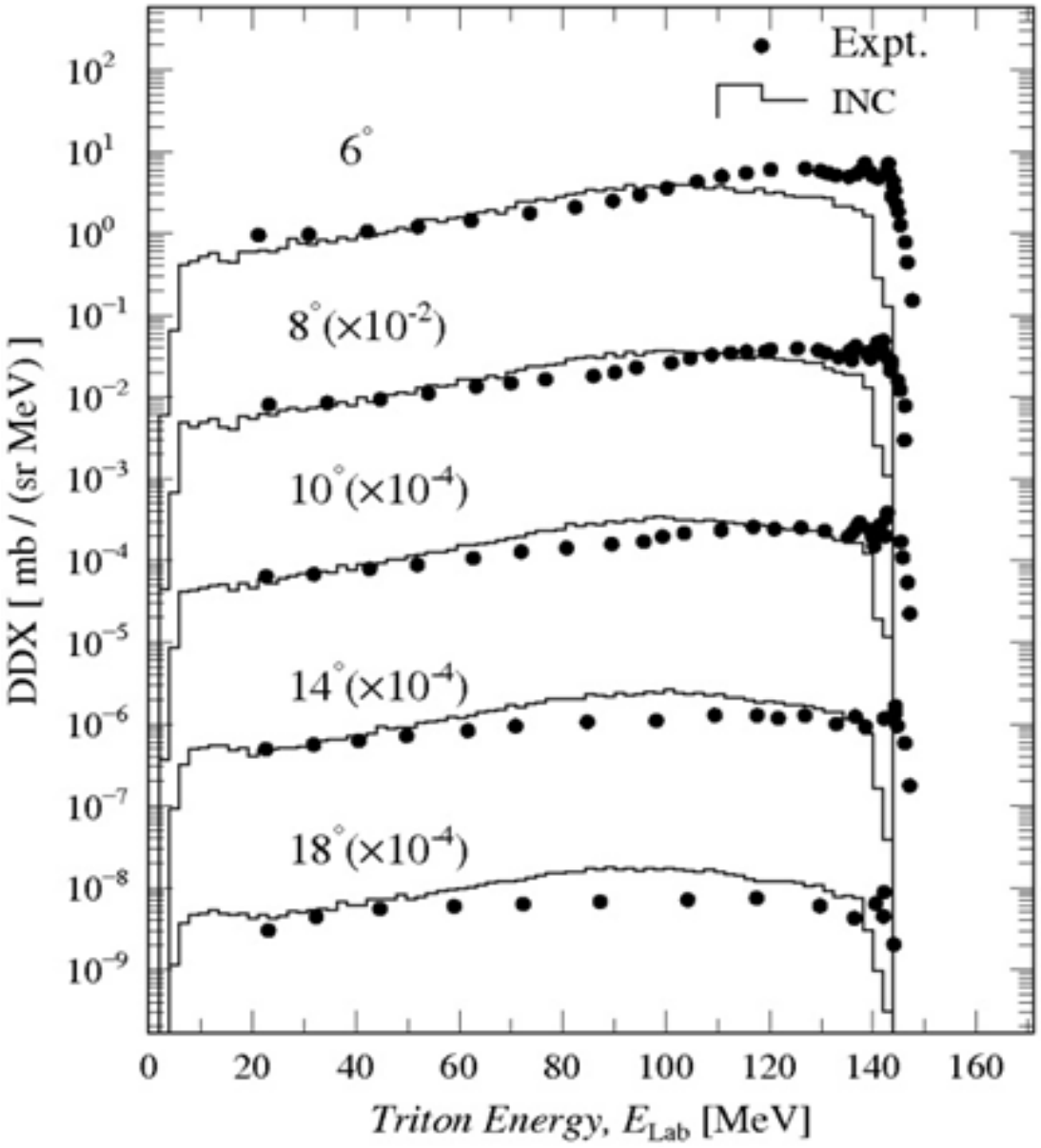

Fig. 4.19 Same as Fig. 4.16, but for ^{58}Ni(α, tx) reactions at 160 MeV.

4.4 Comparison with Other Models

In this section, the experimental data for α-induced reactions on ^{27}Al and ^{58}Ni at incident energy 140 MeV are compared with INCL and JQMD calculation results.

Figs. 4.20 and 4.21 show the comparison of experimental alpha energy spectra with INCL and JQMD results in case of alpha bombardment on ^{27}Al and ^{58}Ni targets, respectively. An evaporation model was coupled to simulate the de-excitation stage of residual nuclei in the two cases. The model simulation was done by the transport codes, PHITS. In both cases, INCL shows better results though severe underestimation is observed in high-energy regions. However, in lower energy regions, the emission DDXs spectra are mainly reproduced by evaporation model. Widely used model for nucleus-nucleus interaction, JQMD also shows poor prediction for (α, α'x) reactions.

Figs. 4.22-4.37 show the comparison of JQMD and INCL calculation results with the experimental data for different channels of alpha-induced reactions at angular positions 20° and 45° or at the angles 20°, 45° and 75°. The prediction capabilities of the two models show the need of a high predictable model for transport codes in case of cluster-induced cluster production reactions.

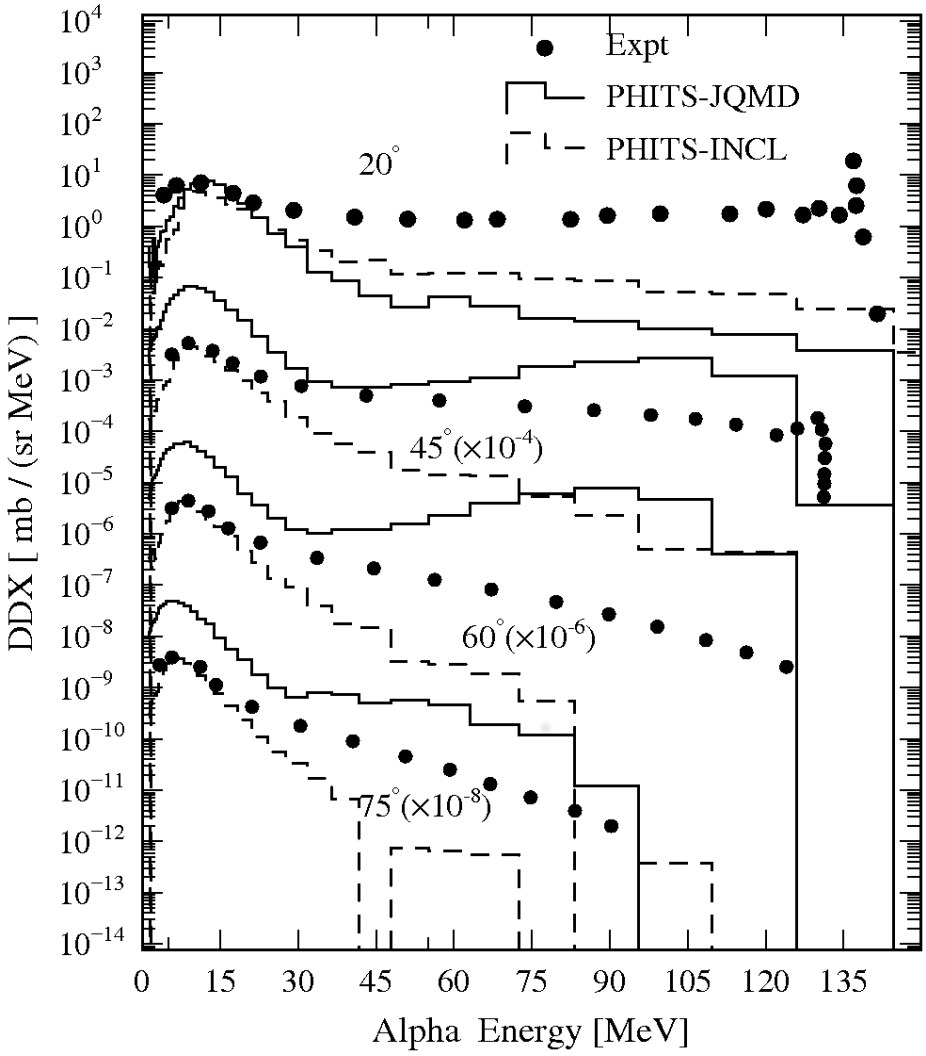

Fig. 4.20 The comparison of experimental DDXs for ^{27}Al(α, α'x) reactions at 140 MeV with the INCL (dashed line histogram) and JQMD (solid line histogram) model calculation results at angles from 20° to 75°. The solid circles represent the experimental deuteron energy spectra. Factors shown in bracket are multiplied for display purpose.

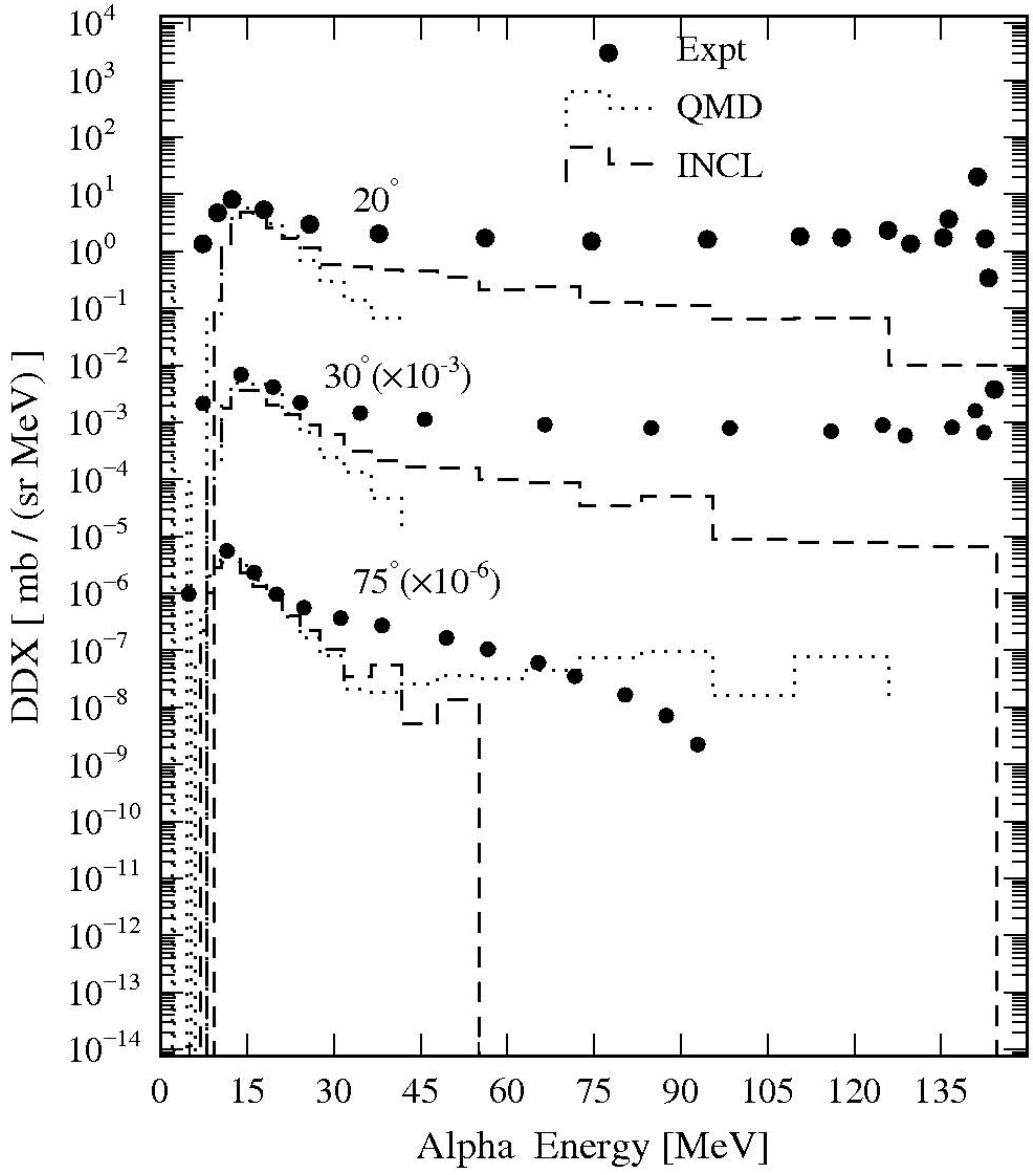

Fig. 4.21 As Fig. 4.20, but for ^{58}Ni(α, α'x) reactions at 140 MeV.

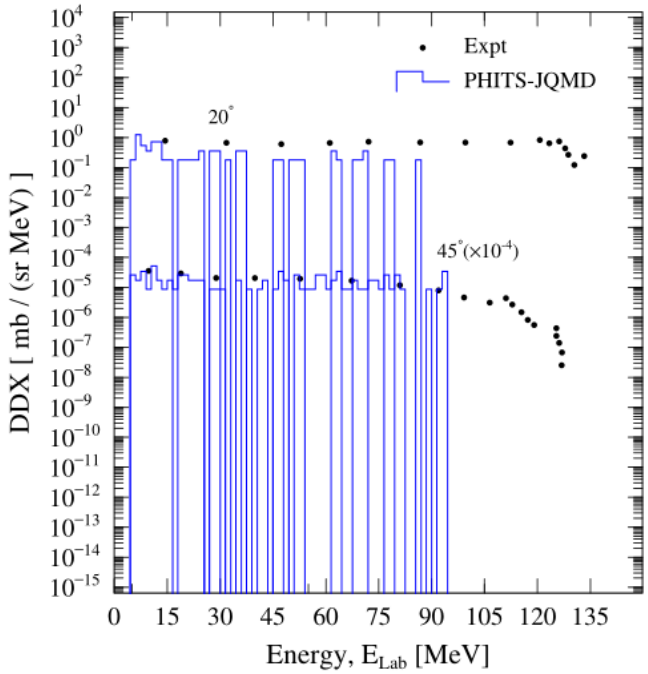

Fig. 4.22 Comparison of experimental DDXs for ^{27}Al(α, tx) reactions at 140 MeV with JQMD calculation result.

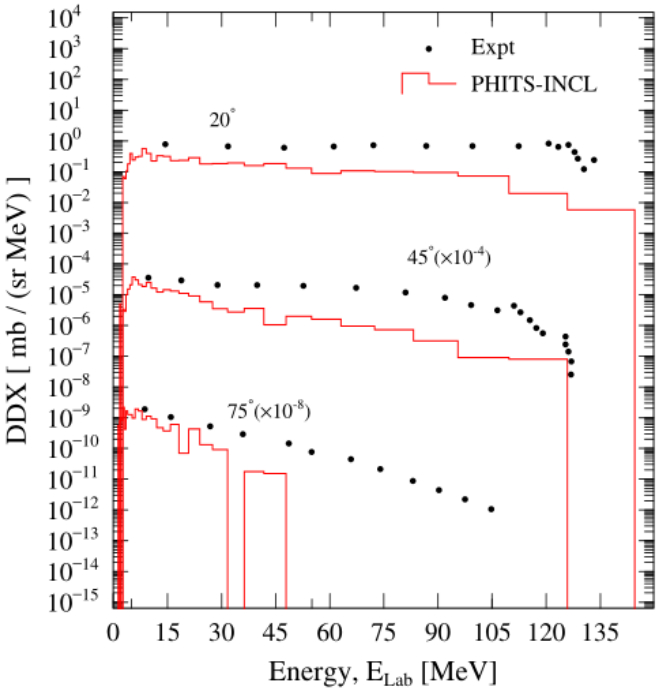

Fig. 4.23 Comparison of experimental DDXs for ^{27}Al(α, tx) reactions at 140 MeV with INCL calculations result.

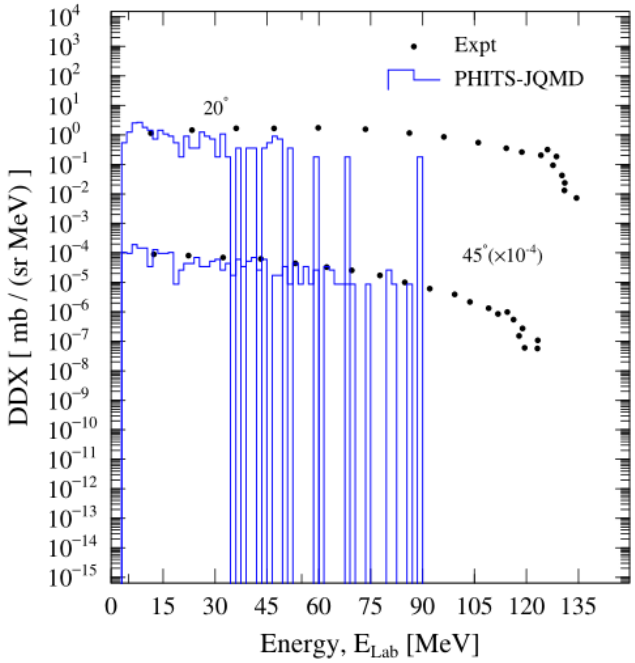

Fig. 4.24 Comparison of experimental DDXs for ^{27}Al(α, dx) reactions at 140 MeV with JQMD calculations result.

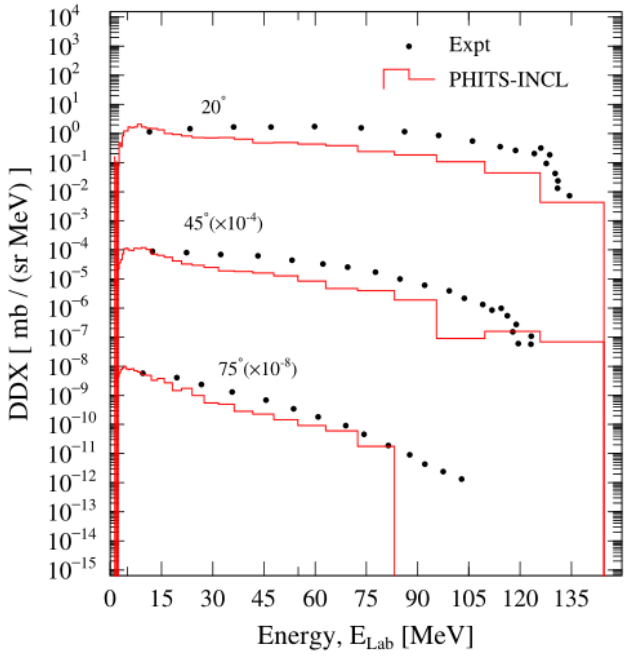

Fig. 4.25 Comparison of experimental DDXs for ^{27}Al(α, dx) reactions at 140 MeV with INCL calculations result.

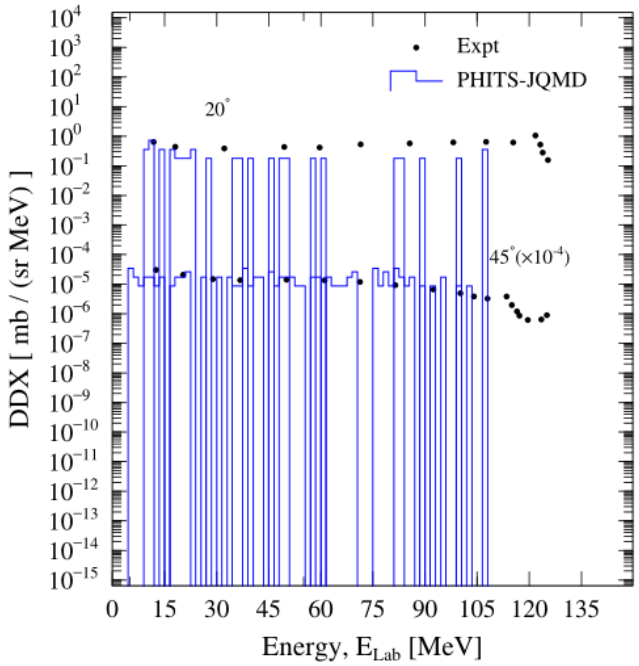

Fig. 4.26 Comparison of experimental DDXs for ^{27}Al(α, ^{3}Hex) reactions at 140 MeV with JQMD calculations result.

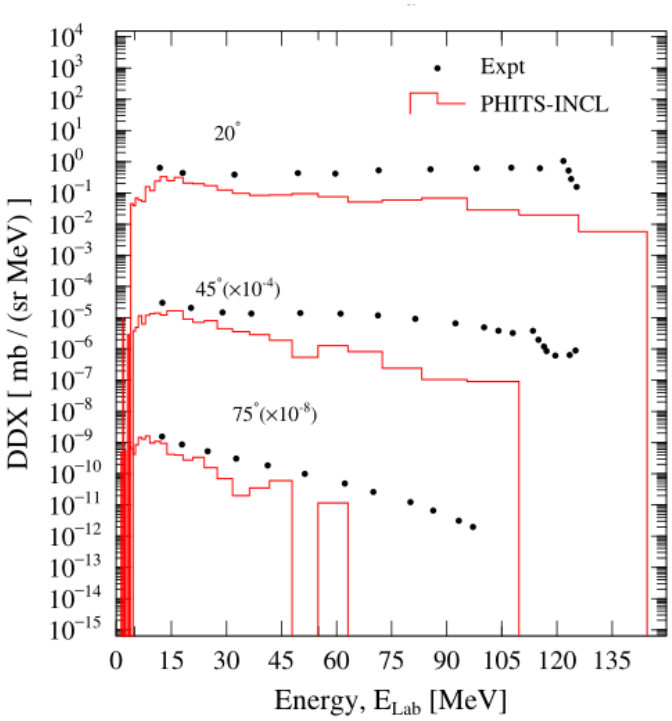

Fig. 4.27 Comparison of experimental DDXs for ^{27}Al(α, ^{3}Hex) reactions at 140 MeV with INCL calculations result.

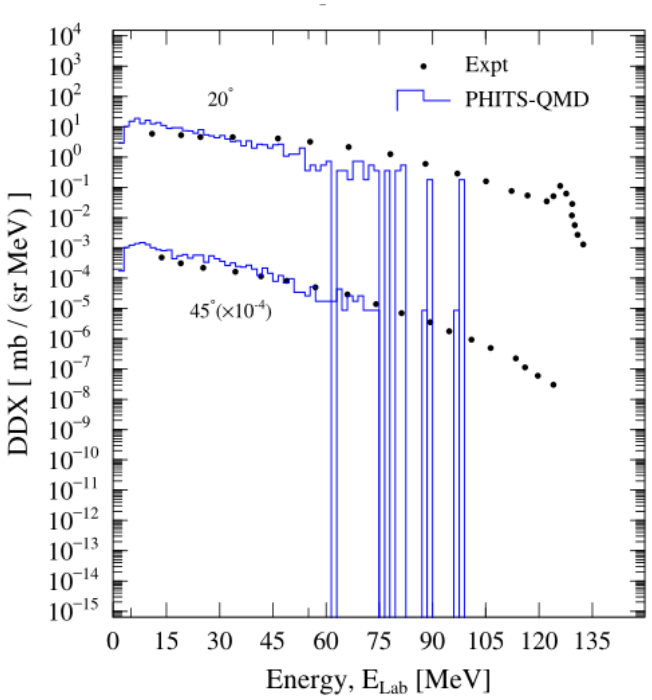

Fig. 4.28 Comparison of experimental DDXs for ^{27}Al(α, px) reactions at 140 MeV with JQMD calculations result

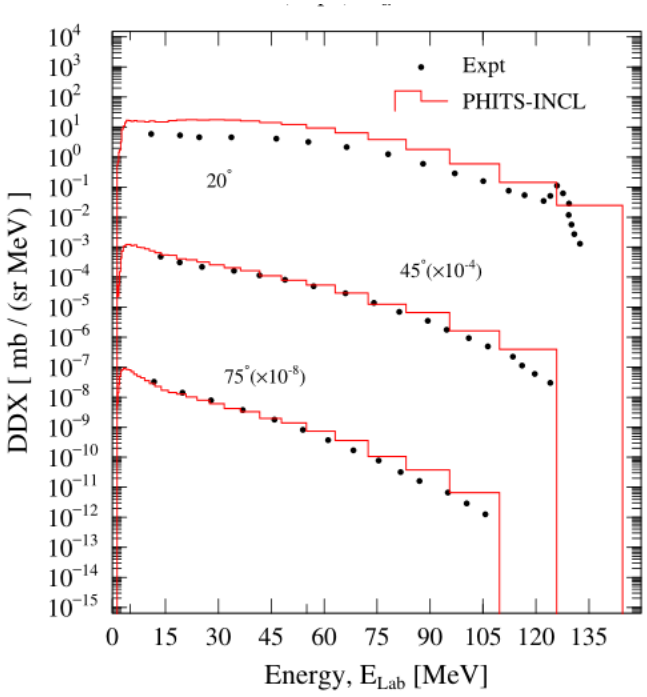

Fig. 4.29 Comparison of experimental DDXs for ^{27}Al(α, px) reactions at 140 MeV with INCL calculations result

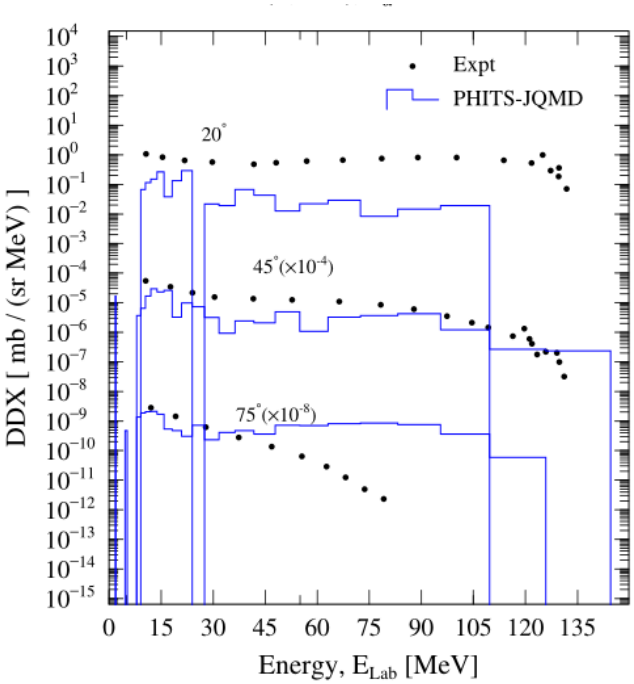

Fig. 4.30 Comparison of experimental DDXs for ^{58}Ni(α, ^{3}Hex) reactions at 140 MeV with JQMD calculations result.

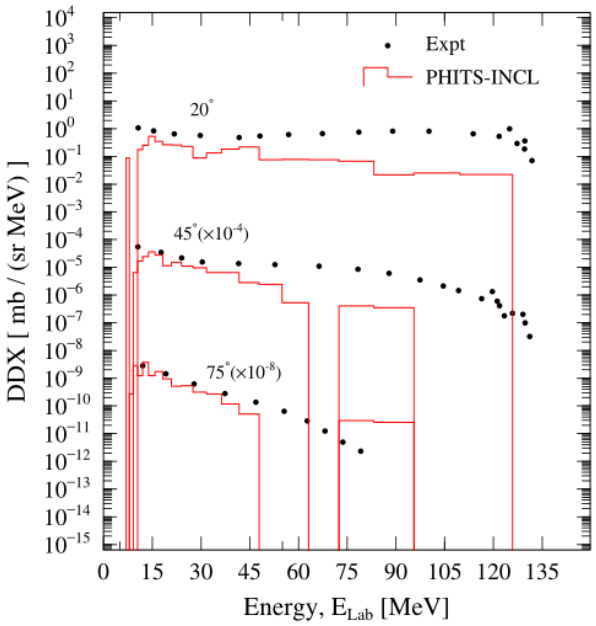

Fig. 4.31 Comparison of experimental DDXs for ^{58}Ni(α, ^{3}Hex) reactions at 140 MeV with INCL calculations result.

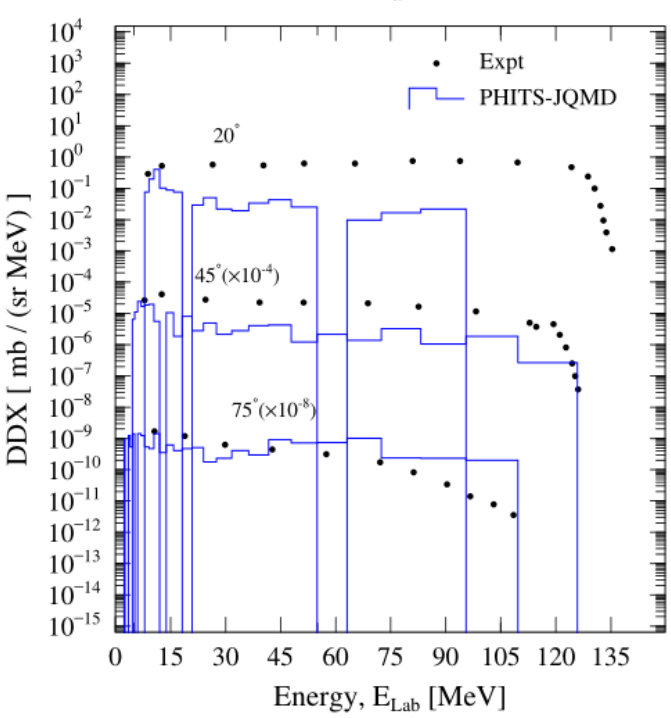

Fig. 4.32 Comparison of experimental DDXs for ^{58}Ni(α, tx) reactions at 140 MeV with JQMD calculations result.

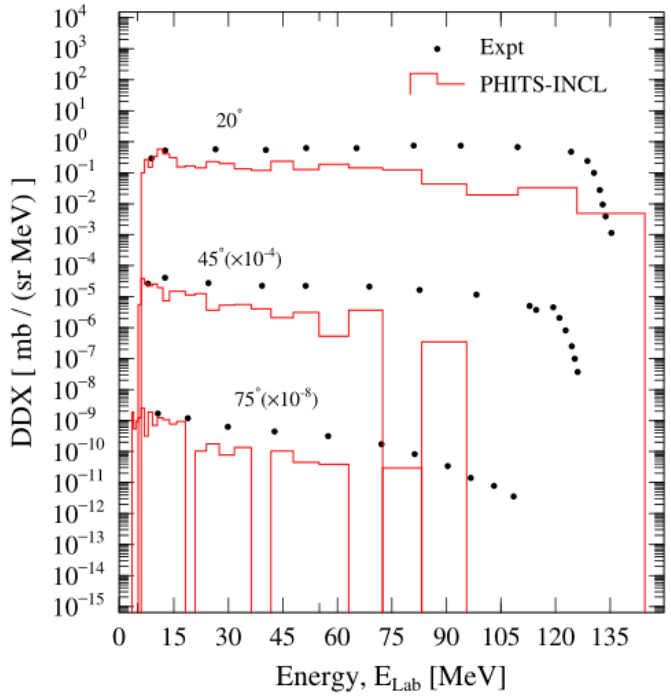

Fig. 4.33 Comparison of experimental DDXs for ^{58}Ni(α, tx) reactions at 140 MeV with INCL calculations result.

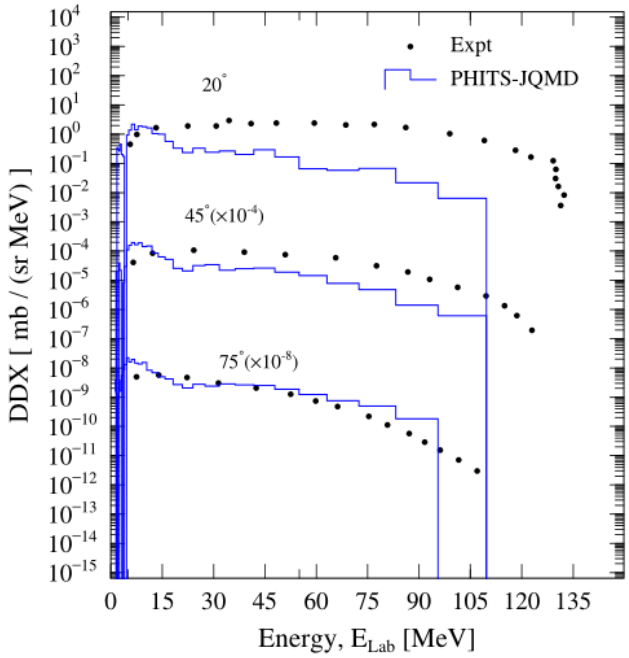

Fig. 4.34 Comparison of experimental DDXs for ^{58}Ni(α, dx) reactions at 140 MeV with JQMD calculations result.

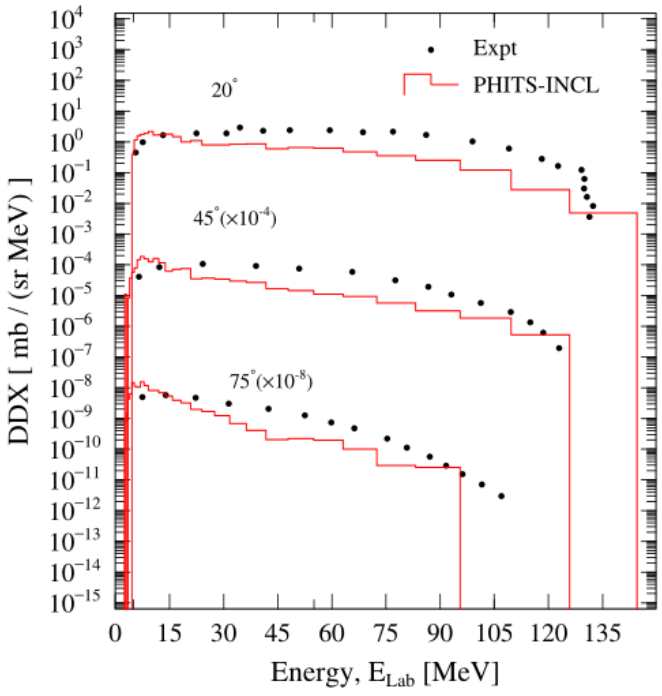

Fig. 4.35 Comparison of experimental DDXs for ^{58}Ni(α, dx) reactions at 140 MeV with INCL calculations result.

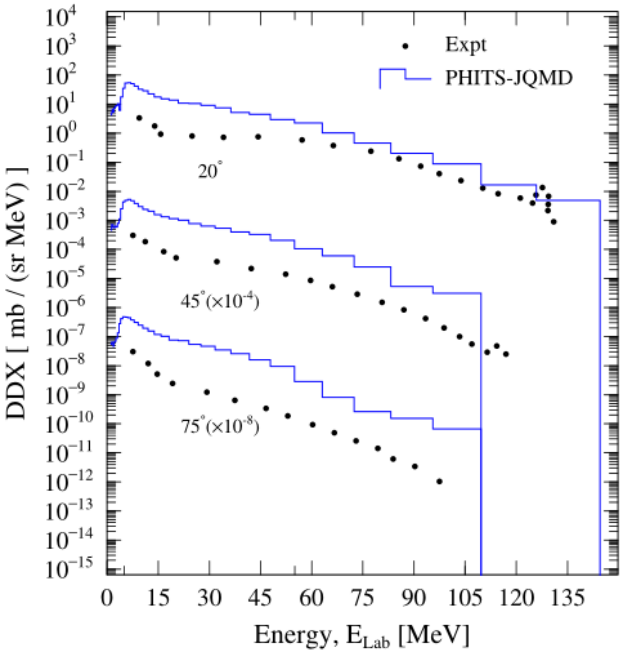

Fig. 4.36 Comparison of experimental DDXs for ^{58}Ni(α, px) reactions at 140 MeV with JQMD calculations result.

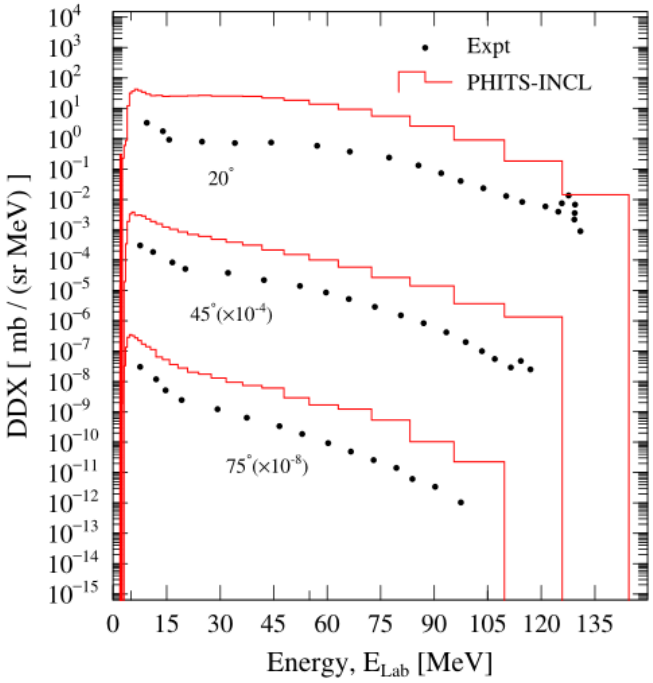

Fig. 4.37 Comparison of experimental DDXs for ^{58}Ni(α, px) reactions at 140 MeV with INCL calculations result.

5 Conclusion

In this research, the previously developed INC model was investigated to widen its applicable range to include cluster-induced (deuteron and alpha) and cluster production reactions. The essential improvement of the model was to incorporate the breakup of the incident cluster at the initial state of interaction. We introduced the idea of virtual excited states of the incoming cluster in the INC framework where the projectile ground state is expressed as a superposition of wave functions of its different states that consists of clusters units. Nuclear potential has a strong impact on the angular distribution of the incoming and outgoing particles. Therefore, the trajectory deflection was considered for both incoming clusters and ejectiles. We performed the calculations within the framework of our INC model together with an evaporation model considering the incident cluster as a collection of independent nucleons.

To verify the extended model energy-angle distributions of (d, $d'x$), (d, px) and (d, nx) reactions for various targets were calculated at intermediate energies. The model showed a good account of observed data for the deuteron-induced inclusive reactions. The model calculations were also performed to verify the extended code for α-induced reactions by comparing with experimental observations. The calculation results indicated that the proposed model has high predictive power for all channels of alpha-induced reactions, namely, (α, $\alpha'x$), (α, ^{3}Hex), (α, tx), (α, dx), (α, px), and (α, nx). The model underestimated the high-energy end of spectra, which are occupied by transitions to discrete levels. We believe that the inclusion of the stripping reaction mechanism would improve the model accuracy.

The present work incorporates the unpreceded physics idea in the framework of INC model. The model extension for deuteron-and alpha-induced reactions for a variety of

final channels for the calculations of cascade stage of nuclear reactions would open the door for further extension of INC model to the light ion induced and cluster production reactions. In near future, the model developed at Kyushu University will be expanded for carbon-incidence nuclear reactions, which has a good interest in the carbon-ion radiotherapy treatment to estimate the amount of dose.

References

[1] Y. Sawada, Y. Uozumi, S. Nogamine, T. Yamada, Y. Iwamoto, T. Sato, and K. Niita, "Intranuclear cascade with emission of light fragment code implemented in the transport code system PHITS," *Nucl. Instruments Methods Phys. Res. B* 291, pp. 38–44, 2012.

[2] T. Sato, K. Niita, N. Matsuda, S. Hashimoto, Y. Iwamoto, S. Noda, T. Ogawa, H. Iwase, H. Nakashima, T. Fukahori, K. Okumura, T. Kai, S. Chiba, T. Furuta, and L. Sihver, "Particle and heavy ion transport code system, PHITS, version 2.52," *J. Nucl. Sci. Technol.*, vol. 50, pp. 913–923, 2013.

[3] S. Pedoux, "Extension of the Liège Intranuclear Cascade Model to the 2-15 GeV Incident Energy Range," University de Liege, 2012.

[4] O. Jäkel, "Heavy Ion Radiotherapy," *New technologies in radiation oncology. Medical Radiology (Radiation Oncology).*, G. A. Schlegel W., Bortfeld T., Ed. Berlin, Heidelberg: Springer, 2006.

[5] M. Durante and J. S. Loeffler, "Charged particles in radiation oncology," *Nat. Rev. Clin. Oncol.*, vol. 7, pp. 37–43, 2010.

[6] F. A. Cucinotta, L. W. Townsend, and J. W. Wilson, "Description of alpha-nucleus interaction cross sections for cosmic ray shielding studies," NASA Technical Paper 3285, 1993.

[7] J. C. Chancellor, G. B. I. Scott, and J. P. Sutton, "Space Radiation: the number one risk to astronaut health beyond low earth orbit," *Life*, vol. 4, pp. 491–510, 2014.

[8] A. Mzhavia, "Study of double differential cross section of nuclear reactions induced by protons, pions, and oxygen-ions," Kyushu University,Japan, 2012.

[9] K. Niita, H. Takada, S. Meigo, and Y. Ikeda, “High energy particle transport code NMTC/JAM,” *15th Meeting of the International Collaboration on Advanced Neutron Sources*, JAERI-Conf 2001-002, pp. 964–970.

[10] T. Sato, K. Niita, N. Matsuda, S. Hashimoto, Y. Iwamoto, T. Furuta, S. Noda, T. Ogawa, H. Iwase, H. Nakashima, T. Fukahori, K. Okumura, T. Kai, S. Chiba, and L. Sihver, “Overview of particle and heavy ion transport code system PHITS,” *Ann. Nucl. Energy*, vol. 82, pp. 110–115, 2015.

[11] Y. Nara, N. Otuka, A. Ohnishi, K. Niita, and S. Chiba, “Relativistic nuclear collisions at 10A GeV energies from p+Be to Au+Au with the hadronic cascade model,” *Phys. Rev. C*, vol. 61, p. 24901, 1999.

[12] A. Boudard, J. Cugnon, J.-C. David, S. Leray, and D. Mancusi, “New potentialities of the Liège intranuclear cascade model for reactions induced by nucleons and light charged particles,” *Phys. Rev. C*, vol. 87, no. 1, p. 14606, 2013.

[13] K. Niita, T. Sato, H. Iwase, H. Nose, H. Nakashima, and L. Sihver, “PHITS-a particle and heavy ion transport code system,” *Radiat. Meas.*, vol. 41, pp. 1080–1090, 2006.

[14] Y. Iwamoto, T. Sato, S. Hashimoto, T. Ogawa, T. Furuta, S. I. Abe, T. Kai, N. Matsuda, R. Hosoyamada, and K. Niita, “Benchmark study of the recent version of the PHITS code,” *J. Nucl. Sci. Technol.*, vol. 54, pp. 617–635, 2017.

[15] R. E. Prael, “A review of physics models in the LAHET code,” *Proceedings of a Specialists’ Meeting, 30 May–1 June Intermediate Energy Nuclear Data: Models and Codes, OECD*. p. 145, 1994.

[16] R. E. Prael and H. Lichtenstein, “User guide to LCS: The LAHET code system”, LA-UR-89-3. Los Alamos National Laboratory, Los Alamos, New Mexico 8754, 1989.

[17] H. W. Bertini, “Intranuclear-cascade calculation of the secondary nucleon spectra from nucleon-nucleus interactions in the energy range 340 to 2900 MeV and

comparisons with experiment,"*Phys. Rev.*, vol. 188, p. 1711, 1969.

[18] Y. Yariv and Z. Fraenkel, "Intrannclear cascade calculation of high-energy heavy-ion interactions," *Phys. Rev. C*, vol. 20, 1979.

[19] J. Allison, K. Amako, J. Apostolakis, P. Arce, M. Asai, T. Aso, …, and H. Yoshida, "Recent developments in GEANT4," *Nucl. Instruments Methods Phys. Res. A*, vol. 835, pp. 186–225, 2016.

[20] G. Folger and J. P. Wellisch, "String Parton Models in Geant4," *Comput. High Energy Nucl. Phys.*, pp. 24–28, 2003.

[21] D. H. Wright, T. Koi, G. Folger, V. Ivanchenko, M. Kossov, N. Starkov, A. Heikkinen, and H. P. Wellisch, "Low and high energy modeling in Geant4," *Proc. Hadron. Show. Simul. Work.*, pp. 11–20, 2006.

[22] M. P. Guthrie, J. R. G. Alsmiller, and H. W. Bertini, "Calculation of the capture of negative pions in light elements and comparison with experiments partaining to cancer radiotherapy," *Nucl. Instruments Methods*, vol. 66, pp. 29–36, 1968.

[23] H. W. Bertini and M. P. Guthrie, "Results from medium-energy intranuclear-cascade calculation," *Nucl. Phys. A*, vol. 169, pp. 670–672, 1971.

[24] A. Ferrari, P. R. Sala, A. Fasso, and J. Ranft, "Fluka : A Multi-Particle Transport Code," SLAC-R-773, 2005.

[25] T. T. Böhlen, F. Cerutti, M. P. W. Chin, A. Fassò, A. Ferrari, P. G. Ortega, A. Mairani, P. R. Sala, G. Smirnov, and V. Vlachoudis, "The FLUKA Code: Developments and challenges for high energy and medical applications," *Nucl. Data Sheets*, vol. 120, pp. 211–214, 2014.

[26] A. Fasso, A. Ferrari, S. Roesler, P. R. Sala, F. Ballarini, A. Ottolenghi, G. Battistoni, F. Cerutti, E. Gadioli, M. V Garzelli, A. Empl, and J. Ranft, "The physics models of FLUKA: status and recent developments," *arXiv*:hep-hp/0306267v1 June, 2003.

[27] S. Roesler, R. Engel, and J. Ranft, The monte carlo event generator DPMJET-III. Springer, Berlin, Heidelberg, 2001.

[28] H. Takado, S. Meigo, and K. Niita, "Present status of nucleon-meson transport code NMTC/JAERI," *Advanced Monte Carlo for Radiation Physics, Particle Transport Simulation and Application*, 2001, pp. 157–175.

[29] R. Serber, "The production of high-energy neutrons by stripping," *Phys. Rev.*, vol. 72, July, pp. 1008–1016, 1947.

[30] IAEA benchmark of spalletion models, https://www-nds.iaea.org/spallations/.

[31] M. . Goldberger, "The interaction of high energy neutrons and heavy nuclei," *Phys. Rev.*, vol. 74, pp. 1269–1277, 1948.

[32] H. W. Bertini, "Low-energy intranuclear cascade calculation," *Phys. Rev.*, vol. 131, p. 160, 1963.

[33] N. Metropolis, R. Bivins, M. Storm, A. Turkevich, J. M. Miller, and G. Friedlander, "Monte Carlo calculations on intranuclear cascades. I. Low-energy studies," *Phys. Rev.*, vol. 110, pp. 185–203, 1958.

[34] K. Chen, Z. Fraenkel, G. Friedlander, J. R. Grover, J. M. Miller, and Y. Shimamoto, "Vegas: A Monte Carlo simulation of Intranuclear Cascades," *Phys. Rev.*, vol. 166, no. 4, pp. 949–967, 1968.

[35] A. Boudard, J. Cugnon, S. Leray, and C. Volant, "Intranuclear cascade model for a comprehensive description of spallation reaction data," *Phys. Rev. C*, vol. 66, p. 44615, 2002.

[36] H. Iwamoto, M. Imamura, Y. Koba, Y. Fukui, G. Wakabayashi, Y. Uozumi, T. Kin, Y. Iwamoto, S. Hohara, and M. Nakano, "Proton-production double-differential cross sections for 300-MeV and 392-MeV proton-induced reactions," *Phys. Rev. C*, vol. 82, p. 34604, 2010.

[37] K. Niita, S. Chiba, T. Maruyama, T. Maruyama, H. Takada, T. Fukahori, Y. Nakahara, and A. Iwamoto, "Analysis of the (N,xN') reactions by quantum molecular dynamics plus statistical decay model," *Phys. Rev. C,* vol. 52, p. 2620, 1995.

[38] S. Furihata, K. Niita, S. Meigo, Y. Ikeda, and F. Maekawa, "The GEM code- A simulation program for the evaporation and the fission process of an excited nucleus," JAERI-Data/Code 2001-015.

[39] J. J. Griffin, "Statistical model of intermediate structure," *Phys. Rev. Lett.*, vol. 17, pp. 478–481, 1966.

[40] R. Serber, "Nuclear reactions at high energies," *Phys. Rev.*, vol. 72, pp. 1114–1115, 1947.

[41] K. M. Watson, "Multiple scattering and the many-body problem applications to photomeson production in complex nuclei," *Phys. Rev.*, vol. 89, p. 575, 1953.

[42] D. Mancusi, A. Boudard, J. Cugnon, J. C. David, P. Kaitaniemi, and S. Leray, "Extension of the liege intranuclear-cascade model to reactions induced by light nuclei," *Phys. Rev. C* vol. 90, pp. 1–36, 2014.

[43] G. J. Mathews, B. G. Glagola, R. A. Moyle, and J. V. E. Viola, "Inclusion of deuteron and alpha-particle collisions in intranuclear cascade calculations," *Phys. Rev. C*, vol. 25, pp. 2181–2195, 1982.

[44] EXFOR: Experimental Nuclear Reaction Data, https://www-nds.iaea.org/exfor/exfor.htm

[45] J. W. Negele, "Structure of finite nuclei in the local-density approximation," *Phys. Rev. C*, vol. 1, p. 1260, 1970.

[46] J. Cugnon, D. L'Hote, and J. Vandermeulen, "Simple parametrization of cross-sections for nuclear transport studies up to the GeV range," *Nucl.Instruments Methods Phys. Res. B*, vol. 111, pp. 215–220, 1996.

[47] F. Atchison, “Spallation and fission in heavy metal nuclei under medium energy proton bombardment meeting on targets for neutron beam spallation sources,” *Proc. of Mtg. on Targets for Neutron Beam Spallation Source*, KFA-Jiilich, Germany, June 1979, 17 (1980).

[48] V. F. Weisskopf and D. H. Ewing, “On the yield of nuclear reactions with heavy elements,” *Phys. Rev.*, vol. 57, pp. 472–485, 1940.

[49] S. Furihata, “Statistical analysis of light fragment production from medium energy proton-induced reactions,” *Nucl. Instruments Methods Phys. Res. B*, vol. 171, pp. 251–258, 2000.

[50] I. Dostrovsky, Z. Fraenkel, and G. Friedlander, “Monte Carlo Calculations of Nuclear Evaporation Processes. III. Applications to Low-Energy Reactions,” *Phys. Rev.*, vol. 116, pp. 683–702, 1959.

[51] T. Matsuse, A. Arima, and S. M. Lee, “Critical distance in fission reactions,” *Phys. Rev. C*, vol. 26, pp. 2338–2341, 1982.

[52] H. Iwamoto, “核内カスケード模型への核子間相関の組み込み,” Kyushu University, 2010.

[53] Y. Uozumi, T. Yamada, S. Nogamine, and M. Nakano, “Intranuclear cascade model including collective excitations and trajectory deflections for (p,p’x) reactions around 50MeV,” *Phys. Rev. C*, vol. 86, p. 34610, 2012.

[54] G. J. Russell, “Spallation Physics - An Overview,” *Int. Collab. Adv. Neutron Sources KEK. Tsukuba*, pp. 291–299, 1990.

[55] A. Krasa, “Spallation reaction physics,” Czech Technical University, Prague, 2010.

[56] D. Ridikas, W. Mittig, H. Savajols, P. Roussel-Chomaz, S. V. Förtsch, J. J. Lawrie, and G. F. Steyn, “Inclusive proton production cross sections in (d,xp) reactions induced by 100 MeV deuterons,” *Phys. Rev. C*, vol. 63, p. 14610, 2000.

[57] S. Nakayama, H. Kouno, Y. Watanabe, O. Iwamoto, and K. Ogata, "Theoretical model analysis of (d,xn) reactions on ^{9}Be and ^{12}C at incident energies up to 50 MeV," *Phys. Rev. C*, vol. 94, pp. 1–9, 2016.

[58] J. R. Wu, C. C. Chang, and H. D. Holmgren, "Charged-particle spectra: 80 MeV deuterons on ^{27}Al and ^{58}NI and 70 MeV deuterons on ^{90}Zr, ^{208}Pb and ^{232}Th," *Phys. Rev. C*, vol. 19, pp. 370–390, 1979.

[59] J. R. Wu, C. C. Chang, and H. D. Holmgren, "Breakup of a particles in the fields of nuclei," *Phys. Rev. Lett.*, vol. 40, no. 15, pp. 1013–1016, 1978.

[60] K. Heyde, *Basic ideas and concepts in nuclear physics*, 3rd ed. London: Institute of Physics, 2004.

[61] Y. Uozumi, T. Yamada, and M. Nakano, "Intranuclear cascade model for 50-MeV-region (p , p ′ x) reactions over a wide target mass range," *J. Nucl. Sci. Technol.*, vol. 52, no. 2, pp. 264–273, 2015.

[62] A. Budzanowski, M. Fidelus, D. Filges, F. Goldenbaum, H. Hodde, L. Jarczyk, B. Kamys, M. Kistryn, S. Kistryn, S. Kliczewski, A. Kowalczyk, E. Kozik, P. Kulessa, H. MacHner, A. Magiera, B. Piskor-Ignatowicz, K. Pysz, Z. Rudy, R. Siudak, and M. Wojciechowski, "Variation of nonequilibrium processes in the p+Ni system with beam energy," *Phys. Rev. C*, vol. 80, p. 54604, 2009.

[63] H. Duarte, "Particle production in nucleon induced reactions above 14 MeV with an intranuclear cascade model," *Phys. Rev. C*, vol. 75, p. 24611, 2007.

[64] Y. Yariv and Z. Fraenkel, "Intranuclear cascade calculation of high energy heavy ion collisions: Effect of interactions between cascade particles.," *Phys. Rev. C*, vol. 24, 1981.

[65] J. Cugnon, "Monte Carlo calculation of high-energy heavy-ion interactions," *Phys. Rev. C*, vol. 22, 1980.

[66] T. Kin, F. Saiho, S. Hohara, K. Ikeda, K. Ichikawa, Y. Yamashita, M. Imamura, G.

Wakabayashi, N. Ikeda, Y. Uozumi, M. Matabo, M. Nakano, and N. Koori, "Proton production cross sections for reactions by 300- and 392-MeV protons on carbon, aluminum, and niobium," *Phys. Rev. C*, vol. 72, p. 14606, 2005.

[67] Y. Uozumi, Y. Sawada, A. Mzhavia, S. Nogamine, H. Iwamoto, T. Kin, S. Hohara, G. Wakabayashi, and M. Nakano, "Deuteron-production double-differential cross sections for 300- and 392-MeV proton-induced reactions deduced from experiment and model calculation," *Phys. Rev. C*, vol. 84, p. 64617, 2011.

[68] J. R. Wu, C. C. Chang, and H. D. Holmgren, "Charged particle spectra: 140 MeV α particle bombardment of ^{27}Al, ^{58}Ni, ^{90}Zr, ^{209}Bi, and ^{232}Th," *Phys. Rev. C*, vol. 19, pp. 659–673, 1979.

[69] J. R. Wu, C. C. Chang, H. D. Holmgren, and R. W. Koontz, "Alpha-particle breakup at incident energies of 20 and 40 Mev/nucleon," *Phys. Rev. C*, vol. 20, pp. 1284–1300, 1979.

Acknowledgement

At first, I would like to express my sincere gratitude to my esteemed supervisor Prof. Yusuke Uozumi. His guidance, wisdom, patience, as well as encouragement, helped me throughout the research and writing the thesis. I have learnt from his values, immense knowledge, and very gentle behavior. His positive outlook and confidence inspired me and gave me confidence. I like to express my gratitude to Prof. Masanobu Yahiro and Prof. Keisuke Maehata for the valuable remarks on the manuscript.

I am highly obliged to Prof. Tatsuya Kawae for his warmhearted suggestions and to Prof. Yujiro Yonemura for his delightful advice at different times. I would like to express my sincere thanks to Professors Nobuo Ikeda and Hidehiko Arima, and all my present and past lab members, especially, G. Watanabe, Y. Yamaguchi, A Sonoda, M Ueda. I must thank all my friends from different countries with whom I spent a great time. I also extend my thanks to Mr. Kawahara, Ms. Fujita and Mr. Yamada for helping at different aspects of daily life. I like to express heartfelt regards to Yoshida Scholarship Foundation for the gorgeous support during my studies.

I express sincere gratitude to my family and extended family members, especially my loving and amazing mother, two younger brothers who have supported me through the years. The greatest thanks go to my loving husband for his patience, support, care and everything. I would like to express a deep sense of regard to my father who used to stand by me like a pillar in times of need with constant encouragement, moral support and blessings. His memory is always a great source of inspiration for me.

During my three years stay in Japan, I have learned many things still having very little understanding of this culture. I believe this experience will help me in different states of my life. I am also thankful to many individuals, but I cannot name all of them here.